2014

Investigation of Pharmaceutical Mass Transfer Phenomena Using Molecular Dynamics Simulations

Yi Gao
Loyola University Chicago

LOYOLA UNIVERSITY CHICAGO

INVESTIGATION OF
PHARMACEUTICAL MASS TRANSFER PHENOMENA
USING MOLECULAR DYNAMICS SIMULATIONS

A DISSERTATION SUBMITTED TO

THE FACULTY OF THE GRADUATE SCHOOL

IN CANDIDACY FOR THE DEGREE OF

DOCTOR OF PHILOSOPHY

PROGRAM IN CHEMISTRY

BY

YI GAO

CHICAGO, IL

AUGUST 2014

ACKNOWLEDGMENTS

I would like to thank every individual who provided me with guidance, encouragement, friendship, and support on my long journey to complete this dissertation.

To my advisor Professor Kenneth Olsen for his inspiration, guidance, generous time commitment, understanding, kindness, and endless patience throughout my dissertation research. I have the highest respect for his knowledge, expertise, and spirit of venturing into a new field of research. What I have learned from him is a gift that I will treasure for a lifetime.

To Professors Daniel Graham, Miguel Ballicora, and Daniel Becker for their guidance and committee service.

To Dr. Geoff Zhang for his mentorship and scientific guidance, not only during my thesis research but also throughout my career at Abbvie. His passion to science is greatly admired. He is also one of the members on the committee.

To Dr. Yihong Qiu, my college classmate, friend, husband, and colleague, who has unconditionally supported my ambitious endeavor. I am fortunate to have unlimited access to his knowledge and expertise. The delicious dinner waiting for me every evening makes every day a Valentine's Day.

To Professors Martina Schmeling, Duarte Fretas, Miguel Ballicora, and Daniel Graham for the wonderful lectures. Their dedication to teaching is unparalleled. I enjoyed every class and wish I could have taken more with them.

To my father for pushing me to aim high, for teaching me, and for being a role model of resilience. He has set an example for me by beginning to study music after retirement and becoming an accomplished amateur musician.

To my dear daughter Allie and son Brynan for being the most devoted cheerleaders to their "crazy" mother. Their love propelled me through every setback on this voyage with joy.

To Dr. Devalina Law and Dr. Michelle Long at Abbvie, who trusted me and steered me toward the Ph.D program at Loyola.

To Dr. Shaoxin Feng, currently at Allergan, Inc., for the stimulating discussions and for teaching me a shortcut to make the complex crystal lattice structure into a useful file for the VMD software.

To my colleagues at Abbvie: Rodger Henry who provided the crystal structure files and scientific discussions, Jianwei Wu who assisted in HPLC analysis, and Dr. Donghua Zhu and Dr. Deliang Zhou for enjoyable scientific discussions.

To Professor Gang Wang at DePaul University for tutoring on probability and other mathematic questions.

To Stacey Lind for helping with all of the graduate school paperwork and course registrations. Without her help, I would have been totally lost.

To Donna Olsen for checking the spelling and grammar of my manuscripts.

To the management at Abbvie who has enthusiastically supported me in pursuing the Ph.D degree over the past eight to nine years. The list includes Dr. Michelle Long, Dr. Juergen Zeidler, Dr. Steven Nowak, Dr. Sue Semla, Dr. John Skoug, Dr. Wolfgang Fraunhofer, Dr. Eric Schmitt and Dr. Thomas Borchardt, especially to Wolfgang who

integrated this degree into my developmental goals and made sure I did not get sidetracked too often.

To Abbvie, Inc. for the Employee Tuition Assistance Program, which provided me with the opportunity to continue my education.

To the Department of Chemistry at Loyola University Chicago for providing a part-time student program, which made it possible for me to realize my dream.

To all of my colleagues at the Pharmaceutics and Formulation departments of Abbvie for their friendship and for supporting my Abbvie projects. In particular, I would like to thank Jianwei Wu, Julia Markworth, Socrates Vela, Nathaniel Catron, Ken Gleason, and Ji-an Wu.

Last but not least, to many close friends who have given me strong moral support and made my life much more enjoyable. The immense help from them will always be remembered.

To my father Gao Xinghua, and mother Chen Lan
and
husband Yihong, daughter Allie and son Brynan

有志者，事竟成.

—语出《后汉书.耿弇传》

Nothing is impossible to a determined mind

—Chinese proverb from Han Dynasty (~2000 years ago)

TABLE OF CONTENTS

LIST OF TABLES

LIST OF FIGURES

LIST of ABBREVIATIONS

α	Alpha
Å	Angstroms
ASD	Amorphous Solid Dispersion
APAP	Acetaminophen
API	Active Pharmaceutical Ingredient
β	Beta
CLogP	Calculated Logarithmic Partition Coefficient
C_p	Heat Capacity
DSC	Differential Scanning Calorimetry
ΔG	Gibbs Free Energy Change
GI	Gastrointestinal (Tract)
ΔH	Enthalpy Change
Hf	Heat of Fusion
HPLC	High Pressure Liquid Chromatography
HPMC	Hydroxypropyl Methylcellulose
IDR	Intrinsic Dissolution Rate
M	Molar Concentration
MD	Molecular Dynamics
mm	Millimeter
m.p.	Melting Point

ns	Nanosecond
ρ	Density
PEG	Poly(ethylene glycol)
pKa	Acid Ionization Constant
PLA	Poly(lactic acid)
PEG-b-PLA	Poly(ethylene glycol)-block-poly(lactic acid)
PLM	Polarized Light Microscopy
ps	Picoseconds
PVP	Poly(vinyl pyrrolidone)
PXRD	Powder X-ray Diffractometry
γ	Gamma
R	Ideal gas constant
RH	Relative Humidity
ΔS	Entropy Change
S	Supersaturtion
SMPT	Solution Mediated Phase Transformation
SurFPT	Surface Facilitated Phase Transformation
VDW	van der Waals
VMD	Visual Molecular Dynamics
TLZ	Tolazamide
USP	United States Pharmacopeia

ABSTRACT

Molecular dynamics (MD) simulation has been widely used in understanding the physical basis of the structure and function of biological macromolecules. However, its application in pharmaceutical research is still at an early stage. This dissertation attempts to establish the use of MD simulation in studying several important pharmaceutical mass transfer processes. The three-series study included (1) the understanding of drug crystal dissolution at molecular level, (2) the elucidation of an unique mechanism for facile polymorphic transformation of crystalline drugs in solutions, and (3) the determination of drug–polymer interactions at water–crystal interface and the implications to crystallization inhibition.

A drug crystal dissolution into aqueous solution was simulated successfully for the first time on acetaminophen crystal Form I. The results revealed distinct corner & edge effect and differentiated dissolution rate among the three crystal surfaces of (001), (101) and (100), which correlated strongly with total interaction energies among the drug molecules and between the drug and water molecules. This study helped us gain additional fundamental understanding in the relationship between dissolution rate and particle size and morphology.

A series of MD simulations and experimental methods were utilized to evaluate the thermodynamic and kinetic forces that control the polymorphic transformation in solutions. Acetaminophen Form II, a metastable crystalline form which readily converts

to the themodymically stable Form I when in contact with solution was studied. It was found that the facile polymorphic transformation is not attributed to the solubility differences; rather it is caused by a unique mechanism of surface facilitated phase transformation (SurFPT). This new mechanism is able to promote faster polymorphic transformation than the well-known mechanism of solution-mediated phase transformation (SMPT), thus it is more detrimental.

In the third study, the molecular mechanism of crystal surface specific drug–polymer interaction was investigated by simulating tolazamide crystals in the presence of hydrated PEG-*b*-PLA, a diblock copolymer. The results from the simulations demonstrated the polymer's strong interaction with the (001) face, weaker interaction with the (010) face and minimal to no interaction with the (100) face, which matched remarkably well with the reported crystal habit alteration by the preferential interaction of PEG-*b*-PLA primarily with the (001) and partially with (010). Interestingly, van der Waals interactions were identified as the dominant forces (accounts for 77–93% of total interaction energies) that enabled such strong drug–polymer interactions. These findings suggest that polymers capable of forming strong hydrophobic interactions are more effective in inhibiting crystallization of poorly-water soluble and hydrophobic drugs in aqueous media than those with hydrogen bonding capacities. Such in-depth analysis and understanding facilitate the rational selection of polymers in designing supersaturation-based enabling formulations.

CHAPTER ONE

BACKGROUND

This dissertation is concerned with three important pharmaceutical mass transfer phenomena taking place in aqueous solutions: (1) the dissolution of drug crystals, (2) the polymorphic transition, and (3) the inhibition of crystal growth through drug–polymer interactions. These three topics will be briefly reviewed in this section. The main focus of this dissertation is to apply new methodologies, especially molecular dynamics (MD) simulation to gain a better mechanistic understanding of these phenomena. Thus, the background of MD simulations will also be briefly reviewed in the context of drug dissolution and drug–polymer interactions.

Drug Dissolution

Dissolution is defined as the process by which a solute forms a solution in a solvent. It is a kinetic process quantified by rate and driven by equilibrium solubility. In the dissolution of crystalline solids, the crystal structure of the solute disintegrates as separate ions, atoms, or molecules. How the solute and solvent interact with one another determines the thermodynamic energies involved, such as the heat and entropy of dissolution. In order for dissolution to occur, the overall Gibbs free energy must be negative. Dissolution will continue until the Gibbs free energy becomes zero at which the equilibrium solubility is established.

Dissolution and Drug Development

The basic theories and laws of dissolution have been established in chemistry since the late 19th century.[1] In the pharmaceutical field, the dissolution process is of fundamental importance to the design, development, manufacture and quality control of drug products for the following reasons: (1) the large majority of active pharmaceutical ingredients (API) and inactive ingredients (or excipients) are solids; (2) these solids often undergo dissolution and precipitation processes during the manufacturing process of the API's and drug products and (3) most importantly, before the therapeutic effect of a drug can be realized, the drug must go into solution at the site of absorption in order to cross the biological membrane into the systemic circulation (Figure 1). Since the rate at which a drug dissolves from a dosage form often affects its rate and/or extent of absorption (also referred to as bioavailability), dissolution is considered one of the most critical steps in oral drug absorption. This is particularly the case for sparingly soluble drugs.

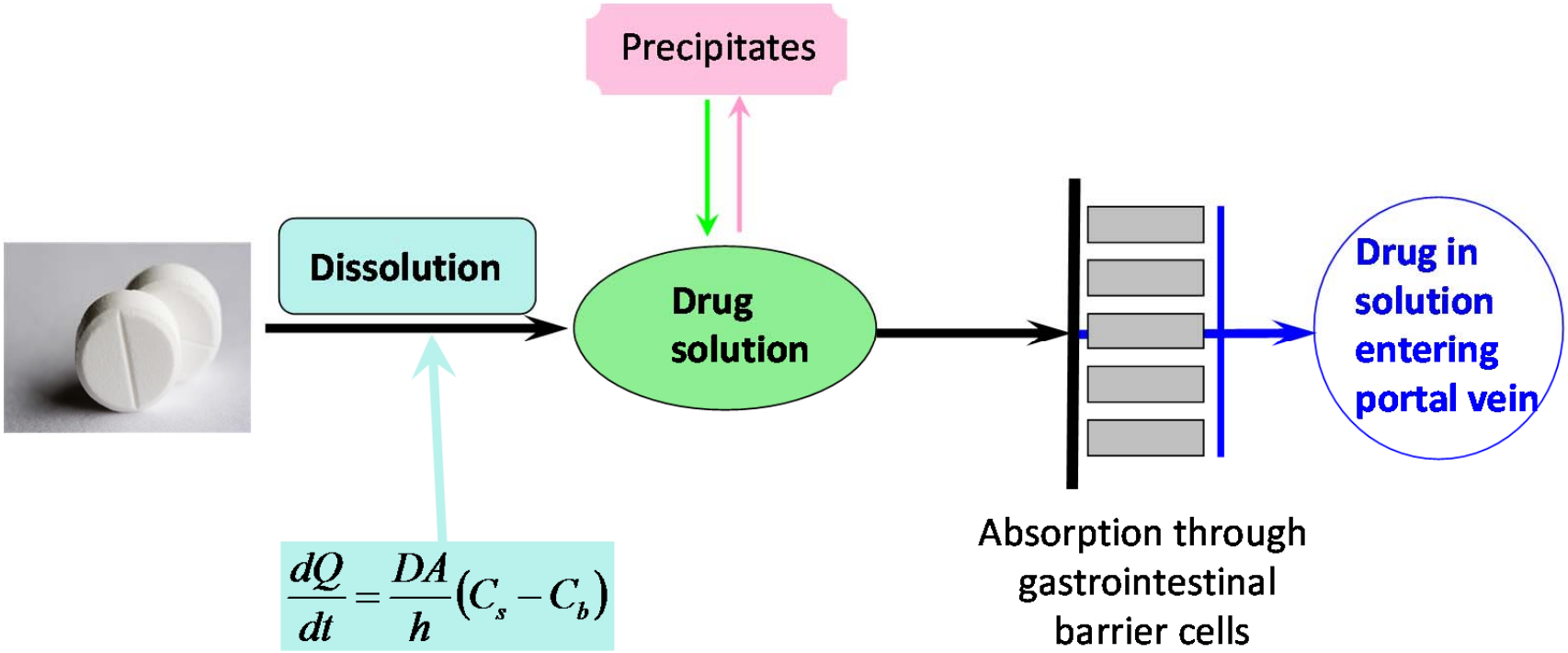

Figure 1. Drug dissolution and absorption of orally administered solid tablet dosage forms in the gastrointestinal (GI) tract.

In general, the rate of drug dissolution is influenced by the physicochemical properties of the drug substance, formulation and manufacturing process of the dosage form. Over the past decades, extensive studies have been conducted to evaluate thermodynamic and kinetic factors affecting dissolution of drug substances. The thermodynamic factors relate to the intrinsic solid-state properties such as solubility which changes with different solid forms (polymorphs and amorphous forms) and with other conditions (dissolution media, temperature, pH, buffer type, and ionic strength). The extrinsic factors that drive the kinetic process include particle surface area, hydrodynamics (stirring rate), and fluid viscosity. Besides the solid form and surface area which may change during dissolution, other aforementioned variables can be controlled in dissolution testing. Polymorphism is very common among drug substances, and different crystal forms have been shown to exhibit different dissolution and *in vivo* performance in both animal models and human subjects.[2,3] As a result, many approaches have been investigated for enhancing the solubility and dissolution properties such as the use of salts and amorphous solid dispersions. These formulation approaches are collectively called enabling technologies. Enabling formulations have a tendency to crystallize back to the parent form crystals after forming supersaturated solutions during dissolution. Therefore, thorough characterization of the supersaturation maintenance and understanding of the likely consequences of crystallization during dissolution are recognized as an essential part of rational drug development.

Methods of Assessing Dissolution

of Pharmaceutical Solids

Models that are widely used to describe dissolution process are the Noyes-Whitney equation[4] and the Nernst-Brunner diffusion layer model,[5] as shown schematically in Figure 2.

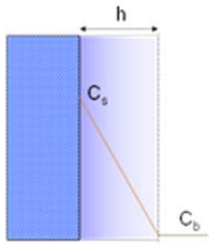

Figure 2. Schematic illustration of diffusion layer dissolution model from a planar surface.

Noyes-Whitney equation: $\frac{dQ}{dt} = k(C_S - C_b)$

Nernst-Brunner equation: $\frac{dQ}{dt} = \frac{DA}{h}(C_S - C_b)$

Where dQ/dt = dissolution rate; k = dissolution rate constant; C_S = solubility; C_b = bulk solution concentration; D = diffusion coefficient of the solute; A = surface area; and h = diffusion layer thickness. They were derived by applying Fick's first law for mass flux under the assumption of (1) presence of a stagnant layer between solid and the bulk solution, (2) constant diffusion layer thickness under fixed hydrodynamics, (3) constant concentration gradient (steady-state), and (4) diffusion-controlled transport.

For particulate dissolution, three diffusion-controlled models have been reported[6] for spherical particles. It is assumed that dissolution rate is proportional to surface area of the sphere, as illustrated in Figure 3.

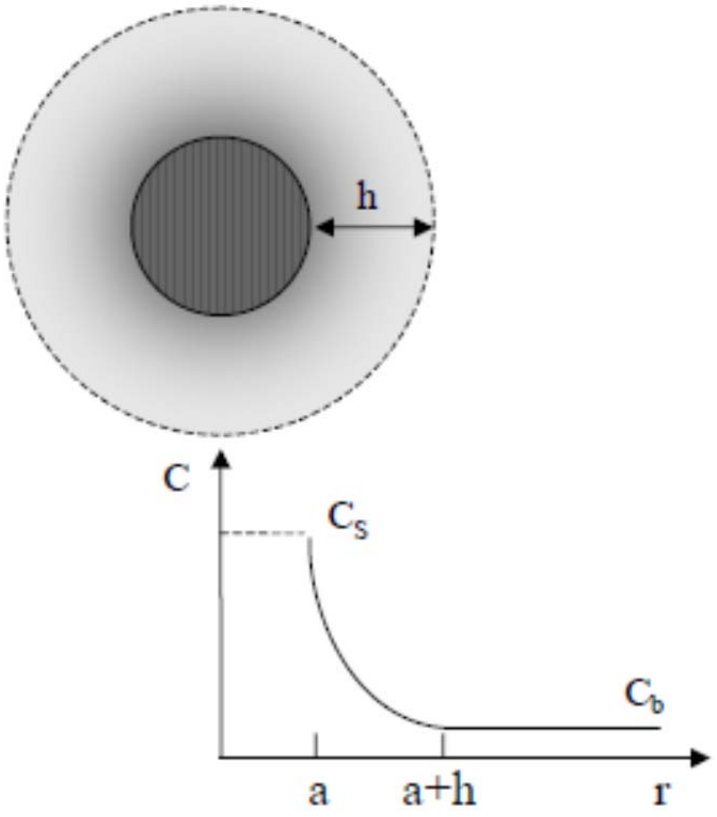

Figure 3. Concentration gradient from the diffusion layer to the bulk in dissolution of a spherical particle,[6] where h is the diffusion layer thickness, C_s is the equilibrium solubility and C_b is the drug concentration in the bulk at any given time, and r is the radius of the spherical particle.

One of the spherical dissolution models is the cube-root law by Hixson and Crowell.[6]

Hixson and Crowell equation: $W^{1/3} = W_0^{1/3} - kt$

In the equation, W is the particle weight, W_0 is the initial particle weight, t is time and k is the dissolute rate constant. During the dissolution of spherical particles, the cubic root of the total weight at a given time, t, is decreasing from the cubic root of the original weight at a rate of kt. The rate constant, k, is expressed as $k = \left(\frac{4\pi\rho N}{3}\right)^{1/3} \frac{DC_s}{\rho h}$, where ρ is particle density, N is number of particles, D is diffusion coefficient, C_s is equilibrium solubility and h is diffusion layer thickness. The particles by the definition of the model should be monosized. Particles with different particle size distributions and different shapes are too complex to model.

Dissolution rate generally is expressed as the mass of solute appearing in the dissolution medium per unit time (e.g., mass×sec^{-1}), but dissolution flux is expressed as the rate per unit area (e.g., mass×cm^{-2} sec^{-1}). Depending on the study objectives, different dissolution test methods are utilized for assessing the drug substance and factors affecting dissolution.

Intrinsic Dissolution

The intrinsic dissolution rate (IDR) refers to the rate of mass transfer per area of dissolving surface under sink conditions ($C_b \leq 0.1 \times C_s$). Essentially, it is the initial dissolution rate long before the saturation solubility is reached. Since $C_b << C_s$, the

Nernst-Brunner equation can be simplified to $\frac{dQ}{dt} = \frac{DA}{h}(C_S - C_b) \approx \frac{DA}{h}C_S$. This simplified equation means that the dissolution rate measured under sink conditions is directly correlated to how fast the compound is released from the crystal lattice into solution which is solely determined by intrinsic solid state properties of the drug. According to the United States Pharmacopeia (USP), IDR is the dissolution rate of pure substances under the condition of constant surface area. This allows different solid forms to be compared in dissolution rate by holding the testing conditions constant (surface area, dissolution medium, stirring rate, temperature, pH, ionic strength, etc.). Thus IDR is considered a tool in the functionality and characterization of bulk drug substances.

Two types of apparatus are described in Pharmacopeias for the intrinsic dissolution test: a stationary disk system, listed only in the USP, and a rotating disk system, known as "Wood's apparatus," listed in the USP, the European pharmacopeias (EP) and the British pharmacopeias (BP).[7] These apparatus measure the release from a compact consisting of pure API with a flat and well-defined surface area into a test medium (Figure 4). A difference between the two procedures is the source of fluid flow over the dissolving surface. In the rotating disk procedure, fluid flow is generated by the rotation of the die, but for the stationary disk procedure, the fluid flow is generated by a paddle or other stirring device.

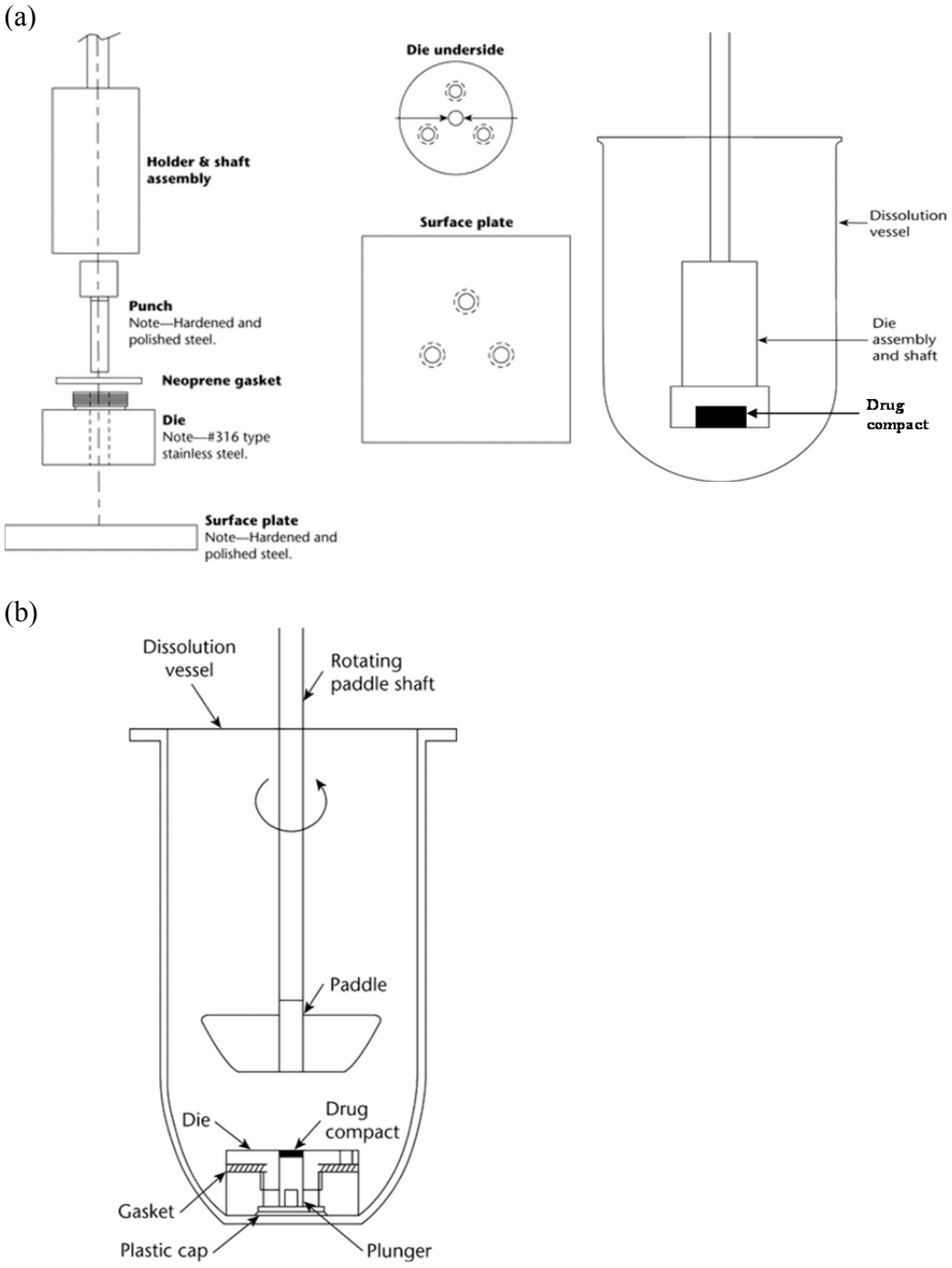

Figure 4. IDR test system. Schematic diagram of (A) the rotating disk apparatus (Wood Apparatus) and (B) the stationary disk apparatus (Source: USP37).

Powder Dissolution

Solid drug substances are, in most cases, harvested through crystallization or precipitation in the manufacturing process. The resultant final APIs are composed of fine particles with a wide range of shapes, sizes and surface properties. For spherical particles, diffusion-controlled dissolution rate can be calculated once IDR of the drug is determined.[8,9] However, the real world drug particles are almost never spherical. It is nearly impossible to accurately and reliably estimate the size, size distribution and surface areas of particles having various irregular shapes. Hence, the dissolution rate of powders needs to be measured experimentally.

To determine the dissolution rate of powders in an aqueous medium, USP Apparatus 1 and Apparatus 2 shown in Figure 5 are usually used. They are also known as basket and paddle dissolution methods, respectively, and are typically used for dissolution testing of tablet and capsule dosage forms as well. The test procedures involve introduction of small and known quantity of sample powders into an appropriate dissolution medium, followed by analysis of solution concentration at predetermined time intervals. The concentration–time curves (dissolution profiles) obtained from the powder dissolution tests can be used for assessing how API variables may affect dissolution rate, assuring consistent quality of the API, comparing drug substance of different solid state properties, helping guide product and process development, and ultimately ensure consistent drug absorption following administration of solid dosage forms.

(a)

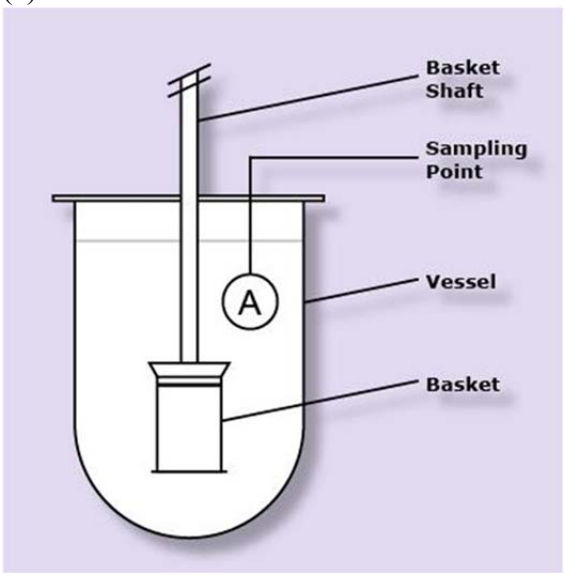

(b)

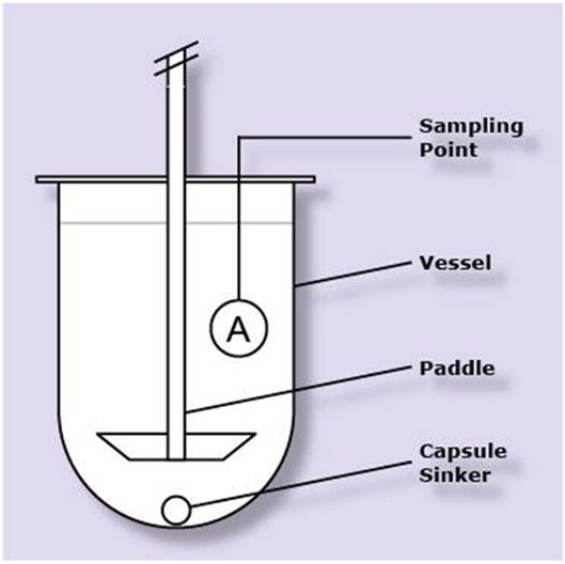

Figure 5. Powder dissolution system. Schematic diagram of (A) USP Apparatus 1 where the dosage form is placed inside the basket and the basket rotates during dissolution to provide mixing, and (B) USP Apparatus 2 where the dosage form is place on the bottom of the flask in a sinker and the paddle rotates to provide mixing (Source: Metrolab).

Despite the well-established dissolution methods to control the product quality and understand formulation performance, dissolution at the molecular level in large part has not been adequately studied.

Polymorphism and Polymorphic Transition

Drug Property Change due to Polymorphism

The active pharmaceutical ingredient (API) is the drug portion in the pharmaceutical dosage forms. Most APIs are crystalline solids due to the ease of purification by crystallization processes and a better chemical stability in the solid state. However, a crystalline solid may not be physically stable because it can rearrange into different internal crystalline structures by varying molecular packing, conformation, hydrogen bonding pattern, chirality and tautomerization. This physical instability gives rise to *polymorphism*, the ability of a substance to exist as two or more crystalline phases that have different arrangements and/or conformations of the molecules in the crystalline lattice.[10]

Polymorphism induces a long list of solid state property changes.[10,11] The different molecular packing affords changes in molar volume and density, refractive index, electrical and thermal conductivity, and hygroscopicity. The thermodynamic properties are altered, resulting in differences in melting and sublimation temperatures, internal energy, enthalpy, entropy, heat capacity, free energy and chemical potential, thermodynamic activity, vapor pressure, and solubility. Spectroscopic properties are also different, such as electronic (UV), vibrational (IR), rotational (far-IR or microwave), nuclear interactions. The kinetic properties that are modified include dissolution rate and

rates of solid state reactions. In the surface property arena, the changes are in surface free energy, interfacial tensions, and crystal habit. Finally, mechanical properties are also different including hardness, tensile strength, compatibility, tableting, powder handling, flow, and blending.

These changes formed the basis for analytical methods to detect and analyze polymorphism. The commonly used characterization techniques include optical microscopy (based on reflective index change), thermal analysis such as differential scanning calorimetry (DSC), based on the thermodynamic property, heat capacity and melting point changes), single crystal or powder X-ray diffraction (PXRD, based on different packing distance), Infrared and Raman spectroscopy (based on vibrational property changes), solid-state nuclear magnetic resonance spectroscopy (SSNMR, based the chemical shift anisotropy and the internuclear dipolar coupling), and so forth.

A lot of these changes have a profound impact to pharmaceutical formulation development. For example, mechanical property changes lead to a difference in powder flow, blending and tableting. Different reaction rates cause the chemical stability differences among the polymorphic APIs. However, the most substantial impact is the change in solubility and dissolution rate. When a solid form converts to the thermodynamically more stable form, its solubility decreases, and so does its dissolution rate, resulting in significantly altered pharmacokinetic factors such as rates of absorption and drug bioavailability. This problem became significantly worse for poorly water-soluble drugs for which the solubility and dissolution rate are already undesirable. If the thermodynamically stable form is not discovered during the earlier stages of development

and a metastable form is used in the formulation, there is a risk that the metastable form will recrystallize into the stable form during product manufacturing and storage resulting in reduced product performance *in vivo*. For this reason, rigorous polymorph screening and characterization to discover the most stable form and to understand the complex polymorphism of each drug candidate have been implemented in the early stages of drug development in every pharmaceutical company.

Polymorphic Transformation

Polymorphic transformation from the metastable polymorph to the stable polymorph is dictated by thermodynamics. In a pair of polymorphs, Polymorph I and Polymorph II, the stability relationship between the two polymorphs is determined entirely by their free energy differences at different temperatures.[12] The free energy of a particular solid is expressed by the following equation:

$$\Delta G = \Delta H - T\Delta S$$

where G is the Gibbs free energy, H is the enthalpy, T is temperature, and S is the entropy. Thus, the free energy for the transition from Polymorph I to Polymorph II:

$$\Delta G_{\mathrm{I}\to\mathrm{II}} = G_{\mathrm{II}} - G_{\mathrm{I}} = (H_{\mathrm{II}} - TS_{\mathrm{II}}) - (H_{\mathrm{I}} - TS_{\mathrm{I}}) = \Delta H_{\mathrm{I}\to\mathrm{II}} - T\Delta S_{\mathrm{I}\to\mathrm{II}}$$

where $\Delta H_{\mathrm{I}\to\mathrm{II}} = H_{\mathrm{II}} - H_{\mathrm{I}}$ and $\Delta S_{\mathrm{I}\to\mathrm{II}} = S_{\mathrm{II}} - S_{\mathrm{I}}$. At any given temperature, three possibilities exist:

1. $\Delta G_{\mathrm{I}\to\mathrm{II}} < 0$: Polymorph II has lower free energy, is therefore more stable than Polymorph I. The transition from Polymorph I to Polymorph II occurs spontaneously.

2. $\Delta G_{\mathrm{I}\to\mathrm{II}} > 0$: Polymorph I has lower free energy, therefore, the transition from Polymorph II to Polymorph I is a spontaneous process.

3. $\Delta G_{\mathrm{I}\to\mathrm{II}} = 0$: Polymorph I and Polymorph II has the same free energy. Therefore, both polymorphs have equal stability. There will be no overall transition between the two polymorphs.

The temperature at which $\Delta G_{\mathrm{I}\to\mathrm{II}} = 0$ is defined as the transition temperature (T_t). If T_t is located below the melting points of both polymorphs, the two polymorphs are enantiotropically related, the representative phase diagram of which is shown in Figure 6*a*. Therefore below T_t, Polymorph I is more stable. Above T_t, Polymorph II is more stable.

If T_t is located above the melting points of both polymorphs, the two polymorphs are monotropically related, the representative phase diagram of which is shown in Figure 6*b*. In this system, Polymorph I is more stable throughout the temperature range.

In either monotropic or enantiotropic systems, polymorphic transition can occur. In the monotropic system (Figure 6*b*), Polymorph II has a higher free energy than Polymorph I until it melts. Therefore, below the melting point, Polymorph II will sooner or later convert to Polymorph I. The rate of conversion depends on the experimental conditions. The enantiotropic system (Figure 6*a*) is a little more complicated. The free energy relationship reverses when T_t is reached. Below T_t, Polymorph 2 will eventually converts to Polymorph 1. However, above T_t, Polymorph 2 will never convert to Polymorph 1. For polymorphic forms exhibiting an enantiotropic relationship,

determination of the T_t, is essential to control polymorphism. For example, if the T_t is 55 °C and the temperature used in API manufacturing ranges from 45 to 65°C, then the drug could crystallize out as Polymorph I in one batch and as Polymorph II in another. In order to consistently manufacture Polymorph I, the crystallization temperature needs to be maintained significantly below 55 °C.

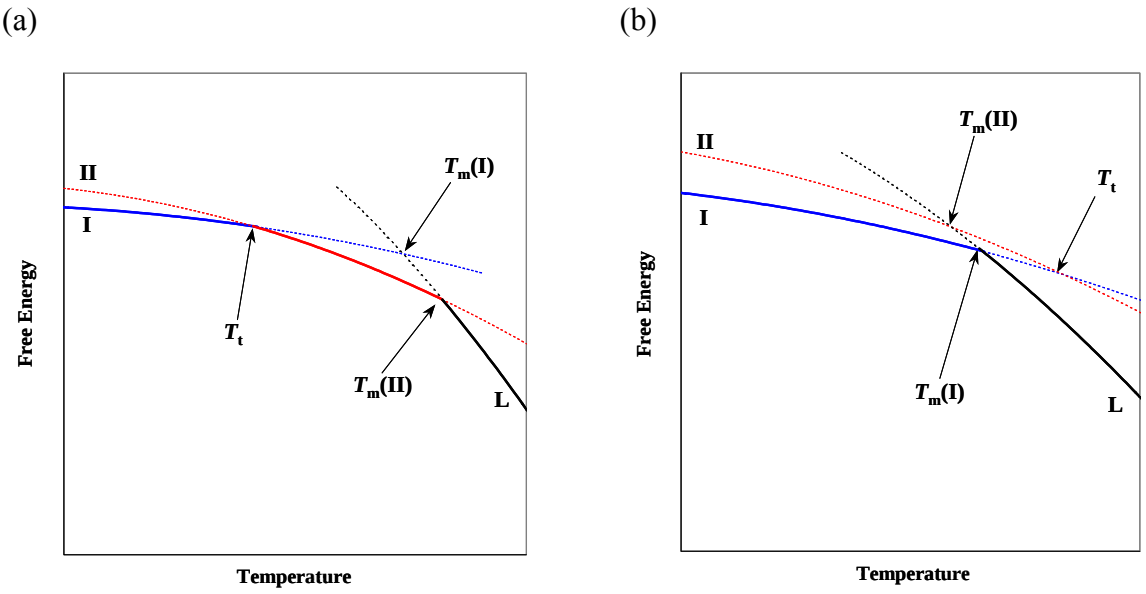

Figure 6. Thermodynamic phase diagrams of polymorphs. (a) Enantiotropy; (b) Monotropy. The stable phases are indicated using solid lines and dotted lines for the meta-stable phases. L is for liquid which is the melt of the solid. T_m is the melting point.[12]

Transformation from the metastable polymorph to the stable polymorph is mainly via four routes: vapor, melt (liquid state), solid state, and solution state. Pharmaceutical solids usually have a low vapor pressure and transition vial sublimation at ambient temperature is not very common. When the crystal is heated to the melting point, crystallization to another form can happen during the cooling of the melt. Conversion in

the solid state usually occurs in response to an energy input. For examples, mechanic milling induces crystal defects or an amorphous phase which are higher energy spots that can promote nucleation to the more stable form. Compaction force during tableting process can also cause polymorphic conversion. Heating the metastable form greatly increases the molecular mobility to trigger recrystallization which can be determined by DSC. The thermal events prior to the melting in a DSC thermogram are indicative of the nature of polymorphic transformation.[12-14] The conversion can also take place when the metastable form is in contact with solution[15] or moisture[16] due to the solubility difference between the two solid forms. The metastable form dissolves into the solution to reach the solubility, which would be supersaturated with respect to the stable configuration. When the supersaturation level is high enough, nucleation of the stable form commences. This solution induced transition is referred to as solution-mediated phase transformation (SMPT).[17,18] The presence of the solvent does not change the thermodynamics and stability relationship unless a solvate/hydrate forms with the solvent. However, owing to the much higher mobility in the solution state than in the solid, the transformation to the stable phases is much faster.

SMPT is the most relevant solid form conversion mechanism when considering the drug dissolution into the aqueous medium *in vivo*. It not only describes the phase transformation from a metastable form to the stable form, but also that from an amorphous solid to a crystalline solid[19] and from a salt to its parent[20] or from co-crystal to another co-crystal.[21] For poorly water-soluble compounds for which the absorption *in vivo* is highly dependent on drug concentration (dissolution rate or solubility-limited

absorption), conversion to a thermodynamically more stable form is detrimental to bioavailability and performance of the final drug product.

Crystallization Inhibition by Polymers

As stated previously, APIs are predominantly crystalline solids manufactured through crystallization from solutions. Crystallization in solution occurs under conditions of supersaturation with the first step being nucleation followed by crystal growth. As shown in Figure 7, crystallization includes two processes: nucleation, and crystal growth after nucleation. The mechanism of nucleation is divided into primary and secondary (induced by crystals only) nucleation with the primary route further categorized into homogenous and heterogeneous nucleation. Homogeneous nucleation is driven by concentration fluctuations in a multicomponent fluid systems at the limit of Gibbs free energy stability (spinodal decomposition), which is not a common event.[22] Heterogeneous nucleation is induced by foreign surfaces such as impurity particles or even glass walls which are ubiquitous. The large sale crystallization of APIs is often done by secondary nucleation where seed API crystals are added deliberately to induce faster crystallization and to control the polymorphism.

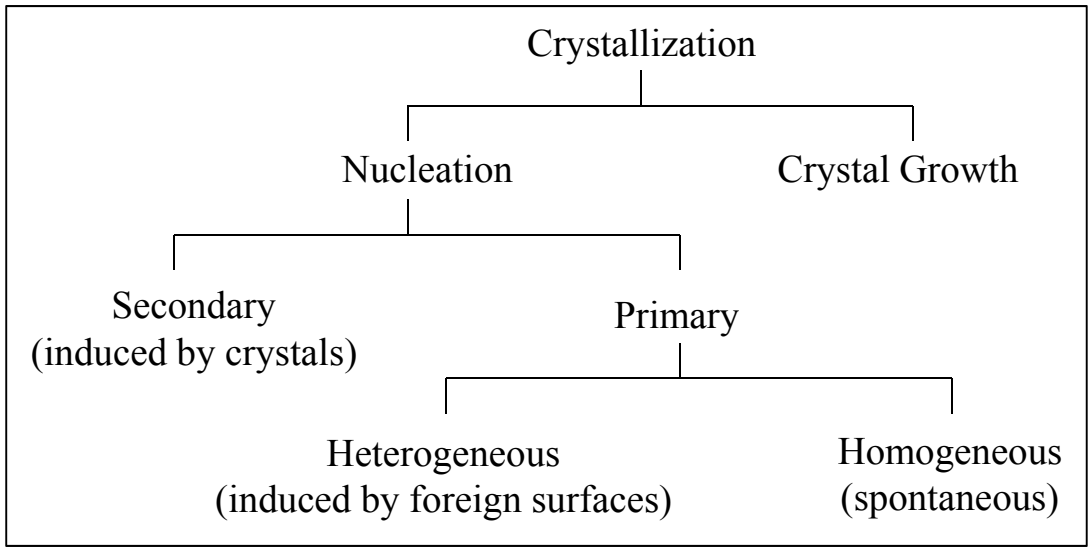

Figure 7. Crystallization from solution. Reproduced based on reference.[22]

However, the situation changes when the API enters the formulation development phase, where particle size control and crystallization inhibition become the central focus. Poorly soluble compounds often require an enabling technology to deliver, including salt formation, lipid based formulation delivery systems, amorphous solid dispersions and nanotechnology. Without exception, these formulations are metastable when administered orally or by injection. Salt in water could disproportionate into the parent drug plus the counter ion depending on the pH, and the drug molecule could crystallize into less soluble parent crystals. Lipid based formulations as well as amorphous solid dispersions upon dilution or dissolving could quickly reach high supersaturation concentration, a driving force for crystallization. Nanoparticles can also be unstable in aqueous solutions due to particle aggregation and size growth which threaten the formulation performance. Even for less insoluble compounds, particle size growth is a problem in formulating a pharmaceutical suspension common for ophthalmic or pediatric

use. APIs used in suspension formulations are milled by crushing and grinding operations, yielding particle surfaces with higher free surface energy. These particles have a tendency of growing or knitting together to form a hard cake, causing difficulties in re-suspending and producing a gritty texture unsuitable for topical, especially ophthalmic, applications.[23] Thus, inhibiting crystallization is an important task in pharmaceutical formulation development.

Nucleation Theory

Before going into crystallization inhibition, it is necessary to understand the basics of nucleation and crystal growth. Although crystals are ubiquitous, they have an accidental nature to them.[24] The molecules located in the internal lattice have a lower chemical potential (μ) and are more stable, while those on the surface are coordinated with fewer neighbors and thus they have a higher chemical potential (μ) and are less stable. Assuming a tiny crystal with a radius, *r*, which is comprised of N interior molecules (N_{int}) contributing to the stabilization of the tiny crystal, the stabilizing free energies equal to $-N_{int}\mu_{int}$. The volume of the interior crystal is $V = \frac{4}{3}\pi r^3$ by assuming spherical nuclei. Correspondingly, the N surface molecules with the surface area of $A = 4\pi r^2$ will contribute to the destabilizing free energy by $+N_{suf}\mu_{ext}$. The tiny crystal can only survive if the free energy of the interior molecules exceeds that of surface molecules. Let *G* stand for the total free energy for a growing approximately spherical tiny crystal, then we have:

$$G = -\frac{4}{3}\pi r^2 N_{int}\mu_{int}\, per\ unit\ volume + 4\pi r^2 N_{sur}\mu_{sur}\, per\ unit\ area$$

The minimal requirement for radius, *r*, is when *G* is minimized. The derivative of *G* gives the following,[24]

$$\frac{dG}{dr} = 0 = -4\pi r^2 N_{int}\mu_{int}\, per\ unit\ volume + 8\pi r N_{sur}\mu_{sur}\, per\ unit\ area$$

$$r = \frac{2 \times N_{sur}\mu_{sur}\, per\ unit\ area}{N_{int}\mu_{int}\, per\ unit\ volume}$$

Above equation indicates that the nucleus radius has to exceed two times the ratio of the surface free energy over the interior free energy in order to be stable.

At this critical radius, the rate of nucleation, *J*, e.g. the number of nuclei formed per unit time per unit volume, can be derived based on the Arrhenius reaction velocity equation and the basic Gibbs–Thomson equation, as shown below.[22]

$$J = Ae^{\frac{\Delta G}{k_b T}} = Ae^{\frac{16\pi\gamma^3 v^2}{3k_b^3 T^3 (lnS)^2}}$$

Where *A* is the pre-exponential factor (the total number of collisions), $e^{-\frac{\Delta G}{K_b T}}$ is the probability of any collisions that lead to the reaction, k_b is the Boltzmann constant, *T* is the absolute temperature, γ is interfacial tension, v is the molar volume and *S* is the supersaturation defined as the ratio of drug concentration over the crystalline solid solubility. It is evident that the nucleation rate is a complex process affected by many factors. At a given *T*, increasing *S* will increase the nucleation rate. A plot of *J* vs *S* at natural log scale will indicate an initial linear increase but *J* becomes extremely fast when some critical level of *S* is exceeded.[22] Higher temperature increases the nucleation rate as

well. *J* is also affected by *A,* the total number of collisions, which is expected to increase with higher temperature and drug concentration. Therefore, an increase in both *S* and *T* will increase the nucleation rate. Nucleation is the rate limiting step in crystallization. Following the birth of nuclei, crystal growth may proceed rapidly.

Crystal Growth

Crystal growth has been described by several theories.[25] The surface energy theories, which have been almost entirely abandoned, are based on the assumption that the total free energy of a crystal would be a minimum. The diffusion theories assume that solute molecules are deposited continuously on a crystal surface at a rate proportional to the concentration gradient between the bulk solution and the crystal surface. It is thus considered a reverse process of crystal dissolution. The mathematical treatment is therefore very similar to other mass transfer processes:

$$\frac{dm}{dt} = K_G A(C_b - C_i)^g$$

The crystal growth rate, $\frac{dm}{dt}$, is proportional to the overall crystal growth coefficient, K_G, the crystal surface area, A, and the driving force for diffusion, $(C_b - C_i)$ where C_b is the bulk concentration and C_i is the concentration at the crystal surface. The exponent g is the overall process order. When $g = 1$ (first order), K_G will be defined by $\frac{1}{K_G} = \frac{1}{k_d} + \frac{1}{k_r}$ where k_d is the diffusion coefficient of mass transfer and k_r is the rate constant for surface integration. This indicates that crystal growth is a two-step process, the first being the diffusion of the molecules to the crystal surface and the second being the integration of

the molecules into the crystal layer. If integration is fast, then the crystallization is rate-limited by diffusion. If the diffusion is fast, then integration becomes the rate limiting step.

Adsorption-layer theories, on the other hand, assume that crystal growth is not a continuous process; rather it is taking place by adsorption, growing layer by layer. There will be a loosely absorbed layer of molecuels on the crystal surface, which will link into the lattice in positions where the attractive forces are the greatest. Before the next layer commences, a monolayer island nucleus is created. This is called two-dimensional nucleation. The mathematical equation for the velocity of the two-dimensional nucleation is $J = Ae^{-\frac{\Delta G}{kT}} = Ae^{-\frac{\pi h \gamma^2 v}{k_b^2 T^2 lnS}}$ which was developed similarly as the classical nucleation theory described above with the letters having the same meanings. Similar to nucleation rate, the crystal growth rate is faster when increasing temperature and supersaturation levels.

Crystallization Inhibition by Polymers

It has been known as early as 1958 that polymers can be added to pharmaceutical suspensions to increase viscosity and thus, to retard the overall crystal nucleation and growth process.[23] More recent pharmaceutical research in crystallization inhibition by polymers has done mainly to meet the need to deliver poorly water-soluble compounds by enabling technologies, particularly amorphous solid dispersions. A large number of publications have been focused on how to screen polymers for making amorphous solid dispersions of selected model compounds. As a comparison, studies with an objective to

elucidate polymer–drug interaction mechanism are fewer. Simonelli *et al.*, in 1970 first described the underlying principles of using polymers to inhibit crystallization of drug molecules.[26] By studying sulfathiazole crystal growth at different concentrations and different molecular weights of polyvinylpyrrolidone (PVP), Simonelli *et al.* established a kinetic model to describe the dependence of crystal growth rate on the diffusion rate of the polymer relative to that of the drug. The model entails that the polymer in solution needs to reach the crystal surface from the bulk solution ahead of the drug molecules, and the polymer concentration needs to be high enough to sufficiently cover the crystal surface to cause inhibition of crystal growth. Their data also indicate that the polymer must be tightly bound to the surface in order to be effective at low concentrations. Therefore, the adsorption of the polymer to the crystal surface is of great interest. Many models have been developed ever since[27-31] for modeling polymer adsorption to a surface using the Langmuir adsorption equation addressing polymer chain flexibility, molecular weight, pH, rate of adsorption, etc. Recently, Alonzo *et al.*[32] studied HPMC (hydroxypropyl methylcellulose) for inhibiting nucleation and crystal growth of felodipine. In the presence of HPMC, the crystal growth of felodipine shifted toward an integration-controlled mechanism from a diffusion-controlled mechanism.

Based on these mechanistic studies, it was believed that the adsorption of a large linear polymer molecule is due to the binding of particular sites; the remainder of the chain projects into the aqueous phase as tails (the ends of the polymer) or loops (the middle of the chain), as envisioned in Figure **8**. The strong adsorption is due to the collective energies of many binding sites on the polymer.[28] Clearly, more studies are

beneficial to understand exactly how the long polymer chain interacts with a crystal surface and which energy forces are involved in the adsorption. This will also help to understand the selectivity of the polymer adsorption to drug molecules which may lead to better ways to design the most efficient formulations.

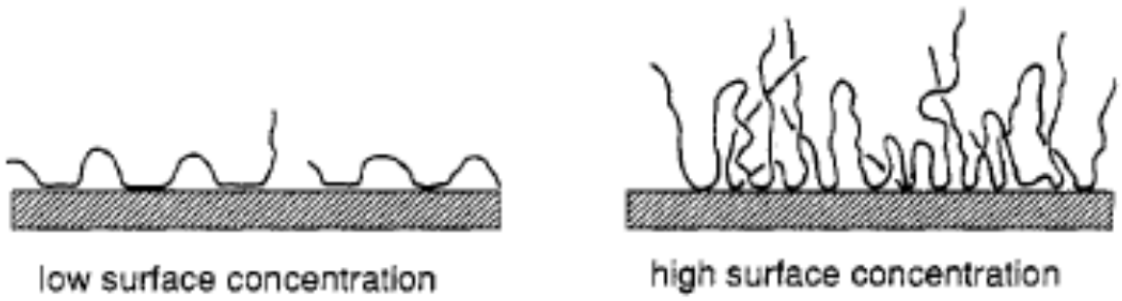

Figure 8. Schematic of the configurationally change of adsorbed polymers with increasing surface concentration.[27]

Molecular Dynamics Simulation

The first molecular dynamics (MD) simulation of a macromolecule of biological interest was published in 1977,[33] which changed the early view of proteins as relatively rigid structures to a dynamic model. Since then, computational biology, particularly MD simulations, have advanced rapidly in methodology and applications in parallel with advances in computing power and simulation programs.[34-36]

Molecular modeling takes its roots from quantum mechanics (QM) which is based on the solution of the Schrödinger wave equation.[37] The wave equation describes the motions of the electrons and nuclei in molecular systems. The 3D molecular structure, molecular energies and many associated properties can be calculated by this equation. However, the level of complexity to solve the Schrödinger equation is prohibitive in

calculating a large system. To simply the calculation, Born and Oppenheimer made an approximation by assuming the nuclei, which are much heavier than the electrons, are fixed on the time scale of electronic vibration.[37] There are primarily two QM methods derived from the Born-Oppenheimer approximation: *ab initio* QM and semi-empirical QM. The former is more rigorous than the latter; therefore it requires more computational time. DFT (density function theory) is a variation of *ab initio* QM which improved the calculation efficiency. Nevertheless, all of the QM methods are still very demanding in terms of computational expenses and time, therefore they are not practical in calculating larger systems, such as proteins. This led to the development of an alternative approach – the molecular mechanics (MM).

The MM model treats all of the atoms as spheres connected by springs representing bonds. Internal forces experienced in the model structure are described using simple mathematical functions[38] forming the potential energy function. MD simulation uses molecular mechanics (MM) models to numerically solve Newton's equations of motion, thus allowing atomic or molecular motions to be observed with respect to time,[38] and providing the ultimate details of motional phenomena.

Potential Energy Function

The success of a MD simulation is highly dependent upon a suitable potential energy function which is called a force field. The current study uses the CHARMM (Chemistry at HARvard Molecular Mechanics) force field[39] which has been separately parameterized for proteins, nucleic acids, lipids, and carbohydrates, making it highly versatile and widely used. The potential function, $V(\vec{R})$, is a sum over individual terms

representing the internal and nonbonded contributions as a function of the atomic coordinates, as described in the following equation.[38]

$$V(\vec{R}) = \sum_{\text{bonds}} K_d(d - d_0)^2 + \sum_{\text{Urey-Bradley}} K_{UB}(S - S_0)^2 + \sum_{\text{angle}} K_\theta(\theta - \theta_0)^2 + \sum_{\text{dihedrals}} K_\chi(1 + \cos(n\chi - \delta)) + \sum_{\text{impropers}} K_\varphi(\varphi - \varphi_0)^2 + \sum_{\text{nonbond}} \left\{ \epsilon_{ij} \left[\left(\frac{R_{ij}^{\min}}{r_{ij}} \right)^{12} - \left(\frac{R_{ij}^{\min}}{r_{ij}} \right)^{6} \right] + \frac{q_i q_j}{\epsilon_l r_{ij}} \right\}$$

Equation 1. Potential energy function of CHARMM27.[38]

As summarized in Table 1, each term in Figure 1 represents a simple functional form and describes an intermolecular or intramolecular force within the system. These terms are additive in nature, resulting in the potential-energy function to describe the energy landscape of the system from a single set of atomic coordinates. The force constants for bonds (K_d), angles (K_θ and K_{UB}), dihedrals (K_χ) and improper dihedrals (K_φ) are empirically determined. The reference (or equilibrium or ideal) values for bonds (d_0), angles (θ_0 and S_0) and dihedrals (φ_0) were determined by both experimental techniques and quantum mechanical calculations which are included in the force field in the MD simulation programs. Besides the CHARMM force field, there are others available, such

as AMBER (preferred by nucleic acid modelers), ECEPP (dihedral angle program for proteins), and GROMOS, OPLS, CFF, and SIGMA.[37]

Table 1. Individual Terms in CHARMM27 Potential Function.

Term	***Function***
$\sum_{\text{bonds}} K_d(d - d_0)^2$	Bond stretching. K_d: bond length force constant. d: bond length. d_0: reference value of bond length.
$\sum_{\text{Urey-Bradley}} K_{UB}(S - S_0)^2$	Angle bending using 1,3-nonbonded interactions. K_{UB}: Urey-Bradley force constant. S: Urey-Bradley. S_0: reference value of Urey-Bradley.
$\sum_{\text{angle}} K_\theta(\theta - \theta_0)^2$	Angle bending. K_θ: bond angle force constant. θ: bond angle. θ_0: reference value of bond angle.
$\sum_{\text{dihedrals}} K_\chi(1 + \cos(n\chi - \delta))$	Dihedral (torsion angle) motion. K_χ: dihedral angle force constant. χ: dihedral angle. n: periodicity of the dihedral angle δ: phase shift
$\sum_{\text{impropers}} K_\varphi(\varphi - \varphi_0)^2$	Improper dihedral motion (out of plane bending). K_φ: improper angle force constant. φ: improper dihedral angle. φ_0: reference value of improper dihedral angle.
$\sum_{\text{nonbond}} \left\{ \epsilon_{ij} \left[\left(\frac{R_{ij}^{\min}}{r_{ij}} \right)^{12} - \left(\frac{R_{ij}^{\min}}{r_{ij}} \right)^{6} \right] + \frac{q_i q_j}{\epsilon_l r_{ij}} \right\}$	Nonbonded interactions. Coulombic equation for the electrostatic energy and Lennard-Jones potential for van der Waals (VDW) energy. ϵ_{ij}: Lennard-Jones well depth. R_{ij}^{min}: distance at which the Lennard-Jones potential is zero. r_{ij}: distance between atoms i and j. q_i: partial atomic charge of atom i. q_j: partial atomic charge of atom j.

Newtonian Molecular Dynamics

Under the influence of the force, particles in a system move according to Newton's equation of motion,

$$F = ma = m\frac{dv}{dt} = m\frac{d^2x}{dt^2} = -\nabla V$$

where *F* is the force exerted on the particle, *m* is mass of the particle, *a* is its acceleration, *v* is the velocity, *t* is the time, *x* is the distance the particle moves and ∇V is the gradient of the potential function. The force, *F,* is the negative gradient (first partial derivative) of the potential energy. The velocity of the particle can be obtained by integrating $a = \frac{dv}{dt}$ to give the following equation.

$$v = at + v_0$$

Similarly, integration of the velocity ($v = \frac{dx}{dt}$) give the following equation.

$$x = vt + x_0$$

Combining of above two equations leads to the following expression,

$$x = at^2 + v_0t + x_0$$

which correlates the position of the particle to the acceleration *a*, the initial velocity v_0, and the initial position x_0 at time *t*. This means that if the initial position and the initial velocity of the particle are defined, the position at a given time can be calculated because the acceleration can be obtained from the derivative of the potential energy function with respect to the particle position ($a = -\frac{1}{m}\frac{dV}{dx}$).

The initial positions are determined by the starting coordinates (e.g. crystal structure). The initial velocities are typically set pseudorandomly from a Maxwell-

Boltzmann or Gaussian distribution at a given temperature, which is accomplished by many software packages.[40]

In simulation of a large system, the potential energy is a function of the atomic positions of all the atoms in the system. Due to the complicated nature of this function, a numerical integrator is needed. Among the numerous numerical algorithms available, the Leapfrog/Verlet Algorithm is the most commonly used. The Verlet algorithm is based on a Taylor series expansion. It uses the positions at time *t* and the velocities at time $t - \left(\frac{\Delta t}{2}\right)$ for updating both positions and velocities via the acceleration *a*. The equation to update velocity is $v\left(t + \frac{\Delta t}{2}\right) = v\left(t - \frac{\Delta t}{2}\right) + a(t)\Delta t$. The equation to update the coordinates is $r(t + \Delta t) = r(t) + v(t + \frac{\Delta t}{2})\Delta t$.[38]

In practice, a successful MD simulation requires implementing many details, such as obtaining appropriate parameters, coordinates and topology files, setting initial conditions, selecting a program, acquiring high speed computers, and visualizing and analyzing the large size data set, and so forth.

Applications of MD Simulations to Pharmaceutical Research

MD Simulation to Study Drug Dissolution

MD simulation of drug crystal dissolution into anaqueous medium has not been reported prior to 2013.[41] However, there have been several dissolution simulations of non-drug crystals in the literature. The earlier work was on inorganic salt crystals (i.e. NaCl) by Ohtaki and his co-authors in the late 1980's.[42-44] The motivation to study NaCl was that sea salt (i.e. NaCl) crystal dissolution is one of most crucial dissolution process

in atmospheric chemistry. Due to the limitation of computational resources, these earlier studies simulated very small crystals in a small water box. The first study[43] reported in 1988 was a 7 ps long MD simulation of a 32 NaCl molecule crystal in 216 water molecules to calculate ion–ion, ion–water and water–water interactions. Based on their results, chloride ions from the five corners dissolved but the sodium ions did not. A year later, a follow-on study[42] simulated the dissolution of the NaCl (111) face which was covered with chloride ions only and the (–1–1–1) faces which was with the sodium ions only. Similarly, 28 NaCl molecules were put into the water box containing 189 waters which was simulated for 7 ps. This second simulation repeated the previous results in that only the chloride ions dissolved and sodium ions remained on the crystals. It was hypothesized that the repulsive forces arising between the chloride ions and the water molecules push the chloride ion out from the crystal surface as they possess a smaller hydration energy than the sodium ions. These authors reported another study[44] in 1993 that expanded the salt list to include many alkali halide crystals (LiCl, NaCl, CsF, KCl, NaF, and KF). Within 12 to 20 ps, the anions in the LiCl, NaCl and CsF crystals have dissolved but none of the cations have. Interestingly, for crystals of KCl, NaF and KF having similar size of cations and anions, no ions have dissolved within 20 ps. Using anion solution X-ray diffraction, NaCl and KCl were found to form 1:1 ion pairs in solution. On the other hand, KF and CsF solutions formed ion clusters larger than 1:1 ion pairs. It appears no conclusion could be made based on these results. In 2011 (eight years later), Liu *eta al.* did a simulation on NaCl dissolution in water[45] using the state-of-the-art *ab initio* molecular dynamics and free energy sampling techniques. Their results shed

some light on the anions preferential initial dissolution. The crystal was comprised of 3 layers of NaCl covered with a 15 Å thick water layer. The simulation was performed for a total of 1 μs with classical force fields [molecular mechanics (MM)] and a separate 0.6 ns of *ab initio* QM (quantum mechanics simulation). In the force-field MM description, the Born–Mayer–Huggins potential was used for NaCl and the TIP3P model was for water. For the QM description, density-functional theory (DFT) with the PBE27 exchange–correlation function was used. They showed that NaCl dissolution is a complex multi-step process triggered by the initial departure of Cl ions from the lattice followed by the departure of Na ions. A well-defined intermediate state was identified in which the departing Cl ion is partially solvated and still retains contact with the crystal. Based on the calculated QM free energy barriers, the initial rate of Cl ions dissolution will be about 1000 times larger than that of Na ions. The departure of Cl ions disrupts the surface and leaves a Na ion in an almost fully solvent-exposed location, primed for subsequent dissolution. The better results from the 2011 study seem related to the use of more advanced simulation methods including a different force field, *ab initio* MD, and a longer run time. Nevertheless, the very early studies by Ohtaki and his co-authors did indicate that Cl ions should departure first in NaCl crystal dissolution. This reminds us of the remark Martin Karplus made in his review article in 2002, "The conceptual changes resulting from the early studies make one marvel at how much of great interest could be learned with so little—such poor potentials, such small systems, so little computer time."[46]

The simulation of salt crystal continued in 2012 with KCl dissolution. The study employed density-functional theory (DFT) calculations and molecular dynamics studies using the GROMACS force field.[47] In the MD simulation, three crystal surfaces each with 105–120 KCl molecules were simulated in about 3000 waters for 2.5 ns. The observations were similar to the NaCl study in 2011. The DFT calculation indicated the departure of Cl ions was before the Na ions and has been found to be more significant from the edge of the KCl crystal. At least four water molecules were found to be necessary to initiate the separation of the ions from KCl crystal. The observation from MD simulation indicated different ion departure profiles with the three different KCl faces.

Simulations were also done on poorly water-soluble salts. In 1999, Parker and coworkers[48] modeled different stepped surfaces of a calcium carbonate crystal with a small amount of water using a molecular dynamic simulation. This process represents the aqueous corrosion which is of importance in geological science. By simulating a monolayer of water on the calcium carbonate surface, they found that water has a stabilizing effect causing slower dissolution than that *in vacuo*. The same authors conducted another MD simulation study[49] in 2006 on the interaction of two solid surfaces, namely the (001) hematite (α-Fe_2O_3) and (104) calcite ($CaCO_3$) surfaces in contact with aqueous electrolyte solutions containing different concentrations of NaCl. A few layers of water were added and the simulation lasted for 1 ns. They observed a characteristic double layer of water at neutral surfaces and that the charge distribution

oscillates into the bulk. The presence of dissolved ions was found to make a small but significant reduction to the dissolution free energies.

MD simulation on organic molecule dissolution has been rare before 2013 and only two papers were found. In the study reported in 2005, a flat crystal surface of urea (001) was built and simulated using the GROMACS force field in the presence of water to monitor the dissolution and subsequent recrystallization.[50] They observed that at 298 K the dissolution proceeded until two layers of urea were completely dissolved. At this point, the surface layer concentration was calculated as 2–7 M which is still below the saturation solubility of 11 M, but it is probably high enough to slow down the dissolution rate to the point that it is no longer measurable by MD simulation. They then decreased the temperature to 260 K and simulated a further 38 ns. After a short induction period, formation of a nucleus on the crystal face was observed which continued to grow until a new layer was formed on the crystal surface. The supersaturation on the surface for nucleation was assumed due to the solubility difference between 298 and 260 K. The paper did not discuss what the solubility of urea is at 260 K which may not be measurable in frozen water (ice).

The second organic molecule dissolution was published in 2011 by Hayakawa and co-authors.[51] The dissolution process of cellulose triacetate (CTA) II crystal was studied in dimethyl sulfonamide (DMSO). The nanocrystal consisting of 18 CTA chains in an 8 × 8 × 8 nm box with DMSO molecules was simulated for 9 ns using the CHARMM program and carbohydrate force field. As illustrated in Figure 7, one CTA chain detached from the crystal surface and entered the DMSO solution at 9 ns. The three types of H-

bonds with varying degrees of bond strength responsible for forming the crystal all disappeared during the dissolution. The two stronger H-bonds provide the major resistance to solvation with DMSO based on the energetic calculation.

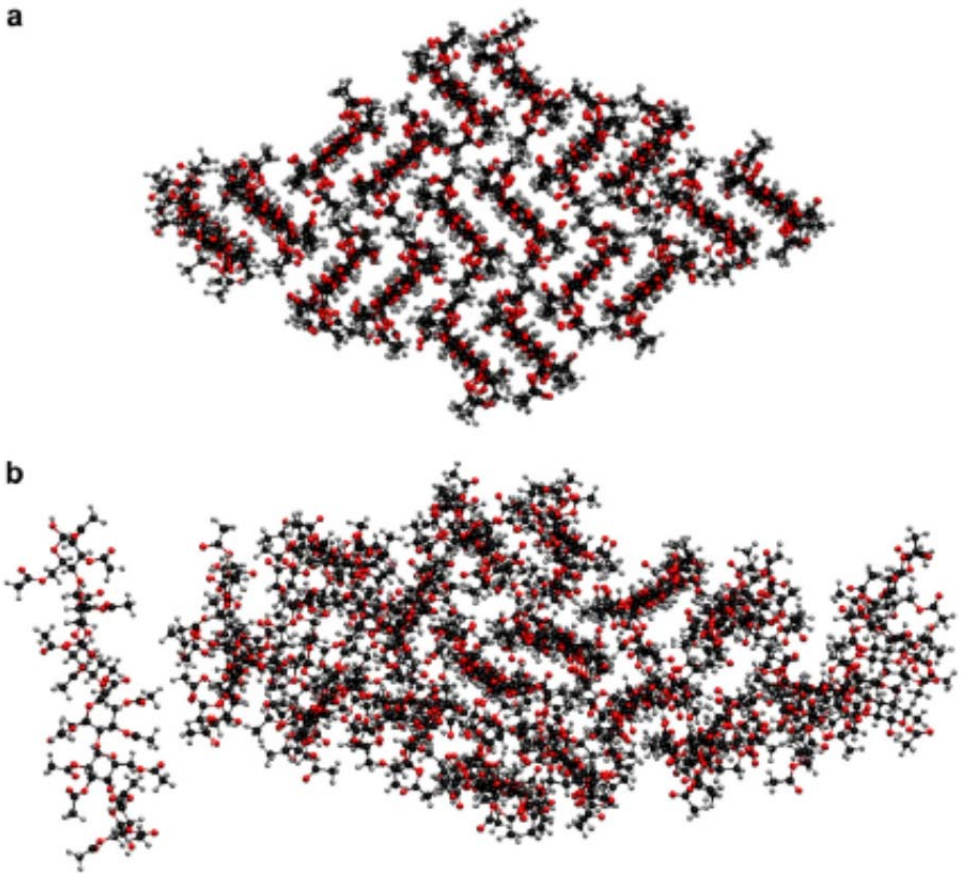

Figure 9. MD Simulation of dissolution of cellulose triacetate II nanocrystal into DMSO at time 0 (a) and 9 ns (b) (from Figure 2 of reference 51).[51]

Several papers emerged in 2014. Toroz *et al.*[52] reported MD simulations of two polymorphs of para-aminobenzoic acid (which is not a drug *per se* but structurally similar to some drugs) at temperatures of 0, 50 and 100 °C for 5 ns. The crystals were solvated using TIP3P model but the water box size was not described. The two polymorphs, α form and β form are enantiotropically related, with the transition temperature (T_t) at 13.8–16 °C. Below the T_t the β form is more stable, and above the T_t the α form is more stable. Thus, simulation at 0 °C should identify β form as the stable form, while at 50 °C or 100 °C should identify the α form. Their results showed that at 0 °C both forms remained as ordered crystal, but at 50 °C the two forms became partially disordered and 100 °C both lost long range order. The stability of the nanocrystals appeared to be an issue, and will need more investigations in the future.

In summary, the practice of using MD simulation to study crystal dissolution has been demonstrated in the literature; and the methodology has gradually improved over the last two decades. There have been very few reported studies limited to small salt crystals and two organic molecules (urea and cellulose). There have been no reported studies on drug crystal dissolution. Hence, it is necessary to establish MS simulation of drug crystal dissolution as a special focus in pharmaceutical research considering that (1) the small salt crystals or large molecular weight cellulose crystals are structurally different from the majority of organic drug crystals, and (2) the purpose of drug dissolution is to understand the effect of surface area, polymorphism, polymorphic transition, supersaturation level, dissolution media, etc. which are very different from the dissolution studies done in the above surveyed disciplines.

MD Simulation to Study Polymer Interaction with Drug Crystals

There are quite a few papers in recent years reporting the simulations of the interaction of polymers with drug or drug like molecules in solution. The purpose of these studies was to understand or identify polymer systems for polymer based drug delivery (i.e. polymeric nanoparticles), therefore, single or multiple drug molecules rather than a drug crystal was simulated with the polymers.[53-57] For example, in 2011, Subashini *et al*.[57] conducted MD simulations to model drug uptake by polymers. The structures of three drugs and six polymers at decamer or hexamer length were built with HYPERCHEM® software. MD Simulations were performed in 11,300 water molecules using the GROMACS forcefield for 300 ps at 300 K, and the interaction energy between various drugs and polymers was calculated. They found the interaction energies were correlated with the experimentally observed drug uptake values. In another example, Kasimova *et al.*[55] in 2012 studied how four different lipophilic drugs (cyclosporine A, griseofulvin, ketoconazole, and quercetin dihydrate) were loaded into a polymeric micelle consisting of six chains of amphiphilic copolymer PEG−hexPLA (built at molecular weight of 5000 g/mol). The four drugs and monomers were parameterized using the general AMBER force field (GAFF), and simulated in TIP3P explicit water for 10 ns after equilibration in vacuum. The interactions between the PEG−hexPLA and the drugs were evaluated by Flory−Huggins interaction parameters which are routinely used to measure the miscibility of two polymers or polymer with other materials. The

Flory−Huggins parameters calculated from the MD simulations were consistent with the experimentally measured Flory−Huggins parameters.

MD simulations with the objective to study drug crystallization inhibition by polymers have also been reported. They can be divided into two main areas: (1) polymer–drug interactions in amorphous solid dispersion systems which primarily investigated the solubility or miscibility of the drug and polymer(s) in the solid state,[58-63] and (2) polymer–drug interactions in crystal systems to investigate crystal growth inhibition in the solution state.[64-66] In the former, the rationale is that if the drug is fully dissolved in the polymer or miscible with the polymer, then the crystallization of the amorphous drug in the polymer matrix will not take place. Described here are the two representative papers. Gupta *et al*.[60] performed MS simulations using the COMPASS force field to predict the miscibility of indomethacin with polyethylene oxide, sucrose and glucose through the calculated cohesive energy and the solubility parameter. An amorphous cell with 60 indomethacin molecules with either 72 sucrose molecules, or 144 glucose molecules or 14 chains of polyethylene oxide (PEO) each containing 30 monomer units were made into a 3 × 3 × 3 (nm) box. The system was equilibrated for 2 ns followed by a 500 ps production simulation. The MD simulations predicted indomethacin to be miscible with polyethylene oxide and to be borderline miscible with sucrose and immiscible with glucose. The MD simulation of indomethacin with PVP by Xiang and Anderson[63] was done differently. Five assemblies with varied indomethacin and PVP compositions with parameters assigned from the Amber force field were first equilibrated in their molten states and cooled to generate amorphous glasses. Prolonged aging dynamic runs (100 ns)

at 298 K were then carried out, from which the solubility parameters, the Flory–Huggins interaction parameters, and associated hydrogen bonding properties were obtained. It was found that inter-drug molecule H-bonding was decreased and replaced by drug–polymer intermolecular H-bonding. The calculated Flory–Huggins interaction parameter was able to predict the miscibility accurately when compared to experimental results.

In the second area involving polymers to inhibit drug crystal growth in aqueous media, there are only three published studies. Zhu *et al.* simulated the interaction of several additives such as hydroxypropyl methylcellulose (HPMC) in water with crystal surface of fenofibrate[66] and griseofulvin.[65] A short HPMC chain (five repeating units) was constructed and placed into a small water box (1500 water molecules) with the simulation carried over a short duration (600–800 ps). The simulated binding energies between the additives and crystal surface were correlated with the experimental results when these additives were found to reduce the particle size of recrystallized griseofulvin. In 2012, Yani, Chow and Tan reported[64] a 400 ps MD simulation of large polymers (225 monomers for PVP and 62 for HPMC) with different crystal phases of salbutamol sulfate in a vacuum. Hydrogen bonding between PVP and salbutamol sulfate, which was ~40% of the total binding energy, was thought to dominate in prohibiting crystal growth.

Outside of the pharmaceutical area, simulations of polymers with crystals were reported in recent years. The collection of literature includes the simulation in dry state of the (poly(octadecyl acrylate)) incorporating into the surfaces of a paraffin crystal (which is a kind of liquid crystal) to inhibit crystal growth,[67] the simulations of 6 polymers (which have not been used as pharmaceutical excipients) with mineral crystal

hydroxyapatite which identified the importance of the carboxyls at the ends of the polymer chains,[68] and a similar study of other sets of polymers with hydroxyapatite crystal[69] and with calcite.[70]

In summary, in the second area (polymers inhibiting pharmaceutical crystal growth in solutions), very limited MD simulations have been done under only limited conditions (short runs, in vacuum or in small water box with short run times). Thus, this area was identified as a gap to motivate future research.

CHAPTER TWO

STATEMENT OF RESEARCH

The literature review identified several areas in pharmaceutical field which we believe can benefit from the application of molecular dynamics simulation. The areas of focus for this dissertation include drug crystal dissolution, polymorphic transition and drug–polymer interactions. The hypothesis is that MD simulation can potentially help understand these pharmaceutical mass transfer processes in aqueous media at the molecular level. This greater understanding could lead to better control over drug dissolution and polymorphic transformation.

Drug Crystal Dissolution

Understanding drug dissolution has been a subject of extensive pharmaceutical research due to its impact on drug absorption and therapeutic effect in humans. Despite the many mathematical models and well-established experimental methodologies, understanding of how a drug molecule detaches itself from solid phase (mostly crystalline) and enters into solution is quite poor for the most part. The purpose of our research is to:

1. To develop and establish methodology in building crystal structure files using acetaminophen as the model drug. Acetaminophen was chosen because of its relatively simple chemical structure for obtaining the parameters, and the interesting polymorphism which is the second focus of this dissertation.

2. To conduct dissolution simulation in water containing 0.15M NaCl at 37 °C, a condition relevant to *in vivo*.
3. To analyze how each molecule dissolves into water in order to gain a molecular level dissolution profile and the energetics involved in the dissolution.

Polymorphic Transition

Acetaminophen Form II is well known to undergo a fast conversion to the stable Form I in solution. Since the conversion occurs in the presence of solution, it was assumed that the solution-mediated polymorphic transformation is the responsible mechanism for such a conversion. However, the details of the transformation have not been understood, and the reasons for such fast conversion are mostly unknown. The motivation is to elucidate the mechanism of the conversion by conducting the following studies.

1. Determine the thermodynamic driving force for the Form II to Form I transformation through experimental methods and MD simulation.
2. Identify the reason for generating the supersaturation necessary for nucleation using MD simulation and/or experimental methods.
3. Explain the fast kinetics of Form II to Form I conversion

Drug–Polymer Interaction

The ability of polymers to inhibit crystallization of drug molecules has been the subject of intense research in recent years. Polymers are used to stabilize a metastable solid form in formulations, i.e. amorphous solid dispersions and nancrystals to deliver poorly water-soluble small molecular drugs. Polymers also are used to maintain supersaturation during

dissolution of enabling formulations for maximizing formulation performance. Finally, polymers can play an important role in modifying the crystal habit during solution crystallization. In this dissertation, we selected to study a polymer drug system reported to have crystal surface specific interactions with the polymer. The objectives are:

1. To build and obtain the hydrated PEG-b-PLA structure.
2. To develop procedures to build structural files of tolazamide crystals with a large crystal surface area.
3. To conduct MD simulations on the interaction of the hydrated polymer with several crystal surfaces in water and to compare these with experimental results.
4. To understand the mechanism of interaction by calculating and analyzing the interaction energies.

CHAPTER THREE

MOLECULAR DYNAMICS OF DRUG CRYSTAL DISSOLUTION: SIMULATION OF ACETAMINOPHEN FORM I IN WATER

Abstract

In order to gain a molecular level understanding of drug dissolution into aqueous media, we report the first molecular dynamics (MD) simulation of a drug crystal dissolving. The simulation was performed for acetaminophen crystal Form I dissolving in 0.15 M aqueous NaCl solution at 37 °C. The 10 ns simulation revealed interesting details of the dissolution process. Dissolution of the molecules from the crystal surface is far from a random process. On the contrary, the order of which molecules enter the solution depends on their initial positions in/on the crystal. Molecules located on the corners and edges dissolved first followed by those located on (100), (010) and (001) surfaces with slight variation. This corner and edge effect that has been observed by our real dissolution experiment conducted under polarized light microscope was successfully predicted at the molecular-scale by the MD simulation. Further analyses revealed the underlying mechanism: the differences in the molecular interaction energetics between the drug and water molecules. The molecules located on corners and edges of the parallelepiped crystal are not as tightly bound to their surrounding neighbors as those located in other positions, but they are more strongly interacting with the surrounding water molecules. The extent of molecular release is strongly correlated with the interplay between

interaction forces with solvent molecules and with other drug molecules in the crystal lattice. These findings, especially the significant "corner and edge effect", will help us gain additional fundamental understanding in the relationship between dissolution rate and particle size and morphology, and thus are very relevant in the context of particle size reduction in delivering poorly water-soluble compounds. This study has also demonstrated that MD simulation is a powerful tool in studying dissolution phenomena.

Key words: molecular dynamic simulation; crystal form; dissolution; corner and edge effect; electrostatic and van der Waals; acetaminophen

Introduction

The first important step in drug absorption from oral solid dosage forms is dissolution, a process by which the drug molecules detach from the solid particles and enter into the surrounding gastrointestinal (GI) milieu. Thus dissolution rate is of fundamental importance in pharmaceutical dosage form design. Over the years, understanding drug dissolution has been a subject of extensive pharmaceutical research.[6,71-75] Despite the many mathematical models and well-established experimental methodologies, understanding of how a drug molecule detaches itself from the solid phase (mostly crystalline) and enters into solution is quite poor for the most part. One possible reason is that the dissolution mechanism, at a molecular level, is difficult to deduce even with highly sophisticated experimental approaches. In this context, computational methods, molecular dynamics (MD) simulation in particular, are a powerful tool that has the potential to help discern patterns and add insights that are otherwise difficult to gain.[76]

In biological sciences, MD simulation has contributed significantly with manifold applications relating to proteins,[77-79] nucleic acids[80-82] and lipids.[83,84] For example, it changed the earlier view of proteins being rigid molecules and replaced those notions with a dynamic structural model with constant motion that is vital in their biological functions.[85] In drug discovery, MD simulation plays an essential role in drug design and structural optimization.[86-89] Application of MD simulation in other aspects of pharmaceutical sciences is also emerging although publications are limited to date. Recently, Xiang and Anderson[90-93] applied MD simulation to the study of lipid bilayers and gained mechanistic understanding of solute partitioning and transport across biomembranes. They have also studied the mobility of a small peptide, Phe-Asn-Gly, in amorphous glasses of poly(vinyl pyrrolidone) (PVP) containing small amounts of water and ammonia using MD simulation. They were able to observe glass transition, aging processes, and the associated structural and dynamic properties of PVP and the embedded peptide.[24] Li and coauthors[94,95] simulated etching patterns on the acetaminophen monoclinic (010) crystal face by calculating the energies associated with molecular detachment, surface diffusion, and additive molecule adsorption using a refined Monte Carlo simulation model. Fuelled by the dramatic increases in computing power in recent years, the use of computational methods in pharmaceutical sciences has showed a growing trend.[64,96,97] However studying dissolution of organic molecules, such as drugs, using this methodology has not yet been reported. Parker and coworkers[48] modeled different stepped surfaces of calcium carbonate crystal using molecular dynamic simulation. By simulating a monolayer of water on the calcium carbonate surface, they

found that water has a stabilizing effect causing slower dissolution than that *in vacuo*. Dissolution of sea salt crystals (NaCl and KCl) into water was also simulated in the early 1980's by molecular dynamics simulation[42-44] and more recently by quantum mechanics simulations.[45,47] The scope and purpose of these studies are very different from the dissolution concept applied in pharmaceutical fields. The aim of this work is to investigate the dissolution behavior and energetics of key stages in drug molecule dissolution using MD simulations. Acetaminophen (designated as APAP hereafter), a widely used analgesic and fever reducing medicine, was used as a model drug. Its initial dissolution into biologically relevant aqueous medium was studied by MD simulation, the simulated data were analyzed by interaction energy calculations, and key results from the simulation were verified experimentally.

Experimental

Material

Acetaminophen anhydrous polymorph I (Form I) with high purity was purchased from Sigma (SigmaUltra, lot 116K0124), and was used in solubility studies as received. Deionized, distilled water for preparing the dissolution medium (0.15 M sodium chloride in water) was purified to 18.2 mΩ/cm resistivity by passing distilled water through a deionizer/charcoal filter (Milli Q academic model, Millipore Corp., Bedford, MA). Sodium chloride used met ACS Reagent specifications.

Solubility Measurement

Equilibrium solubility of acetaminophen Form I was measured in an 0.15 M aqueous solution of sodium chloride at 37 °C. Sufficient solid was added to 3 mL of medium in six replicates. The suspensions were equilibrated for >2 days at 25 rpm on an end-over-end tumbler, model 30-1200 (Vankel, Cary, NC), in a water bath set at 37 °C. After equilibration, the saturated solution was collected by filtration (13 mm Acrodisc® syringe filter with 0.45 μm GHP membrane, Pall Life Sciences, Ann Arbor, MI), at least 1.5 mL of the filtrate was discarded, and the last 0.5 mL was collected. The filtrate was then immediately diluted into HPLC mobile phase and analyzed by HPLC using a five-point external standard curve. The average concentration of the saturated solutions was reported as the solubility at 37 °C.

Theoretical Methods

Building the Crystal

The single crystal structure of acetaminophen Form I, HXACAN01,[98] was retrieved from the Cambridge Structural Database (Cambridge, UK). The unit cell comprises four APAP molecules. Using the Mercury software (Mercury 2.2, CCDC 2001-2008), a crystal lattice was built by repeating the unit cell at each of the three dimensions for four times. The resultant crystal, referred to as APAP1 4 x 4 x 4, consists of 64 unit cells and 256 APAP molecules. The size of this crystal is 51.72 × 37.60 × 28.40 Å, about 4.6 nm in diameter. The shape of the crystal is parallelepiped in the monoclinic crystal system.

Preparing the Crystal for Simulation

The 4 x 4 x 4 crystal constructed above was prepared using Visual Molecular Dynamics software (VMD, version 1.8.7, August 2009).[99] First, the structure file of the crystal was built using the Automatic PSF Builder function from the input of the Mercury file and the APAP topology file. The topology and atom types for the CHARMM27[39] force field for APAP were obtained by comparison with similar molecules already in the standard topology file. Second, a water box was built to surround the crystal. The water box (containing 0.15 M sodium chloride to mimic the ionic strength of biological fluid) extends 40 Å on each side of the crystal to amount to 58622 TIP3 (water) molecules. The size of the water box is 131.7 × 117.6 × 108.4 $Å^3$, which equals to 1.5×10^{-18} milliliters. The ratio of water molecules to the NaCl molecules in the system is 370 to 1.

MD Simulation

The computer code used for the MD simulations was the parallel, scalable MD program NAMD version 2.5.[100] Periodic boundary conditions were used. The cutoffs for nonbonding (van der Waals and electrostatic) interactions were 12 Å. The switch distance was 10 Å, and a 1.0 1–4 scaling factor was used. The 4 x 4 x 4 crystal in the water box was first subjected to energy minimization (6000 steps) followed by slow heating from 10 to 310 K over 30000 steps. The pressure on the system was equilibrated for 10000 steps using a Langevin piston. The system was then allowed to equilibrate for 30000 steps at constant temperature (310 K) and pressure (1 atm) before production data

was accumulated. Production simulations (10 ns) were performed at constant volume and temperature.

Calculation of Interaction Energies

Interaction energies were calculated using algorithms of the van der Waals and electrostatic energies and the NAMD program.[100] These calculations were performed for specific APAP molecules with their surrounding APAP molecules, water molecules, and Na^+/Cl^-, for defined groups of APAP molecules with the surrounding water molecules within 4 Å. Because partial charges exist in any atom due to the different electronegativities of the atoms, the potential function used in the molecular dynamics simulation considers the partial charge in every atom even when the molecules are neutral (such as APAP). The electrostatic interactions, including ion–dipole interactions and H-bonding, are calculated using these partial atomic charges (CHARMM potential function[39]). The results of interaction energy calculations were analyzed using VMD.

Visualize Dissolution of APAP Crystals under Polarized Light Microscope (PLM)

The purpose of the experiment is to observe whether the dissolution starts from corners and edges. Acetaminophen crystals of sufficient size were prepared by recrystallization from water according to reported procedures.[101] The recrystallized solids were found to be anhydrous Form I by powder X-ray diffractometry (model Ultima II D, Rigaku Corp., Tokyo, Japan). The faces of the crystals were not indexed by single crystal

X-ray diffraction since the observation will be focused on corners and edges. The crystals were stored in a tightly closed jar with desiccants at room temperature until use.

A crystal (size of ~3 mm in length and 1.2 mm in width) was placed on a glass slide under a polarized light microscope (model Eclipse E-600 POL, Nikon Corp., Garden City, NY) with 4× magnification lens. Images were taken using MetaMorph imaging system (version 4.6R8, Universal Imaging Corporation, Downingtown, PA). Drops of dissolution medium (0.15 M sodium chloride in water) were added to completely cover the crystal. Dissolution of the crystal was monitored visually by capturing images periodically.

Results

Model compound APAP is a small molecular drug (molecular weight of 151.16 g/mol). Its chemical structure is shown in Figure 10a. The drug is weakly acidic with a pK_a of 9.5[102] at 25 °C attributed to the phenol moiety. Therefore APAP is neither ionized at physiological pH nor in a 0.15 M aqueous solution of sodium chloride, the dissolution medium used in this study. In a 0.15 M aqueous solution of sodium chloride, the equilibrium solubility of APAP Form I was measured to be 20.0 ± 0.2 mg/mL or 0.132 ± 0.001 M (n = 6) at 37 °C. The reported solubility under the closest conditions is 21.02 ± 0.13 mg/mL in water at 37 °C.[103]

APAP anhydrous Form I has a monoclinic structure[98] with space group $P2_{1/a}$, and a = 12.93 Å, b = 9.40 Å, c = 7.10 Å, α = β = 90.0° and γ = 115.9°. Each unit cell contains four APAP molecules, as shown in Figure 10b. By four times repetition of the three-

dimensional translation of the unit cell, the constructed 4 x 4 x 4 crystal assembly comprises 256 APAP molecules with a size of 51.7 x 37.6 x 28.4 $Å^3$ (Figure 10c). Of the six surfaces of the crystal, two are (100) type, another two are (010) type, and the last two are (001) type of surfaces. The water box consisting of a total of 58622 water molecules as well as 0.15 M sodium chloride extends 40 Å from each side of the crystal to create a water box size of 131.7 x 117.6 x 108.4 $Å^3$ (Figure 10d). The size of the water box was so designed that if the crystal were completely dissolved, the concentration would be 0.28 M, that is, about 2-fold of the solubility. Analogous to a physically performed solubility measurement, extra solids were added to the medium, and the dissolution process was monitored by MD simulation. At the end of 10 ns simulation, the APAP concentration in the water box was about 40% of the solubility.

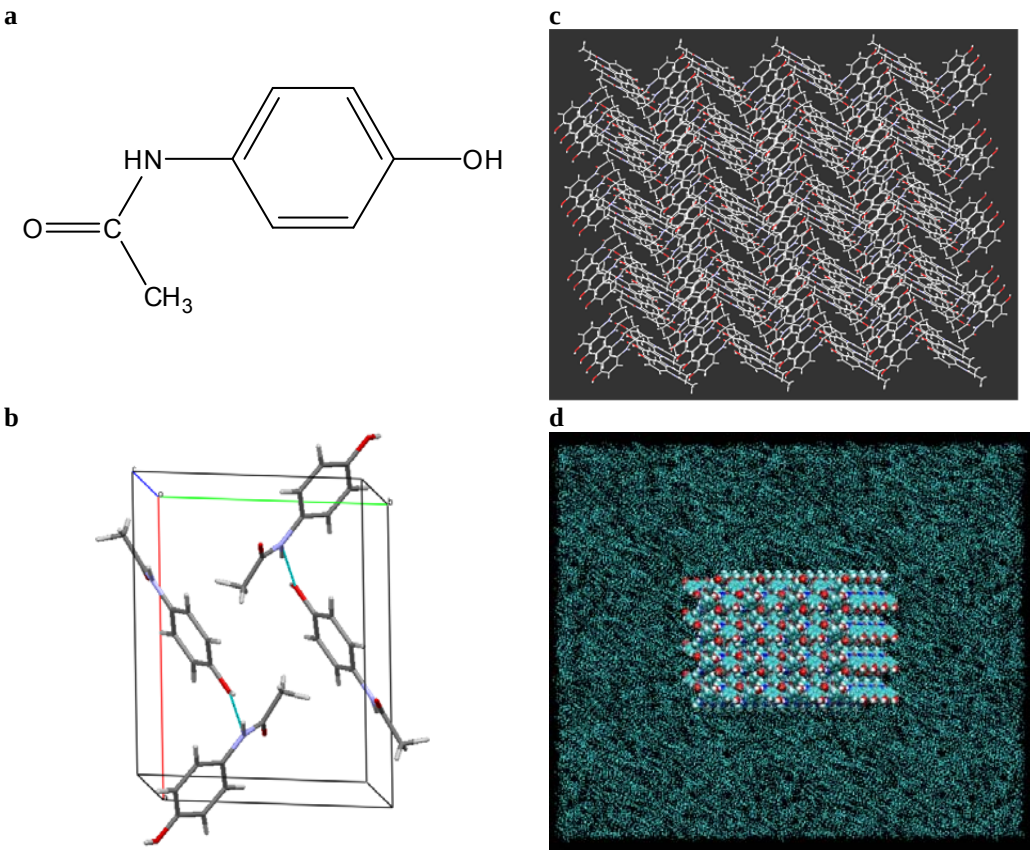

Figure 10. (a) Molecular structure of APAP. (b) Unit cell of APAP anhydrous Form I (dotted line indicating the two hydrogen bonds). (c) The 4x4x4 crystal of APAP anhydrous Form I built by repeating the unit cell four times in all three dimensions, viewed down crystallographic *c* axis. (d) 4 x 4 x 4 crystal of APAP Form I in the 131.7 × 117.6 × 108.4 $Å^3$ water box.

Grouping of APAP Molecules

For the purpose of tracking the molecules that are released, the surface molecules on the crystal were divided into seven groups based on structural insights and the symmetry of the parallelepiped shaped crystal, which has eight corners, twelve edges, and six surfaces. Figure 11 illustrates how the surface bound molecules are grouped. The molecules located on the 8 corners are named as “corner group”. Similarly, the molecules on the 12 edges (except for those in the corner group) formed the “edge group”. The differences among the molecular orientation on the surfaces are significant; the two (100) surfaces are made of APAPs with the phenol group pointing toward external water phase. The two (010) surfaces have the methyl group exposed to the outside, and the molecules on the two (001) surfaces form crossed structures. Further, the top layer of APAP molecules on the (100) and (010) surfaces is completely exposed to water, but the second layer right beneath appears to be partially accessible to water. On the (001) surfaces, on the other hand, the APAP molecules are intertwined, forming a single surface layer accessible to water. Therefore, besides the corner group and edge group described above, other surface bound molecules are logically divided into five additional groups: (100) layer 1 (top layer on the 2 surfaces of (100)), (100) layer 2 (second layer on the tow surfaces of (100)), (010) layer 1 (top layer on the two surfaces of (010)), (010) layer 2 (second layer on the two surfaces of (010)), and (001) layer 1.

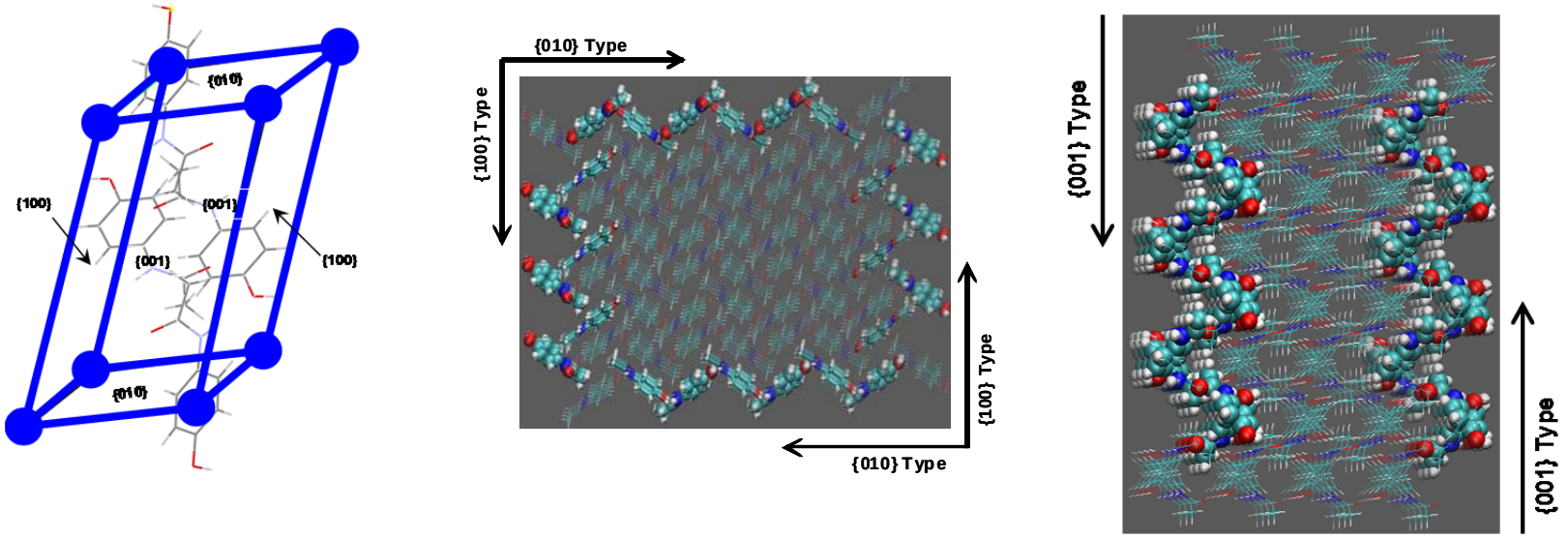

Corners and Edges **(100) and (010) Types** **(001) types**

Figure 11. Illustration of seven groups: (left) Circles indicate positions of corner group molecules; bars indicate positions of edge group molecules. (middle) Surfaces of (100) and (010) types viewed down crystallographic *c* axis, both with layer 1 (bulky VDW style) and layer 2 (smaller VDW style). (right) Surfaces of (001) type (viewed down crystallographic *a* axis).

Observation of the MD Simulation

The crystal in the water box was first equilibrated to reach lower energy. Figure 12*a* is the image of the crystal at the end of equilibration, which exhibits some interesting features. First, the crystal remained intact preserving the overall three- dimensional long-range order as originally built. Second, each molecule moved around within limited boundaries, representing vibrational and rotational movements of molecules in the crystal lattice. Last, the molecules on outer layer appeared much more mobile than those located deeper inside the crystal.

The simulation of dissolution was then initiated and continued for 10 ns. APAP molecules gradually left the crystal and over time accumulated in the water phase. The dissolved molecules display thermal motions. They move around within the water box in a random manner, sometimes wandering back to positions close to the crystal surfaces. Figure 12*b,c* shows snapshots of the system at 3 and 10 ns respectively. It is obvious that with time the crystal became smaller, and the released numbers of APAP molecules were increased. It is also noticeable that only the molecules located on surface layer of the crystal dissolve, and the crystallinity (long- range order) is preserved in the center of the solid. These observations are consistent with the visual observation of a dissolving crystal.

a b c

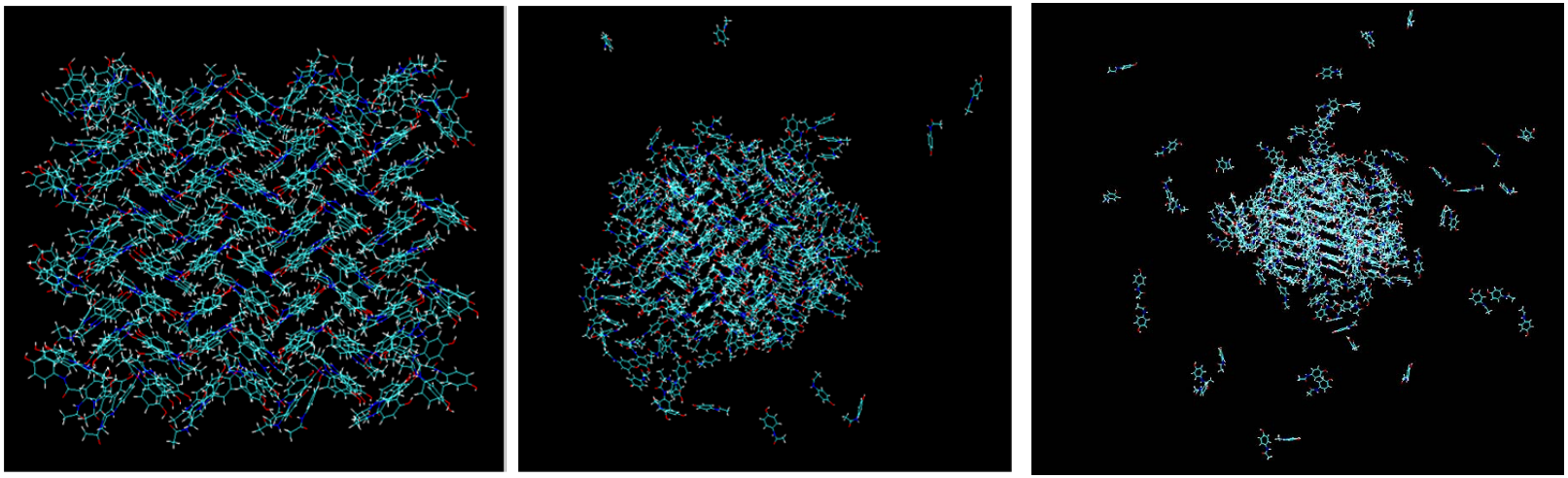

Figure 12. (a) The 4 x 4 x 4 crystal of APAP after equilibration (at 0 ns) viewed down crystallographic *c* axis. (b) Image taken at 3 ns. (c) Image taken at 10 ns.

Order of Molecule Dissolution

As expected, the molecules located on the surfaces of the crystal dissolve into the solution first. To gain understanding in the molecules dissolved and their relationship with the crystal, we used the VMD software to examine the order of release for the molecules. The hypothesis is that a predictable pattern exists between the location of the APAP molecules and their order of release.

In Figure 13, a series of images were captured at different times of dissolution (0.3–10 ns). A clear trend was observed when the dissolved APAP molecules were correlated with the groups that reflect their original locations on the crystal. The preference of initial release is more toward the corners of the crystal, especially along the two more acute corners (sharper corners). The secondary release is from the edges, and finally the flat surfaces release APAP last. This indicates that the molecules are not leaving the crystal surfaces randomly but in an organized fashion.

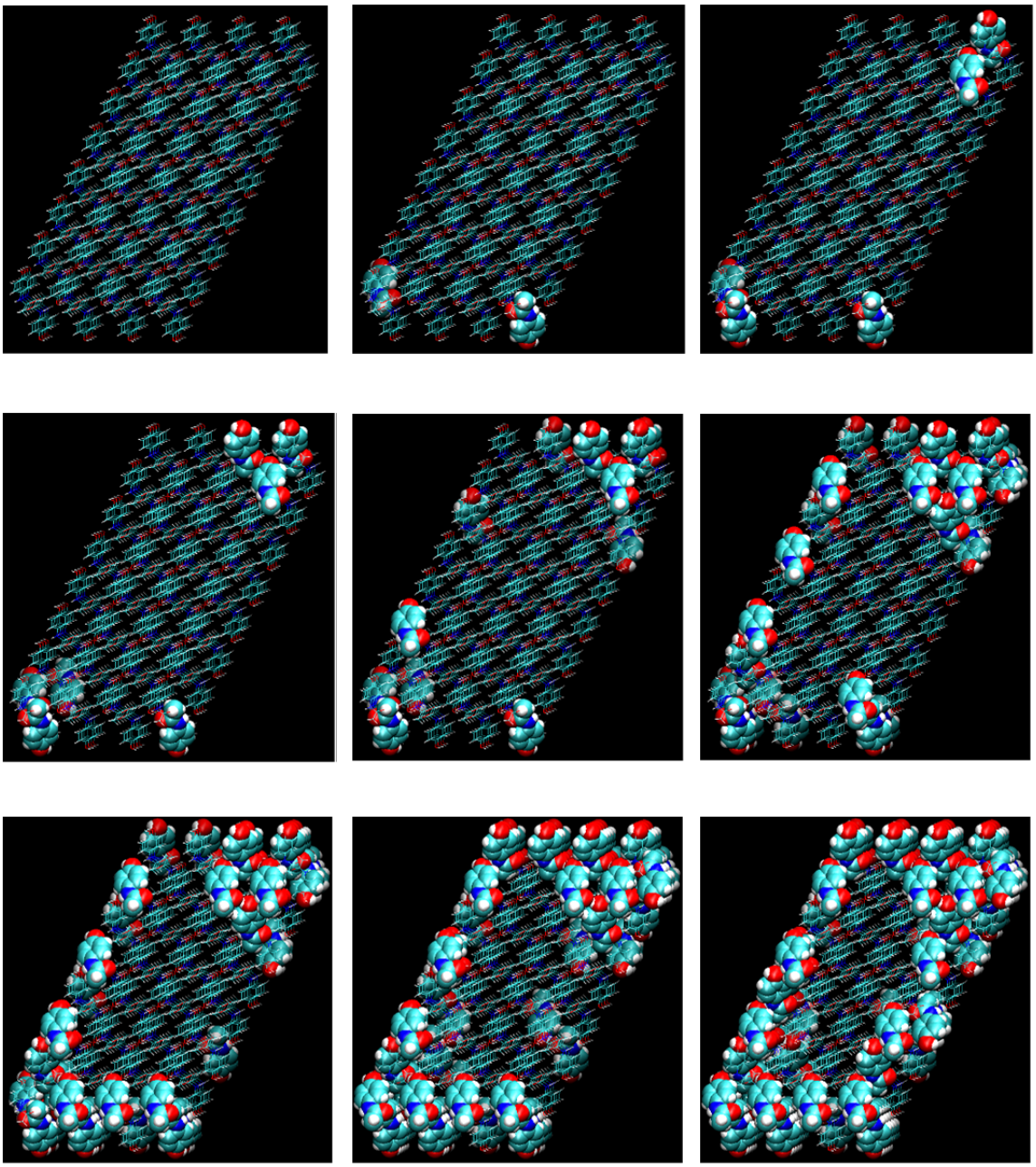

Figure 13. Demonstration of the molecule release profile with time. Undissolved APAPs are shown in line style. Dissolved APAPs are shown in bulky VDW style. From left to right and from top to bottom, 0, 0.3, 0.6, 0.9, 1.8, 2.7, 4.5, 7.5 and 10 ns. All are viewed down crystallographic *b* axis.

Interaction Energy Calculation among APAP Molecules

To determine the theoretical basis of the observed position-dependent release, total interaction energies were calculated between each individual of the 256 APAP molecules and their immediate surrounding APAP molecules within 4 Å over the 10 ns time frame. The total interaction energies are a sum of the van der Waals and electrostatic forces. To illustrate the calculated results, the following APAPs were chosen to represent different initial positions: (1) two molecules that are located in the center of the crystal and have never left their original locations during the 10 ns simulation; (2) a molecule located on (010) layer 2 that has never dissolved; (3) a molecule located on (100) layer 1 that was not dissolved within 3 ns but eventually left at 8.1 ns, and (4) two APAPs that dissolved within 3 ns including one released at 1.2 ns in the corner group and another released at 1.9 ns in the edge group. It was expected that at time zero the APAP molecule being evaluated should interact through electrostatic and van de Waals forces with its surrounding APAPs. When an APAP is dissolving into water, such interactions should decrease significantly or completely since the dissolved APAP is no longer in contact with the neighboring APAP molecules that are initially surrounding it. At the same time, the interaction with the solvent molecules should increase.

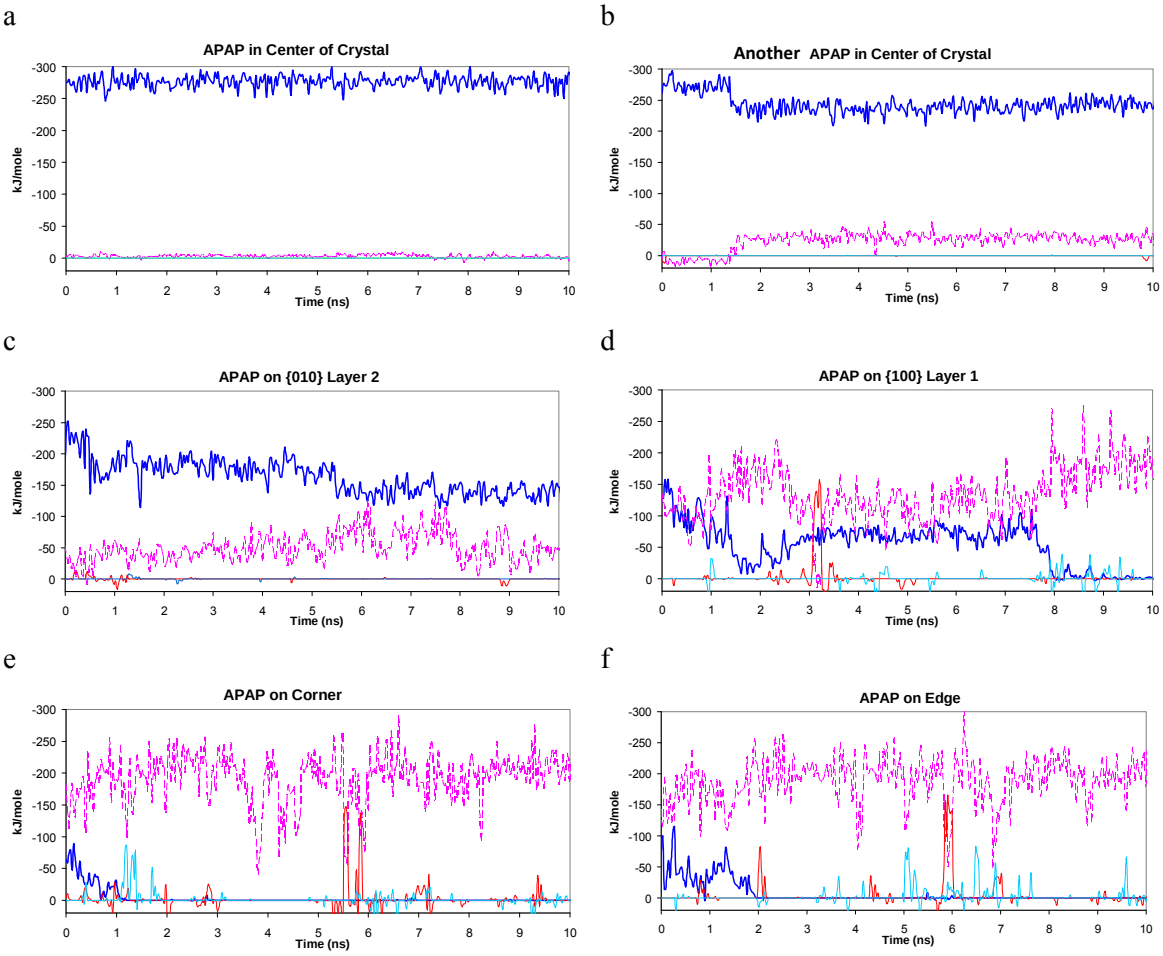

Figure 14. The change of total interaction energy as a function of time for selected APAP molecules: solid blue line (——): energy between APAP and its surrounding APAP molecules; dotted pink line (– – – –): energy between APAP and all water molecules; solid light blue line (——): energy between APAP and all chloride ion $[Cl]^{-1}$); solid red line (——): energy between APAP and all sodium ion $[Na]^{+1}$). (a, b) two APAPs located in the center of the crystal that have never been released. (c) an APAP located on (010) layer 2 that has never been released. (d) an APAP on (100) layer 1 that released at 8.1 ns (later than 3 ns). (e, f) two APAP molecules released within 3 ns, one on corner released at 1.2 ns and one on edge released at 1.9 ns.

A series of plots in blue colored solid lines in Figure 14 depicts the calculated total interaction energy with surrounding APAPs over the course of 10 ns for the preceding list of APAP molecules. The data demonstrate the outcome as what has been predicted. In every plot, the initial total energy is always negative, and the energy level fluctuates from time 0 to 10 ns. However, there are profound differences in the interaction energy profiles among these different APAP molecules. Molecules that are located in the center of the crystal exhibited the highest interaction energies (the most negative) with the surrounding APAP molecules. The total energy exceeded –250 kJ/mole initially and remained with little or no change throughout since their local environments do not change during the course of simulation. The molecule in the (010) second layer also never escaped and started with the total energy close to –200 kJ/mole, which gradually changed to about –125 kJ/mole at the end of 10 ns. However the interaction energy of this molecule never went to 0, suggesting that it maintained strong enough interaction with its neighboring APAP molecules to prevent it from leaving the crystal surface. The APAP molecule located on layer 1 of (100) has an initial energy of about –130 kJ/mole (much less than those of those two preceding cases), but the energy drifts downward to –10 kJ/mole at 1.5 ns, and at 8.1 ns, the energy takes a deep dive down to 0 kJ/mole. This is precisely what was determined by the visual observation using VMD. As illustrated in Figure 15, this (100) Layer 1 molecule was initially wrapped inside a group of adjacent APAPs. At 1.5 ns, the molecule moved half way out of the pocket and lost contact with most of the surrounding APAPs, which is consistent with the interaction energy dropping to –10 kJ/mole. At 8.1 ns, it dissolves and no longer associated with any of the APAPs initially

surrounding it, resulting in the interaction energy decreasing to 0. The earlier released APAP molecules, in the *corner group* and in the edge group have smaller initial interaction energy (–64 to –70 kJ/mole) and released earlier at 1.2 and 1.9 ns, respectively. In all cases, the timing when the total energy changes to zero always corresponds to the time of molecule dissolving into water phase.

The total interaction energies of –250 kJ/mole for the APAP located in the center of the crystal would seem to be too large a number from lattice energy perspective (ΔH_f of APAP Form I is 28.1 ± 2.2 kJ/mole[104]). The reason is that for the entire crystal, this calculation would multiply count interactions. Thus, if an APAP molecule in the center of the crystal is surrounded by 10 other APAP molecules then the actual lattice energy would be 1/10th of the value we calculated. The range of interaction energy values reported by us is in line with other studies.[64]

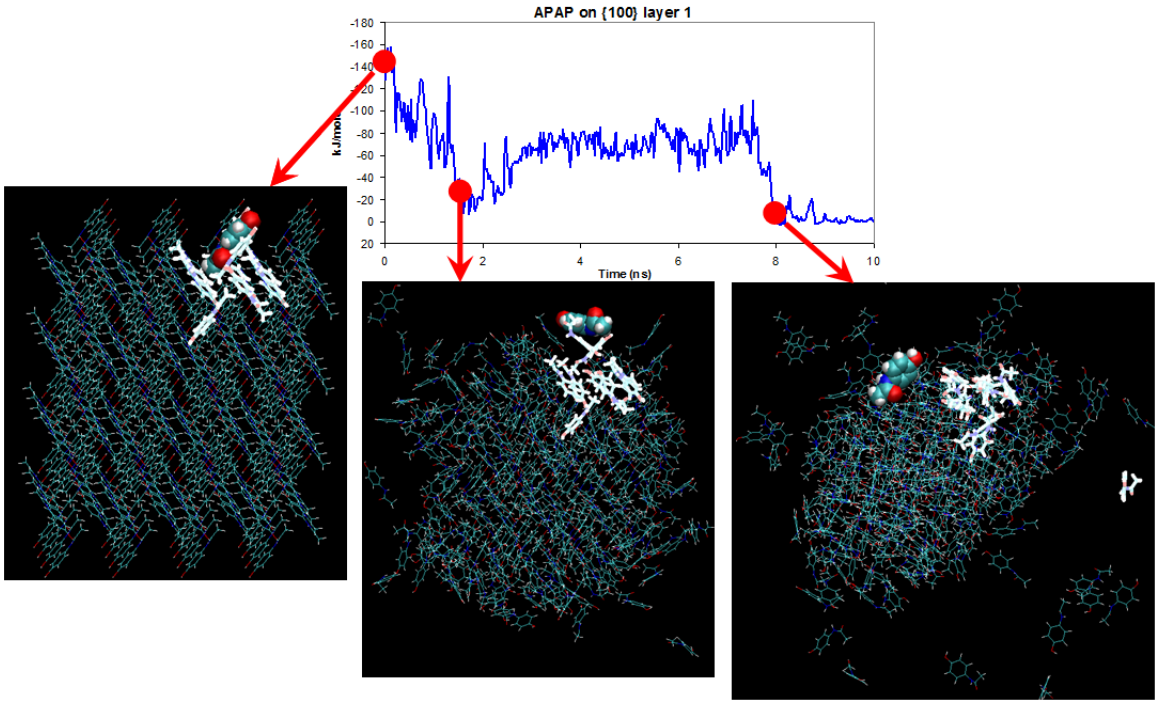

Figure 15. Visual depiction of events occurring at sudden alterations in APAP/APAP interaction curve of the molecule on (100) layer 1 (panel d in Figure 14). From left to right, (1) the molecule surround by nine APAP molecules at $t = 0$ ns; (2) status of the molecule at $t = 1.5$ ns (it only has contact with two of the nine surrounding APAPs; (3) position at $t = 8.1$ ns (it dissolved, losing contact with all APAPs initially surrounding it with interaction energies decreasing to zero).

Interaction Energies between APAP and NaCl Molecules

The MD simulation was conducted in the presence of 0.15 M NaCl. The effect of NaCl on the solubility of APAP was evaluated also through the perspective of interaction energies. The total interaction energies for the same set of selected APAP molecules in Figure 5 with surrounding Na^+ and Cl^- within 4 Å were calculated in the course of 10 ns simulation. The APAP molecules in the center of the crystal (Figure 5*a,b*) and in the

second surface layer (Figure 5*c*) have little or no contact with the dissolution medium; therefore, the interaction energies with Na^+ or Cl^- are zero or almost zero. The surface layer APAP molecules (Figure 5*d,e,f*), on the other hand, were shown to have interactions with Na^+ or Cl^-, especially when the molecules are released into the water phase. The interaction with Na^+ or Cl^- is sporadic and weak in general when compared with the strength of APAP–water interactions. Only rarely the APAP/Na+ interaction became as strong as the APAP–water interactions.

Interaction Energies between APAP and Water Molecules

During the dissolution process, drug molecules interact with water. One way of investigating this interaction is to look at the changes in van der Waals and electrostatic energies between APAP and water molecules over the 10 ns period. The interaction energies between a specific APAP molecule (same groups of APAPs as shown above) and the waters were calculated at 0.03 ns intervals and overlaid with the APAP/APAPs interaction curves in Figure 14. It is clear that the water interaction is complementary to the APAP intermolecular interactions. The loss in interaction between APAPs was gained back from their interaction with water. However, these APAP/water interaction energy profiles are somewhat different from those of APAP/APAPs in that they fluctuate significantly in amplitude after the APAP molecules dissolve. In order to understand this, we calculated the numbers of water molecules within 4 Å of the designated APAP at 0.03 ns resolution. The resultant water number vs time profiles were compared with values of APAP/water and APAP/NaCl interaction energies in Figure 16. It is interesting to note

that the variation in number of waters is completely superimposable with the fluctuation in APAP/water interaction energies, indicating that the primary cause for the big swings in APAP/water interaction energy is the change in numbers of water molecules interacting with the APAP molecules (solvation number). A minor contribution lies in the interaction with NaCl; a few downward spikes (significant decreases) in the APAP/water interaction energies can be attributed to the increases in the APAP/NaCl interactions. Over the entire time, the numbers of waters that are interacting with APAPs vary constantly and dramatically (numbers spanning from 9 to 37 in the case of the APAP on the corner). These results painted a realistic picture of how a molecule interacts with water in solution. The solvation number, if obtained experimentally, will be an average of these dynamics. The MD simulation is able to clearly capture this dynamic image.

a

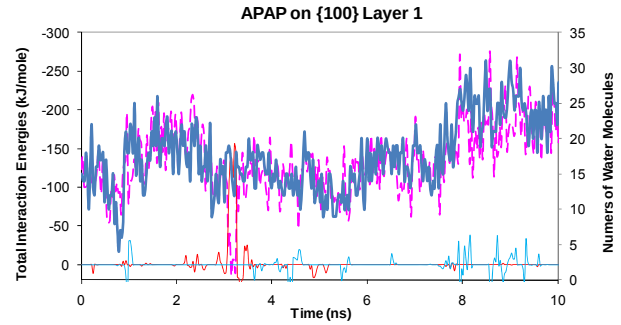

b

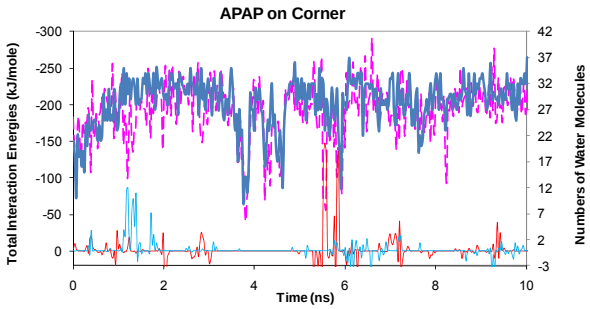

c

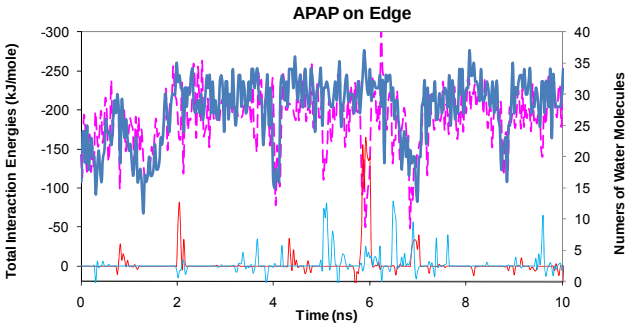

Figure 16. Correlation of APAP–water interaction level fluctuation with the number of surrounding water molecules and the APAP–NaCl interaction. The first *Y*-axis on the left is the change of total interaction energy as a function of time for selected APAP molecules. Dotted pink line (– – – –): between APAP and all water molecules; Solid light blue line (————————): between APAP and all chloride ion $[Cl]^{-1}$); Solid red line (————————): between APAP and all sodium ion $[Na]^{+1}$). The second *Y*-axis on the right is the number of water molecules in the adjacent of the APAP molecule within 4 Å. Solid dark blue line (————————) is the change in number of water molecules over time. (a) an APAP on (100) Layer 1 that released at 8.1 ns (later than 3 ns). (b, c) two APAP molecules released within 3 ns, one on corner released at 1.2 ns, and one on edge group released at 1.9 ns.

Group Average Interaction Energies at Time 0

The initial van der Waals and electrostatic energies among the different groups of APAP molecules were compared to further identify general relationships. This calculation accounted for average interaction energy per APAP residue obtained from the whole group at 0 ns. Both APAP/APAP and APAP/Water interactions for the seven groups were calculated (Figure 17). The corner group on average possesses the *smallest* interaction energy with their surrounding APAP molecules, followed by increasing energy order of edge group, (001) layer 1, (010) layer 1, (100) layer 1, and (001)/(010) layer 2 (Figure 17a). When the interaction energy with water molecules is considered (Figure 17b), the rank order is exactly reversed, with the corner group taking the lead followed by edge group, (001) layer 1, (010) layer 1, (100) layer 1, and (001)/(010) layer 2. This comparison indicates there should be differences in dissolution rate among the different groups. Figure 18 correlates the percentage of molecules released at different times (3, 5 and 10 ns) with the differences in interaction energies. Since the interaction energy among the drug molecules would deter dissolution, while the interaction energy between the drug and water molecules would favor the dissolution, the difference between these two forces (total interaction energy of APAP with water minus that of APAP with APAP) was plotted along the *x*-axis. The percent of release was calculated by taking the ratio of released molecules in the specific group over the total APAP molecules in the same group and plotted on the *y*-axis. There is a clear trend with a rank order consistent with the preferential release profile among different groups at all three time points (Figure 18). These data demonstrate that a strong correlation exists between

the initial energy level and the extent of molecule release. The release rate follows the order of corner group, edge group, (001) layer 1, (010) layer 1, and (100) layer 1.

Figure 17 also shows the different landscapes of van der Waals energy vs electrostatic energy among the different groups. The van der Waals energy comprises a significant portion in the total energies in groups of APAP/APAP interaction, while its role in the APAP/water interaction seems less important than the more dominant electrostatic forces. In the APAP/APAP interaction, electrostatic energy varies greatly among different groups, while the interaction contribution by van der Waals interactions is relatively more uniform.

a

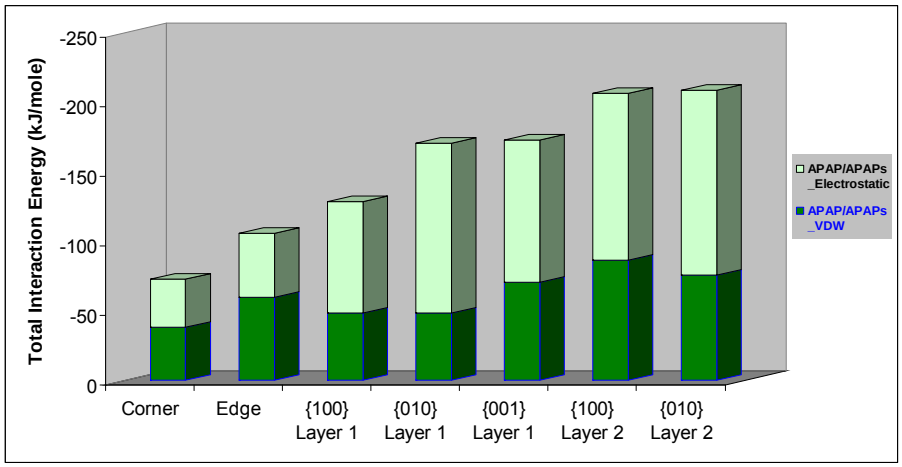

b

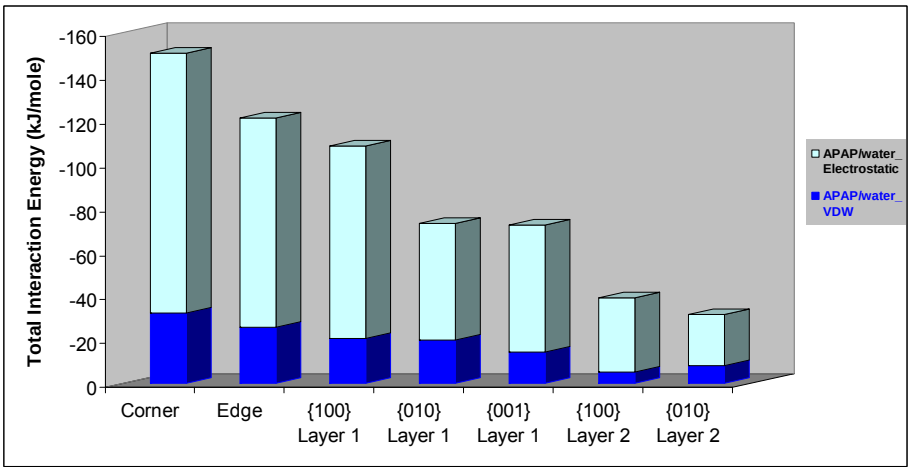

Figure 17. Initial interaction energies expressed as an average for each group. (a) Energy between APAP and its surrounding APAPs; (dark green bar) van der Waals, (light green bars) electrostatic. (b) Energy between APAP and surrounding water molecules; (dark blue bars) van der Waals, (light blue bars) electrostatic.

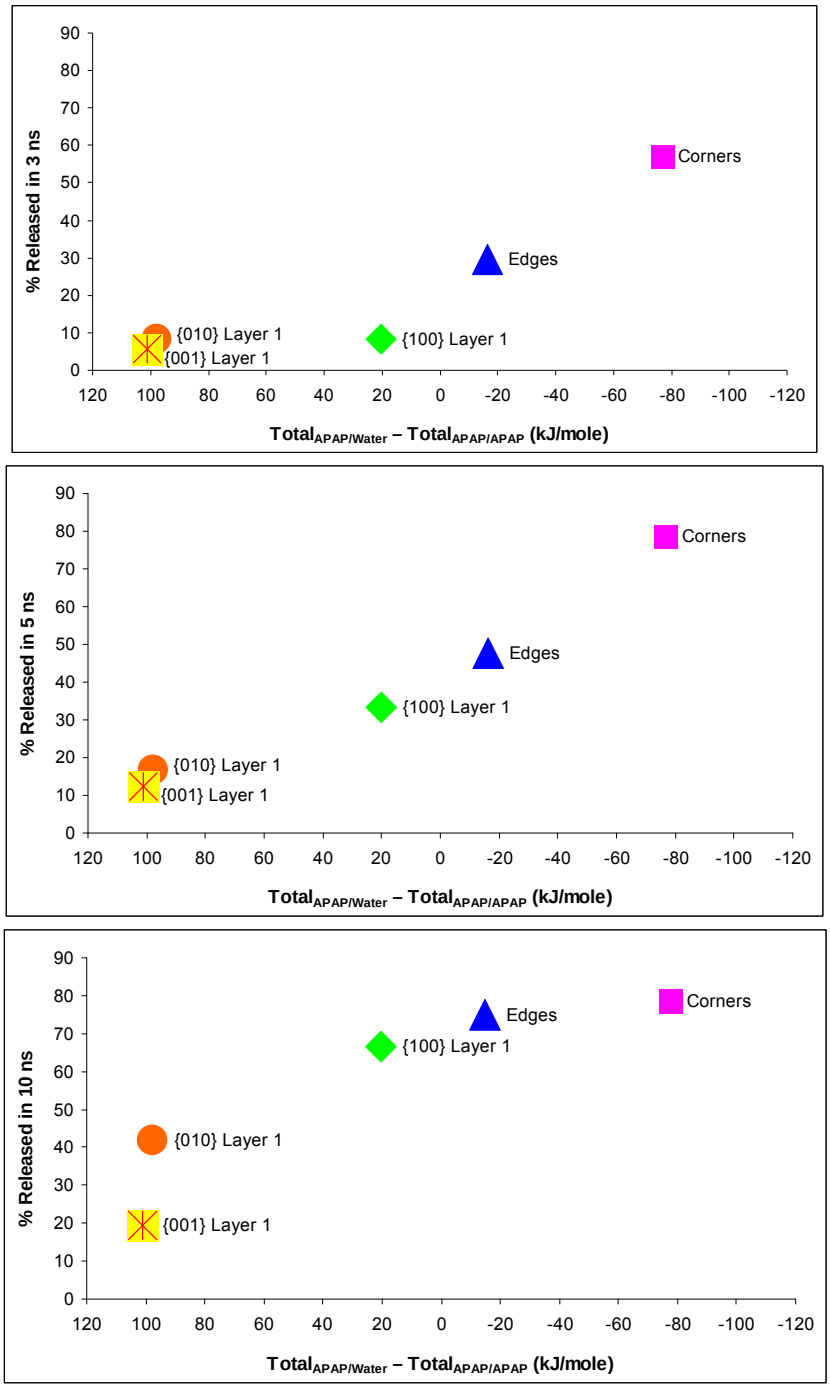

Figure 18. Total interaction energy differences between APAP/APAP and APAP/water and their correlations with percent of molecules released with time. Top graph, t = 3 ns; middle graph, t = 5 ns; bottom graph, t = 10 ns.

Physical Observation of APAP Crystal Dissolution

The molecular dynamic simulation of a nanoscale dissolution showed that the first groups of molecules to leave the crystal surface are located on the corners and along the edges. To test whether this phenomenon would occur during macroscale crystal dissolution, a visual dissolution was performed while observing a large size APAP crystal under a microscope. The visual dissolution results are captured in Figure 19. In the beginning, the crystal has well-defined shape and sharp edges (Figure 19a). However, as dissolution progressed, the corner quickly changed shape, and the edges became blurred and dull (Figure 19b). If the molecules had left all surfaces at a same rate without any preferences, the original shape of the crystal should have remained. Therefore, experimental observations support the simulation results.

a

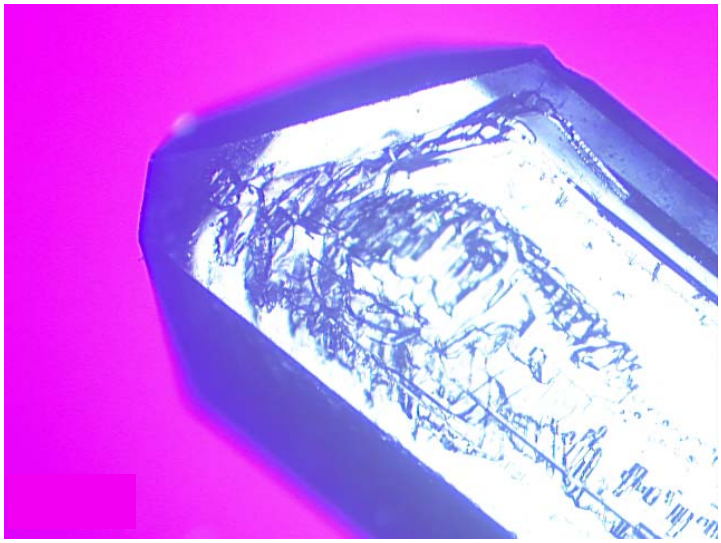

b

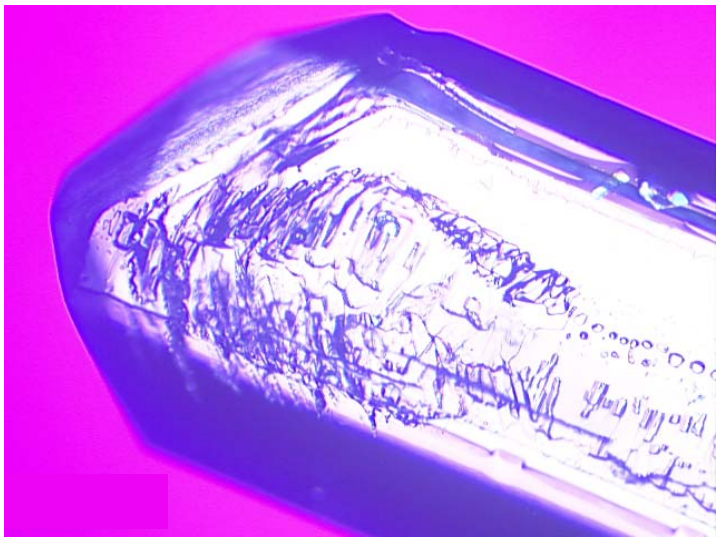

Figure 19. Visual observation of dissolution of an APAP crystal in 0.15 M sodium chloride solution under a polarized light microscope at 4× magnifications. (a) Initial image before adding dissolution medium; (b) Seven min after adding dissolution medium.

Discussion

Molecular Release in Dissolution Process and Interaction Energies

The MD simulation clearly showed how each molecule leaves the crystal surface to enter the water phase. The dissolution process is far from simply a random action. The sequence at which the molecules leave the crystal surface follows a defined pattern: the molecules located at corners, especially at the sharper corners, follow a trend of dissolving earlier, followed by those on edges, and very few from the center of flat surfaces have dissolved (Figure 13). According to Wang and Flanagan,[6] neighboring molecules on a solid (either crystalline or amorphous) are closely associated with each other through intermolecular forces. Dissolution involves the breaking of these existing intermolecular interactions, and then the formation of new interactions with dissolution medium (0.15 M NaCl in our simulation experiment). In the present study, the interaction energies among the molecules located in different places of the crystal were calculated as the sum of the electrostatic forces and van der Waals energies. The APAP molecules located on corners and edges are relatively loosely associated with their surrounding APAP molecules (Figure 17a) indicated by total interaction energies (–60 to –106 kJ/mole) at time zero being smaller than the total energies of their surface bound counterparts (in the vicinity of –130 to –170 kJ/mole) and even smaller than those in the second layers (~ –200 kJ/mole) or buried inside the crystals (total initial energies around -250 kJ/mole) in Figure 14a,b. The larger the bound energy the molecule possesses, the more difficult it is for it to release into the water. Once the molecule is released into the

water phase, the total interaction energy between APAP and surrounding APAP molecules immediately disappears (Figure 14).

Sometimes, the total interaction energy vs time profile for a single APAP molecule (Figure 14b,d) undergoes changes not related to dissolution of the molecule, which were found by visual inspection with VMD to be directly linked to the physical movement of the molecule. For example in Figure 15, both sudden decreases at 1.5 and 8.1 ns in Figure 14d are caused by the loss of contact with its surrounding molecules. In another example, the change at ~1.5 ns to the molecule located in the center of the crystal (Figure 14b) is due to the dissolution of a molecule that initially binds to this center molecule, resulting in some exposure to water (graphical illustration not shown). By plotting the total interaction energy of APAP molecules with their surrounding APAP molecules vs time (Figure 14), one can determine when a molecule dissolves (interaction energy changing to 0) or has changed in its relationship with adjacent molecules. This has been demonstrated in all 256 APAPs (data not shown for all). These results indicate that the energy computational method is a powerful tool in analyzing the dissolution simulation data.

Sodium chloride at 0.15 M to mimic the ionic strength of biological fluid was present in the solubility simulation of APAP. Electrolytes such as sodium chloride are known to potentially affect solubility. They can attract water molecules and reduce the density of the aqueous environment adjacent to the solute molecules, causing lower solubility (salting out effect). They may also interact directly with the solute molecules, resulting in higher solubility (salting in effect). The total interaction energies between

APAP and Na^+ and Cl^- for select APAPs are plotted in Figure 5. As expected, only the surface layer APAP molecules (Figure 5d,e,f) were shown to have interactions with Na^+ or Cl^-. Compared to APAP/water interactions, such interactions take place sporadically with much smaller energy in general. Most of the time, the interaction energies are in the range of –50 to –100 kJ/mole which are much less than the strength of APAP–water interactions (on average at –250 kJ/mole). Only very occasionally and for very short durations, the APAP/Na+ (ion-dipole) interactions reached the level of APAP–water interactions. The reason for the relatively much smaller overall interaction energy is the overwhelmingly larger number of waters vs NaCl molecules present in the system; for every NaCl molecule, there are 370 water molecules. As a result, the effect of 0.15 M NaCl on the solubilization of APAP in water is minimal. This is consistent with the measured solubility values of APAP in the presence and in the absence of NaCl, which are hardly distinguishable (20.0 ± 0.2 in our study vs 21.03 ± 0.13 mg/mL[103]).

The water molecules play a significant role in "dragging" the drug molecules into the aqueous phase, which is the second step in the dissolution process. This can be demonstrated by calculating the interaction energies between APAP molecules and the water molecules. As shown in Figure 14, water molecules do establish new interactions with those APAP molecules that are dissolved, and they have fewer interactions with those APAP molecules that are not dissolved. The group average initial interaction energies with water (Figure 17b) followed the opposite trend as those between APAP molecules (Figure 17a). The stronger interaction with water positively contributed to dissolution.

Figure 14 and Figure 17 revealed that the dissolution pattern observed at the molecular level (Figure 13) is governed by the interplay between the interaction energies formed among the APAP molecules and between the APAP and water molecules. Figure 18 demonstrates that the net difference between these two types of interaction energies is the underlying cause for the differences in dissolution rate from different areas of the crystal. Dissolution rate has been long established to be directly correlated to solubility,[4] a thermodynamic property. The dissolution process can be viewed as a pseudochemical reaction, which is governed by thermodynamics. The Gibbs free energy, ΔG, is the balance between enthalpy, ΔH, and entropy, ΔS, at given temperature T ($\Delta G = \Delta H - T\Delta S$). ΔG needs to be negative in order for dissolution to occur. Since dissolution produces more randomness of molecules in the entire system (including solid and solution states), the ΔS term is generally positive. Thus, net enthalpy is the term to determine whether or not ΔG will become negative.[6] Further, the contribution of entropy to dissolution is the same regardless the location of molecules on the crystal. Therefore, the differences in dissolution rates are determined by the interaction energy based on the location of the molecules. When the net interaction energy difference is negative (interaction of APAP/water overwhelms that of APAP/APAP), dissolution of APAP into water becomes favorable. This can explain why the dissolution in the corner group (with net interaction of –89 kJ/mole) and the edge group (with net interaction energy of –24 kJ/mole) is facile, and why the release percentage of the corner is higher than the edge at early stages. In the surface layers of (100), (010) and (001), the APAP/APAP intermolecular binding energy exceeded that of APAP/water. In this case, the molecules

would favor staying on the crystal surface until the other term, ΔS, overcomes the enthalpy barrier. This explains the very slow initial dissolution of the surface groups. Among the surface groups, however, differences also exist. The (100) layer 1 started with significantly higher water interaction (–108 kJ/mole) than the (010) layer 1 and (001) (both at –72 kJ/mole) owing to the out-facing hydrophilic phenol moiety that presumably facilitates the interaction with water molecules. As a result, this group as a whole is able to dissolve much faster than the other two surface groups. The (010) and (001) crystal faces which are not as hydrophilic have similar level of interactions with water (Figure 17b), and consequently the initial dissolution rate is at a similar level too. Eventually the dissolution of the (010) surface moved ahead of the (100) surface (Figure 8, bottom panel) because (010) surface is smaller than (100) in the 4 x 4 x 4 crystal and closer to the edges and corners. Overall, the correlation is evident: with the decrease of net interaction differences, the extent of dissolution from the fastest to the slowest follows the rank order of corner group > edge group > (100) layer 1 > (010) layer 1 > (001) layer 1 (Figure 18). Explained physically, corners have larger surfaces accessible to water, resulting in more interactions with more water molecules. The same physical argument can explain why edges have higher interaction with water than the flat surfaces.

We have discussed above the total interaction energies that have profoundly influenced the rate of dissolution. The total interaction energies originate from two types of forces: electrostatic (charge–charge, ion–dipole and hydrogen bonds) and van der Waals (dipole-dipole, dipole–induced–dipole and dispersion forces). Various electrostatic interactions are specific and directional. H-bonding has been viewed as the most

important force to hold together organic solid crystals.[105] H-bonding is also responsible for solubility behavior of polar molecules such as drugs in solvents especially polar solvents (e.g. water).[106] Van der Waals interactions are nonspecific attraction forces and proportional to radius^{-6} which fall off rapidly with increase of intermolecular distance.[107] In the literature, the importance of van der Waals forces in the crystal lattice and solubilization has not been emphasized to the degree that the H-bond has been. In Figure 17a, we plotted the group average APAP intermolecular interaction energies divided into electrostatic and van der Waals contributions. These plots revealed that H-bonding is an important force but not the only important force. Van der Waals comprises a significant percent of the total interaction energy in all seven groups. Its contribution in the corner and edge groups is almost at 50%. Similar plots were made to describe the APAP/water interactions at the crystal/water interface (Figure 17b), in which the electrostatic force is shown to be a much more dominating factor because water has an exceptional capability to form H-bonds. Yet the portion of van der Waals contribution is still not negligible. The strong correlation between percent of release and net interaction energy shown in Figure 18 would have been lost if the van der Waals interactions were excluded from consideration. The data in Figure 17 have demonstrated the significance of *both* H-bond and van der Waals in lattice energy and in energetics of crystal dissolution. Since both the electrostatic and van der Waals energies will depend on the structure of the molecule, the relative importance of these two factors would vary for different compounds.

The distribution of van der Waals and electrostatic energy in two crystal surfaces, (100) and (010) (Figure 17), warrants more discussion. These two groups of surface molecules are packed similarly (Figure 11) so the van der Waals force is almost identical. What is intriguing is the much larger electrostatic interaction energy of the (010) face compared with that of (100) face. The answer was found after examining the H-bond motifs on (100) and (010) faces. Each APAP on the (100) layer 1 forms *two* H-bonds: O=C–N–H (1^{st} layer) → O–H–Phe (2^{nd} layer) and Phe–O–H (2^{nd} layer) → O=C–N–H (1^{st} layer), while each APAP on (010) layer 1 is bound by *three* H-bonds to two APAPs in the second layer: Phe–O–H (1^{st} layer) → NH–C=O (molecule no. 1 in 2^{nd} layer), Phe–O–H (molecule no. 2 in 2^{nd} layer) → O=C–NH– (1^{st} layer) and O=C–NH (1^{st} layer) → O–H–Phe (molecule no. 2 in 2^{nd} layer). Therefore, the (010) surface is associated with higher electrostatic energy and should be more stable than the (100) surface just as demonstrated in Figure 18.

The surface correlated dissolution indicates that different morphologies of the crystals should exhibit different dissolution rates. Earlier theoretical assessment of shape factor in dissolution rate suggested minimal influence,[74] however, later reported experimental evidence indicated otherwise. In a dissolution study of five single crystals,[71] the shape factor changed significantly after 50% dissolution, which points to preferential dissolution of different faces. In another theoretical study, the flux of aspirin from crystal phase (100) is approximately 6 times faster than that from phase (001), which is correlated with reported variations in the dissolution behavior of commercial aspirin products.[108] In one more report, single crystal dissolution was studied on APAP crystals

and different dissolution rates from phase (001) and (110) were found.[109] Chow and Grant conducted extensive studies on the physical factors (such as shape) affecting the dissolution rate of APAP crystals.[110] They found that the aspect ratio played a significant role in the intrinsic dissolution rate of APAP, and an empirical equation can be established to correlate the intrinsic dissolution rate with aspect ratio and other physical factors such as incorporated impurity levels. In their empirical equation, the intrinsic dissolution rate is exponentially proportional to the aspect ratio, *l/w* (length/width) [ln (rate) = constant × ln *l/w*]. The aspect ratio affects the morphology and consequently the amount of material in edges. Assume two rectangular crystals have the same solid volume of 1000 nm^3. Crystal no. 1 is a cube with $l = 10$ nm, and $w = 10$ nm, so the total length of edges will be 120 nm (four times 10 nm times three). Crystal no. 2 is a needle with $l = 100$ nm, and $w = 1$ nm, which will result in a total length in edges of 444 nm, almost 4-fold of the edges as in a cubic crystal. Therefore, increasing *l/w* ratio results in more abundance of edges. In a follow-up study,[111] Chan and Grant confirmed that crystal habit is the major factor that determines the intrinsic dissolution rate of acetaminophen crystals. Their experimental findings are consistent with what we have observed here in our MD simulation. The MD simulation demonstrates that morphology is expected to affect the dissolution rate due to different interaction energies intrinsically presented in different surfaces of APAP crystals. Since corners and edges have fewer APAP–APAP interactions and more APAP–water interactions, increasing the aspect ratio would boost the dissolution rate.

Solubility and Dissolution Rate vs Particle Size

Upon completion of the simulation, one question immediately became obvious: why is the dissolution so fast? Within 10 ns, the APAP concentration in the water box reached about 40% of the solubility. The APAP crystal built for dissolution simulation consists of 256 molecules with 5120 atoms. The volume of the crystal is 5.0×10^3 Å^3 which translates to a diameter of about 4.6 nm (radius of 2.3 nm) for a spherical crystal. Based on classical nucleation theory, a crystalline lattice structure will be stabilized when it reaches the critical radius, r_c. Particles smaller than r_c will dissolve or evaporate.[112] The size of a critical nucleus typically falls in the range of 100–1000 atoms,[113] which is far exceeded by the 5120 atoms in the APAP 4 x 4 x 4 crystal lattice. The fact that the 4 x 4 x 4 nanocrystal did not dissolve after being subjected to the initial equilibration step (Figure 12a) further confirmed its stability. Hence, using this 4.6 nm crystal to simulate crystal dissolution is proper and justified.

It is known that the saturation solubility can be increased when the particle size is decreased to smaller than 100 nm and the extent of solubility increase can be calculated by the Thomas–Freundlich equation.[114]

$$\ln \frac{C_{s,r}}{C_{s,\infty}} = \frac{2\gamma V_m}{rRT} \qquad \text{(Equation 1)}$$

Where $C_{s,r}/C_{s,\infty}$ is the ratio of solubilities when particle size is decreased from a large particle (∞) to a smaller one with radius of r, γ is the interfacial tension, V_m is the molar volume of the particle (the molecular weight divided by the density), R is the gas

constant, and T is the absolute temperature. With APAP's molecular weight of 151.16 g/mol, density of 1.2 g/cm^3, the interfacial free energy of 30 mJ/m^2 at 310 K (37 °C),[114] the solubility of a r = 2.3 nm APAP crystal is calculated to be 3.6 times of the solubility of a macro crystal.

It is also known that the dissolution rate of the nanosized crystal will increase over that of a large particle. The dissolution rate constant, k, can be calculated by Higuchi and Hiestand equation (also known as two-thirds-root expression), which was derived for diffusion layer based dissolution of very small particles:[6]

$$k = \left(\frac{4\pi\rho N}{3}\right)^{2/3} \frac{2DC_s}{\rho} \qquad \text{(Equation 2)}$$

Where ρ is the density of the particle, N is the number of particles, D is the diffusion coefficient, and C_s is the solubility.

The dissolution rate constant of a small particle, k_S, vs the dissolution rate constant of a large particle, k_L, can be calculated by taking the ratio of k_S/k_L from eq 2. When comparing k_S with k_L in this calculation, it is assumed that the same amount of drug sample was added into the dissolution medium so that the weight portion from the ρ term can be canceled out. It is also assumed that diffusivity, D, between the large and small particles is similar. After simplification of eq 2, the ratio of k_S/k_L is expressed in the following equation:

$$\frac{k_S}{k_L} = \frac{C_{sol,S}}{C_{sol,L}} \times \left(\frac{r_L}{r_S}\right)^2 \qquad \text{(Equation 3)}$$

where $C_{sol,S}$ is the solubility of the small particle, $C_{sol,L}$ is the solubility of the large particle, r_L is the radius of a large particle and r_S is the radius of a small particle. Notice that the solubility of the nanocrystal of APAP is 3.6 times that of the large particle from the Thomas–Freundlich equation. Assuming a large particle has a particle size of 10 μm (a commonly used particle size for drugs), the dissolution ratio, k_s/k_L, is $3.6 \times (10000 \text{ nm}/ 2.3 \text{ nm})^2 = 6.8 \times 10^7$. Putting this value in practical perspective, if the large particle (10 μm) takes 20 min to reach 40% saturation, the 2.3 nm nanocrystal will take 17.6 μs ($20 \times 60 \text{ s}/6.8\times10^7$) to reach the same level of saturation. This 17.6 μs dissolution time is still 3 orders of magnitude longer than the 10 ns simulation time. Thus, in our MD simulation of the dissolution, the crystal takes a shorter time to dissolve than it would in a conventional experiment. The reason is not clear; however, it is consistent with the other published MD simulations. For example, Parker and co-workers[48] simulated dissolving a small surface layer of a calcium carbonate crystal over 200 ps (0.2 ns). In another paper by Bhargava and co-workers,[115] the initial aggregation of surface active ionic liquid was simulated within 4 ns although the complete aggregation process takes microseconds to milliseconds. In a recently published work by Yani and co-workers,[64] the production run on the interaction between polymer and salbutamol sulfate crystal utilized simulation time less than 1 ns. Apparently, the time scale differences will not discount the important findings discovered by MS simulations.

Corner and Edge Effect

A perfect crystal surface is more difficult to dissolve. Indeed there are no molecules from the center of the *perfect* APAP 4 x 4 x 4 crystal surfaces to dissolve initially

(Figure 13). In our simulation, the first three dissolved molecules are all located at corners, followed by several on edges. The strong trend where the APAP molecules at the corners and edges, especially at the corners, dissolved before other molecules persisted all the way to the end of the 10 ns in this simulation. The same was observed in another two MD simulations we have completed earlier using different sizes of crystal and water box (detailed data not shown). The first simulation was done on a much smaller crystal (3 x 3 x 3 crystal lattice, 27 APAP molecules) in a 20 Å water box. The second one was on the same large size crystal (4 x 4 x 4 lattice, 256 APAPs) but in a smaller 25 Å water box containing about 1/5 of the water molecules presented in the 40 Å water box. Both of these additional MD simulations also show without doubt that molecules released first from corners and edges. We have also conducted a real dissolution experiment of a large crystal, millimeter size (Figure 19). The results confirmed that corners and edges disappear first, which rendered dull the edges of the crystal. Therefore, the corners and edges serve as the initial sites for dissolution in *perfect* single crystals.

The corner and edge effect has an underlying theoretical basis. In a reported study using bond valence calculations, Schindler and Mutter[116] explained that the cluster of crystals on the edge of a mineral sheet would develop activated sites first and dissolve into aqueous solution. In our MD simulation, the order of molecule dissolution is a result of the interplay between the interaction energies formed among the APAP molecules and between the APAP molecules and water with the corner and edge groups clearly differentiating themselves from the surface groups (Figure 18). This interaction energy calculation provides strong evidence that corners and edges should dissolve first in a

perfect crystal. Once a molecule breaks free from the corners or edges, new corners and edges will be created instantaneously, forming new sites for the next wave of molecules to dissolve. This domino wave will gradually reach the molecules originally on surfaces, where the relatively weakly associated surface molecules will dissolve prior to the more tightly bound surface molecules. Such a dynamic dissolution process will proceed until the whole crystal disappears or until saturation is reached. In practical crystallization processes, a variety of surface imperfections can be produced as a result of mechanical or thermal stress or irregular growth.[112] In this case, besides corners and edges, the imperfect surface spots can also take the lead in dissolution, creating new corners and edges on the way.

It was widely accepted that the dissolution rate correlates with the total particle surface area. Now based on our findings, the initial dissolution rate probably is more correlated with the number, the length and the shape of the corners and edges in the particles. The knowledge of the corner and edge effect allows us to better understand particle size reduction, a very useful technology to increase dissolution rate of poorly water–soluble drugs. Common knowledge holds that particle reduction technology works by creating more surface area. Based on our study, the important underlying mechanism is, at least in part, the creation of proportionately more corners, edges, and other defects when the particles are turned into smaller ones. The advantage of smaller particles lies in the superior accessibility to dissolution media; the molecules in the center of the smaller particles need not wait as long as those in the center of the bigger ones to “see the light at

the end of the tunnel". The presence of larger numbers of the faster dissolving defect spots in milled tiny particles essentially accelerates the accessibility to dissolution media.

Conclusions

We have presented here molecular dynamic simulation of acetaminophen Form I dissolving into an isotonic aqueous medium at 37 °C. The results clearly demonstrate that dissolution from a crystal is not a random process. It is strongly governed by the electrostatic and van der Waals interaction energies among the solute molecules and solute–solvent molecules, with a non-negligible contribution from van der Waals forces. The distribution of the interaction energies has a unique geometric entity: the molecules located on corners and edges of the rectangular parallelepiped crystal are not as tightly bound to their surrounding neighbors as those located in other surfaces. Therefore they are less restricted and tend to dissolve more readily. Furthermore, the simulation results were confirmed by the dissolution experiment. These results prompted us to rethink the fundamentals of particle size reduction in enhancing dissolution rate. The presence of larger numbers of the faster dissolving corners, edges, and other defect spots produced by milling accelerated the accessibility of small particles to dissolution media. This is different from the conventional view of attributing to the flat surface area, although the accompanying consequences, the increases in dissolution rate, are the same. The findings presented here are very relevant in the context of particles size reduction and delivery of poorly soluble compounds.

Acknowledgement

The authors express their sincere gratitude to Drs. Geoff G. Z. Zhang, Yihong Qiu, Rodger Henry, Deliang Zhou and Donghua Zhu at Abbott Laboratories and Dr. Shaoxin Feng at Allergan, Inc., for insightful discussions and to Abbott's Tuition Assistance Program for financial support.

CHAPTER FOUR

UNIQUE MECHANISM OF FACILE POLYMORPHIC CONVERSION OF ACETAMINOPHEN IN AQUEOUS MEDIUM

Abstract

For acetaminophen (APAP), the fast conversion from the metastable orthorhombic crystal Form II to the stable monoclinic Form I in solution has been observed ever since the Form II was discovered decades ago. Since the conversion taken place when the solid comes in contact with solutions, it has been believed that the process followed a solution-mediated phase transformation. However, little has been understood as to exactly which factors are contributing to the fast kinetics. The present study was undertaken to examine both thermodynamic and kinetic driving forces that lead to this facile polymorphic conversion. The thermodynamic solubility of Form II in 0.15 M aqueous NaCl solution at 37 °C was obtained for the first time using a new solubility method with the aid of low level (0.02%) of poly(vinyl pyrrolidone) (PVP) to inhibit crystallization of Form I. The solubility ratio of Form II over Form I, which represents the thermodynamic driving force for the conversion, is only 1.27 ± 0.04. Further experiments to monitor crystallization at supersaturation levels at or even much greater than Form II solubility did not result in any crystallization in ten days at 37 °C. Essentially, Form II is not able to generate sufficiently high supersaturation to nucleate Form I *through dissolution* at 37 °C. In other

words, the fast conversion is not possible through the solution-mediated phase transformation. To identify other possibilities, molecular dynamics (MD) simulations were conducted that investigated the molecular level dissolution behavior and the solid state differences between the two crystalline forms. It was found that Form II behaves very differently from Form I when exposed to solution. Form II showed much higher rate of H-bond breaking, causing the accumulation of large numbers of APAP molecules on the crystal surface. This thick disordered molecular layer on Form II surface provides high local acetaminophen concentration for fast Form I crystallization. This was further supported by the rapid surface recrystallization from a Form II crystal in solution monitored under polarized light microscopy and by powder X-ray diffraction. Therefore, the hydrated surface layer is the "catalyst" for the facile phase conversion. This new mechanism, termed as SurFPT (surface facilitated phase transformation), could be much more powerful in promoting polymorphic transformation in solutions than the well-known solution-mediated phase transformation.

Key words: acetaminophen, molecular dynamics simulation, dissolution, metastable form, solubility, orthorhombic, monoclinic, crystallization inhibition, polymorphic transformation, and surface facilitated phase transformation.

Introduction

Polymorphic transition has been extensively studied in the pharmaceutical field due to its significant impact on manufacturing and *in vivo* performance of pharmaceutical dosage forms.[17,117-119] A metastable solid form is energetically unfavorable and can convert to the

thermodynamically stable form either through solution-mediated transformation in solution or solid-solid transition over-time.[17,120]

Acetaminophen, a widely used analgesic and fever reducing medicine, has multiple crystal forms. Among them, monoclinic Form I and orthorhombic Form II are the most widely studied.[121-126] Form I and Form II are monotropically related, Form I being more stable[127] and used commercially. Form I is difficult to compress into tablets. Thus, a more costly wet granulation process needs to be performed prior to tableting.[128] The dry blend of orthorhombic Form II can be compressed directly to reduce manufacturing cost.[124,128] Unfortunately, efforts to produce Form II on an industrial scale have proved unfruitful because of the facile conversion to Form I in crystallization solvents.[129] In aqueous solutions, Form II also converted quickly to Form I[130] which is why accurate Form II solubility and dissolution data are missing from the literature for such a well-known drug and polymorphic system. Even a large single crystal of Form II gradually recrystallized into Form I at ambient temperature due to the inclusion of a small amount of water.[131] Since the conversion occurs in the presence of solution, it was assumed that the solution-mediated polymorphic transformation is the mechanism responsible for such a conversion.[121,125,132] However, the details of the transformation have not been understood, and the reasons for such fast conversion are mostly unknown. In particular, the following important questions have not been addressed.

1. What is the thermodynamic driving force for the Form II to Form I transformation?

2. Will Form II dissolution be able to generate the supersaturation level necessary for Form I to nucleate?
3. Are there other pathways to create the required supersaturation?
4. Are there alternative mechanisms that can account for the faster conversion?

Our present work is directed toward elucidating the mechanism of APAP Form II to Form I conversion in 0.15 M aqueous solution of NaCl (designated as solubility medium hereafter) at 37 °C. First, solubility measurement of Form II in the solubility medium at 37 °C was done accurately for the first time using a new experimental procedure. This answers the first question regarding thermodynamic driving force. Molecular dynamics (MD) simulations were then conducted to elucidate the structures of the solid phases during dissolution of both Form I and Form II. The energetics of the molecule association in the residual solids was studied through hydrogen bonding, pair correlation functions and interaction energy calculations, which provide molecular or even atomic level analysis that is not possible for any existing experimental methodology. The findings from MD simulation led us to propose a new solid-form conversion mechanism (surface facilitated phase transformation, SurFPT). Further experimental evidence is consistent with this new mechanism.

Experimental

Material

Acetaminophen anhydrous monoclinic polymorph (Form I) with high purity was purchased from Sigma (SigmaUltra, lot 116K0124). Deionized, distilled water for preparing all solutions was purified to 18.2 mΩ/cm resistivity by passing distilled water

through a deionizer/charcoal filter (Milli Q academic model, Millipore Corp., Bedford, MA). Poly(vinyl pyrrolidone) (PVP) grade K30 was from Spectrum (lot XM3057). Sodium chloride and other solvents and reagents used met ACS Reagent specifications.

Powder X-ray Diffractometry (PXRD)

Powder X-ray diffraction patterns of the samples were obtained using an Ultima+™ diffractometer controlled by DMAX2000 software (Rigaku Corp., Tokyo, Japan). The X-ray source was a copper filament X-ray tube operated at 50 kV and 40 mA. Calibration of the goniometer was monitored using standards (Sodalite and Si) prior to use. Micro cover slides (0.15 mm in thickness) with a thin layer of samples were top-loaded onto a zero background holder, and were scanned from 2–40° 2θ at 2–3°/min in a non-spinning mode. Data analysis was accomplished using Jade software (Version 6.5, Materials Data, Inc., Livermore, CA).

Preparation of APAP Form I and Form II Crystals

Form I

Crystals of Form I of sufficient size were prepared by recrystallization from water according to reported procedures.[133] The recrystallized crystals were monoclinic Form I by PXRD (data not shown). The crystals in a sealed bottle were stored in a desiccator at ambient temperature until use.

Form II

Multiple solution crystallizations were attempted in order to obtain sufficient amount of metastable Form II. In one method, crystallization was conducted from ethanol at 0 °C with seeding of melt-quenched Form II and harvesting crystals at 15 min.[125]

Many repetitions of this method resulted in Form II contaminated with Form I. Variations to this method by harvesting crystals at 2.5 min, by adding polymers (PVP or HPMC) to crystallization medium, by switching to a different solvent with lower APAP solubility (i.e. ethyl acetate and acetonitrile), and by lowering temperature using dry ice, all resulted in mixture of Form I and II in repeated experiments. Additionally, crystallization in the presence of 10 mg/mL alginic acid sodium salt was conducted according to a published method,[134] but without success.

Pure metastable Form II used in the studies was crystallized from the melt of Form I following a published method[125] with some modifications. A thin layer (~10 mg) of Form I powder was spread in the center of a micro cover glass (18 × 18 × 0.15 mm, no. 1, VWR International, Pennsylvania, US), which was heated for ~3 seconds on a hot plate set at 170 °C (above m.p. of 168.6 °C[104]). The clear melt on the cover glass was cooled down to ambient temperature (~23 °C). Crystallization started at about 5 min. After 30–60 min, the cover glass was stored flat in a sealed glass petri dish under ambient conditions. The sample was allowed to age for at least two days. Right before use, each cover glass was directly placed on an X-ray sample holder for PXRD analysis. Only those confined to pure Form II according to PXRD were selected in solubility and surface crystallization studies.

Solubility Measurement of Form I and Form II

Form II

The first step was to identify a polymer that can retard or inhibit the conversion of Form II to Form I in solubility medium. PVP was selected based on its interaction with

APAP.[135] The PXRD-confirmed pure Form II on the cover glass was topped with the solubility medium in the absence and presence of 20 μg/mL PVP (0.002%). After 45 min at ambient temperature, the liquid was removed by a filter paper, and the cover glasses were brought for PXRD scan. The sample without PVP was found to contain Form I peaks, while PVP was shown to effectively prohibited the formation of Form I (data not shown). Therefore, 20 μg/mL PVP was added to the solubility medium in the solubility measurement.

Equilibrium solubility of Form II was carried out at 37 °C in the solubility medium containing 20 μg/mL PVP. A procedure very different from conventional shake flask method was designed to enable this measurement. Solubility medium with PVP (150 μL) was added to the cover glass to top the surface of the Form II crystal layer. The cover glass, supported by an X-ray sample holder, was placed inside a container with a loose lid (i.e. a 60 mm × 15 mm cell culture dish). The dish was then loaded into a large diameter glass bottle (100 × 50 mm) and tightly sealed with a lid. Further, to prevent the loss of the solubility medium through evaporation which might lead to inaccuracy of the solubility, the water vapor pressure inside the glass bottle was maintained by including two beakers, each holding 5 mL of solubility medium with 20 μg/mL PVP. Finally, the whole assembly was equilibrated at 50 rpm in a horizontal shaker (Incubating Orbital Shaker, VWR International, Pennsylvania, US) set at 37 °C. Sampling was made by taking out the X-ray sample holder and inserting a pipette tip into the clear solution phase at multiple time points of about 20, 40 and 60 hrs. The clear solution sample was diluted with water in a volumetric flask and analyzed by a HPLC assay using a five-point

external standard curve. After taking the last sample, the residual solid on the cover glass was again scanned for PXRD patterns. A total of 11 replicates were tested. The solubility values obtained from samples with final solid form remaining as pure Form II or mostly Form II were averaged and reported as the solubility of Form II.

Form I

Equilibrium solubility was determined at 37 °C in the solubility medium in the absence and presence of 20 μg/mL PVP (0.002%). Several crystals of recrystallized Form I (total weight of ~35 mg) were weighed into a 4 mL glass vial and 0.5 mL of solubility medium was added. The glass vials, in triplicate under each condition, were agitated in the same way as the Form II samples on the horizontal shaker. Sampling and concentration analysis were also performed following the same procedure used for Form II. The average concentration of the saturated solutions was reported as the solubility at 37 °C.

Physical Stability of APAP Solutions Supersaturated at Concentrations of Form II Solubility and Above

This experiment determined if Form I can crystallize in solutions when the APAP concentration is at or greater than saturation solubility of Form II. Concentrations selected to study were 25, 26, 27, 28, 29, 30, 32, 34, 35 and 45 mg/ mL in the solubility medium, each in triplicate. These supersaturated solutions were prepared by heating suspensions of APAP Form I in sealed 4 mL glass vials on a heating block initially at 50 °C and then briefly at 60–70 °C with shaking. The 45 mg/mL samples were further heated at 80 °C for ~2 min. The clear solutions were quickly transferred to the orbital

shaker set at 37 °C and 50 rpm (same conditions as used in the solubility study). Crystallization was monitored visually up to 12 days.

Theoretical Methods

Building the Crystal

Virtual crystals of Form I and Form II were constructed using the unit cell as a building block in Mercury software (Mercury 2.3, CCDC 2001-2009), following the method previously published in MD simulation of APAP Form I.[41] The two crystal lattices were built to render the best match in terms of overall geometric shape. As reported before,[41] the monoclinic anhydrous Form I lattice repeated the unit cell four times along all three axes. The resultant lattice is referred to as APAP I 4 x 4 x 4. The orthorhombic anhydrous Form II lattice extended the unit cell at *a*, *b*, and *c* directions for 3, 3 and 4 times, respectively, producing the APAP II 3 x 3 x 4 crystal lattice. The single crystal structure of Form II was taken from HXACAN[136] available from the Cambridge Structural Database (Cambridge, UK). More details of crystal lattice parameters of both APAP polymorphs built for MD simulation are listed in Table 2.

Table 2. Comparison of the Built Crystal Lattices of APAP I 4 × 4 × 4 and APAP II 3 × 3 × 4

Polymorph	Unit cell dimension (Å)			*Z*	Lattice built	Crystal dimension (Å)			no. of molecules in lattice	Crystal surface area ($Å^2$)	Length of edges (Å)	Crystal size (nm)
	a	*b*	*c*			*a*	*b*	*c*				
Form I, monoclinic	12.93	9.40	7.10	4	4×4×4	51.72	37.60	28.40	256	8.67×10^3	1430.9	4.56
Form II, orthorhombic	11.81	17.16	7.39	8	3×3×4	35.42	51.49	29.57	288	8.79×10^3	1426.0	4.69

Preparing the Crystal for Simulation

The crystals constructed above were prepared using Visual Molecular Dynamics software (VMD, version 1.9, March 2011).[99] First, the structure file of the crystal was built using the Automatic PSF Builder function from the input of the Mercury file and the APAP topology file. The topology and atom types for the CHARMM27[39] force field for APAP were obtained by comparison with similar molecules already in the standard topology file. Second, a water box was built to surround the crystal. The water box (containing 0.15 M sodium chloride) extends 40 Å on each side of the crystals. The final size of APAP I 4 x 4 x 4 in water box is 131.7 × 117.6 × 108.4 $Å^3$ (equal to 1.51 × 10^{-18} milliliters, with 58622 TIP3 molecules), and that of APAP II 3 x 3 x 4 is 115.4 × 131.5 × 109.6 $Å^3$ (equal to 1.66 × 10^{-18} milliliters). The ratio of water molecules to NaCl molecules in the system is 370 to 1.

1a

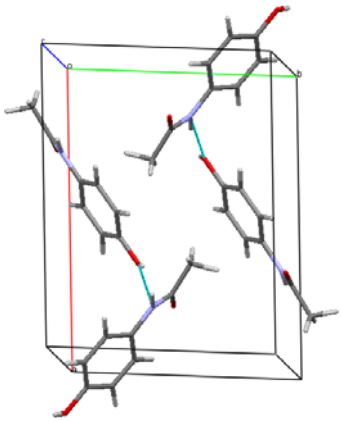

1b

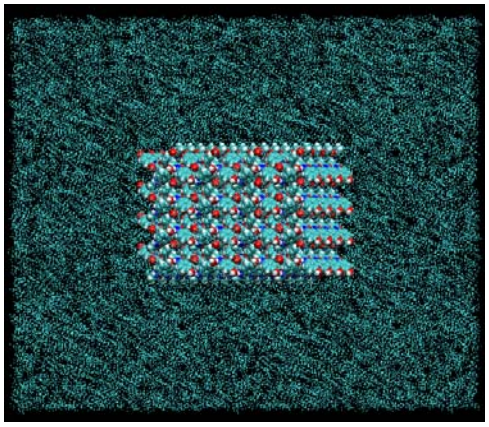

2a

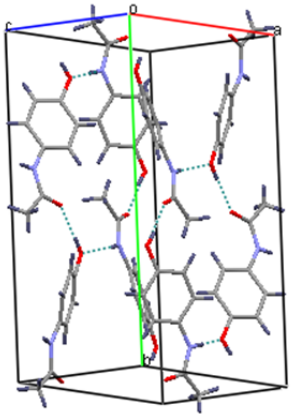

2b

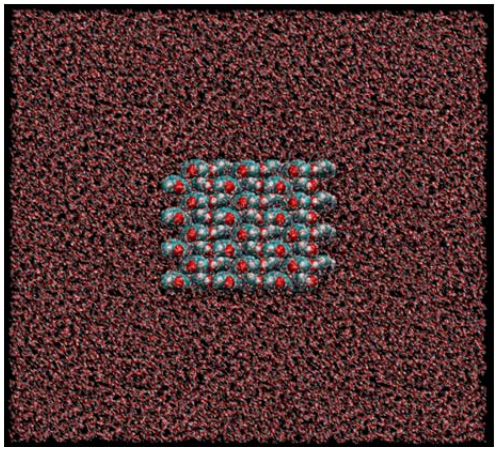

Figure 20. (1a) Unit cell of monoclinic Form I (dotted line indicating hydrogen bonds). (1b) APAP I 4 x 4 x 4 crystal in the 131.7 × 117.6 × 108.4 $Å^3$ water box. (2a) Unit cell of orthorhombic Form II (dotted line indicating hydrogen bonds). (2b) APAP II 3 x 3 x 4 crystal in the 115.4 × 131.5 × 109.6 $Å^3$ water box.

MD Simulation

The computer code used for the MD simulations was the parallel, scalable MD program NAMD version 2.5.[100] Periodic boundary conditions were used. The cutoffs for nonbonding (van der Waals and electrostatic) interactions were 12 Å. The switch distance was 10 Å, and a 1.0 1–4 scaling factor was used. The crystal in the water box was first subjected to energy minimization (6000 steps) followed by slow heating from 10 to 310 K over 30000 steps. The temperature and pressure of the system were equilibrated for 10000 steps using a Langevin piston. The system was then allowed to equilibrate for 30000 steps at constant temperature (310 K) and pressure (1 atm) before production data was accumulated. Production simulations (10 ns) were performed at constant volume and temperature.

Analysis of MD Simulation Data

Calculation of Number of Molecules Dissolved vs Time

The number of APAP molecules out of the sphere of the original crystal lattice and into the water box were tracked at 0.03 ns intervals for 10 ns simulations for both Form I and Form II, using a script written for the VMD program (version 1.9).[99] The data were plotted using Microsoft Excel (Version 2010).

Calculation of Interaction Energies

Interaction energies were calculated as previously described[41] using algorithms of the van der Waals and electrostatic energies and the NAMD program.[100] These calculations were performed for APAP molecules located on corners and edges with their surrounding APAP molecules or water molecules within 4 Å. The electrostatic

interactions, including ion–dipole interactions and H-bonding, and van der Waals were calculated using the partial atomic charges (CHARMM 27 potential function[39]). The sum of electrostatic and van der Waals interaction energies is the total interaction energy reported here.

Calculation of Hydrogen Bonds

The numbers of hydrogen bonds formed throughout a trajectory among APAP molecules in both Form I and Form II were calculated by HBonds Plugin (version 12) in VMD program (version 1.9).[99] A hydrogen bond was counted between an atom with a hydrogen bonded to it (the donor, D) and another atom (the acceptor, A) by defining that the distance D-A is less than 3.4 Å and the angle D-H-A is less than 30 degrees. The percentage of H-bond broken normalized to the initial H-bond numbers was constructed for both Form I and Form II, and plotted against the time scale.

Calculation of Radial Distribution Function g(r)

The radial distribution function g(r) of APAP, also called pair correlation function, over a given trajectory of Form I or Form II in the water box was computed by g(r) GUI Plugin (version 1.2) in VMD program (version 1.9).[99] An APAP molecule located in the center of the crystal was the chosen origin. The spherical shell was defined as 50 Å from the origin. The periodic boundary conditions were enabled during the calculation. The calculated g(r) describes the variations in atomic density as a function of distance from the origin to the coordinates of other APAP molecules within the defined spherical shell.

Polymorphic Transformation Determined by PLM and PXRD

Polarized light microscopy (PLM) was used to visualize the re-crystallization of Form I from Form II and the crystallization from amorphous form and PXRD was to confirm the polymorph transformation. Form II was prepared on a micro cover slide as described above. The amorphous form was made the same way; the melt-quenched amorphous solid was used prior to any crystallization. The sample was placed under a polarized light microscope (model Eclipse E-600 POL, Nikon Corp., Garden City, NY) with a 200× magnification lens. Images were taken using MetaMorph imaging system (version 4.6R8, Universal Imaging Corporation, Downingtown, PA). Droplets of solubility medium were added to completely cover the solid. Changes were monitored visually by capturing images periodically. In the end, the cover slide with the sample on the top (after the added liquid was removed) was loaded directly on a X-ray holder and scanned for PXRD patterns.

Results

Solubility of APAP Polymorphs

Form I

Solubility was measured by dissolving crystals in the solubility medium at 37 °C. The resulting clear solution phase was directly analyzed without phase separation through centrifugation or filtration. The thermodynamic solubility of Form I was found to be 19.7 ± 0.3 mg/mL in the absence of PVP, and 19.4 ± 0.3 mg/mL in the presence of PVP. The polymer at a low concentration of 20 μg/mL did not impact the solubility of APAP in

aqueous solution to any measurable level. These values are consistent with our previously reported solubility using the classical solubility method.[41]

Form II

The thermodynamic solubility was measured from dissolving Form II crystals on micro cover glasses. The clear solution phase was analyzed directly without centrifugation or filtration. Eleven of these micro cover slides with no detectable Form I by PXRD were subjected to solubility measurement at 37 °C. The solubility medium contained pre-dissolved 20 μg/mL of PVP. After about 57–62 hours of equilibration, seven of the eleven replicates were found to have changed to either pure Form I or mainly Form I by PXRD, resulting in concentrations reaching or approaching the solubility of Form I (data not shown). Data from these seven replicates were not used. However, four replicates remained as either pure Form II or mainly Form II at the end of equilibration (Figure 21). These four replicates maintained a higher concentration than that of Form I up to 60 hours (Figure 22). The slight conversion to Form I in some of the Form II replicates did not decrease the concentration at ~60 hours because substantial Form II was still present to feed into the solution. The concentration reached for the four replicates at time greater than 33 hours is taken as the thermodynamic solubility of APAP Form II. The average value of the Form II solubility was calculated as 24.7 ± 0.6 (n=4), about 5.3 mg/mL higher than Form I solubility at 37 °C. The solubility ratio between the two APAP polymorphs is thus calculated to be 1.27 ± 0.04, which corresponds to –0.62 kJ/mole difference in free energy.

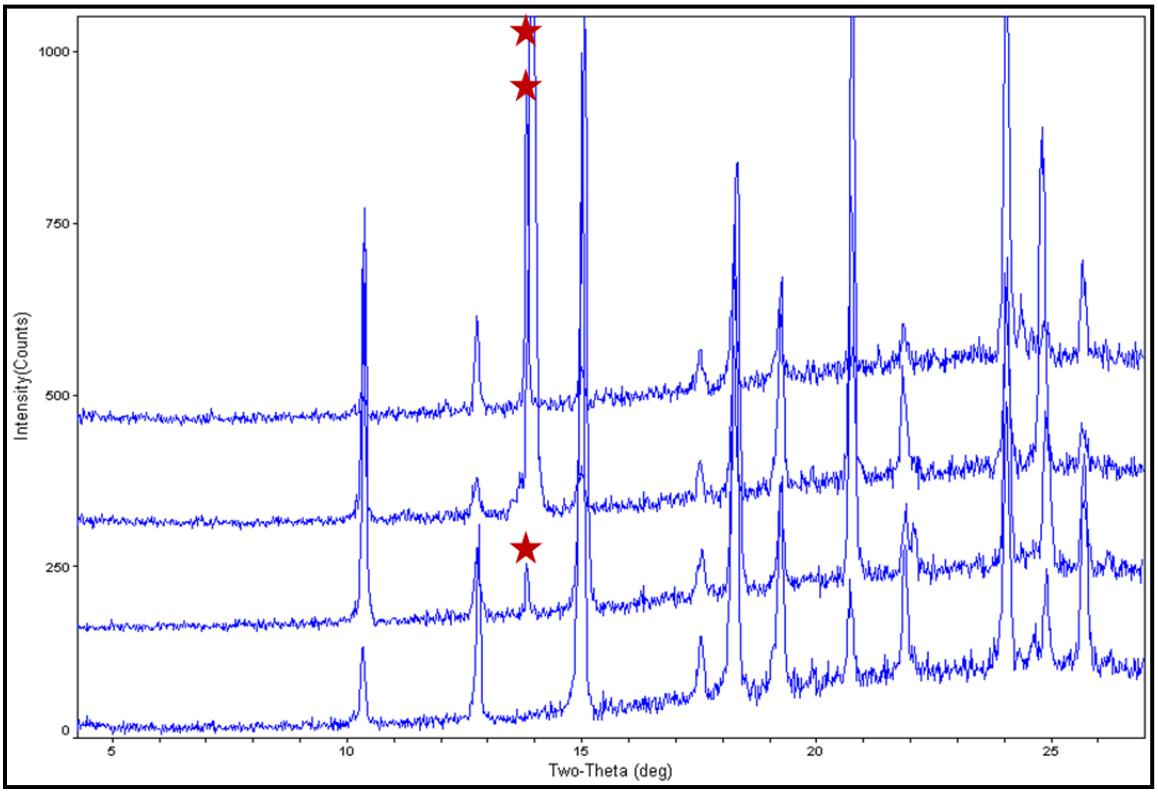

Figure 21. PXRD patterns of residual solid recovered from solubility measurement of Form II in 0.15 M aqueous solution of sodium chloride in the presence of 20 µg/mL of PVP at 37 °C. The four patterns from bottom to top correspond to Form II replicate no.1 to replicate no.4 in Figure 22. Only one Form I peak was observed in three of the four replicates as marked with the star. PXRD pattern of pure Form I is shown in Figure 30.

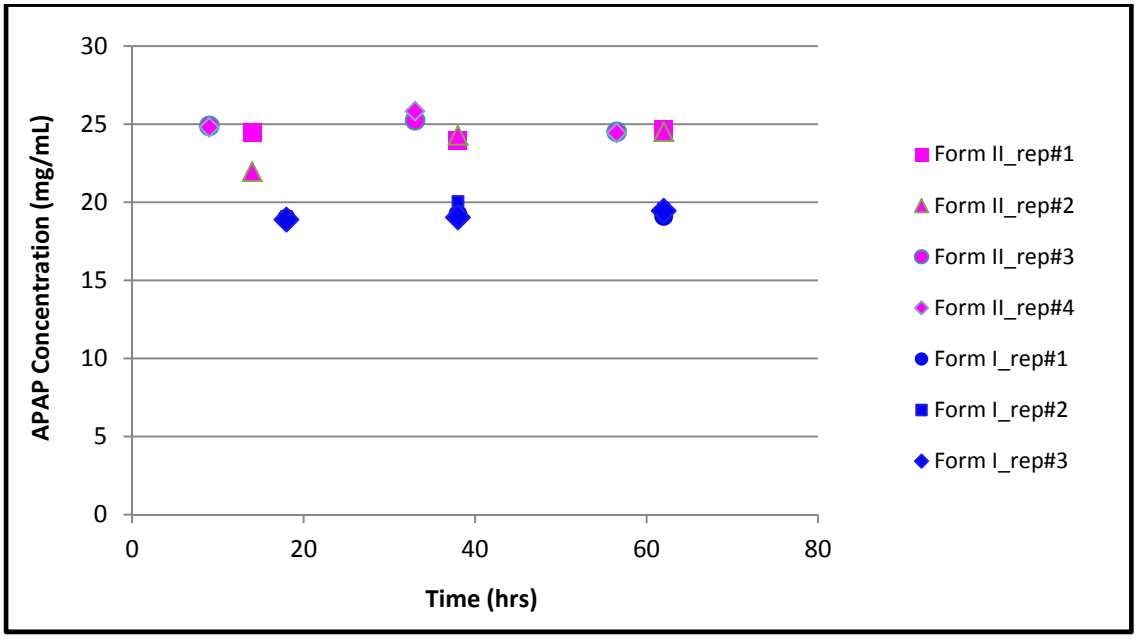

Figure 22. Concentration vs time course during solubility measurement of APAP Form I (three replicates) and Form II (four replicates) in 0.15 M aqueous solution of sodium chloride at 37 °C.

Physical Stability of Supersaturated APAP Solutions

Supersaturated APAP solutions in the solubility medium at concentrations at and above solubility of Form II were studied for physical stability. Supersaturation (S) is defined as the concentration divided by Form I solubility. Ten APAP solutions at 25 (≈ Form II solubility), 26, 27, 28, 29, 30, 32, 34, 35 and 45 mg/mL (S = 1.27x – 2.28x), each with three replicates, were agitated at 37 °C, and the crystallization was monitored visually. As shown in Figure 23, no crystallization was observed for up to 10 days at 25–30 mg/mL (S = 1.27x – 1.52x), and for 4.5 days at 32–34 mg/mL (S = 1.62x – 1.73x),

indicating that Form I is not able to nucleate from the solution at and even significantly above the Form II solubility within the time window of the solubility measurement.

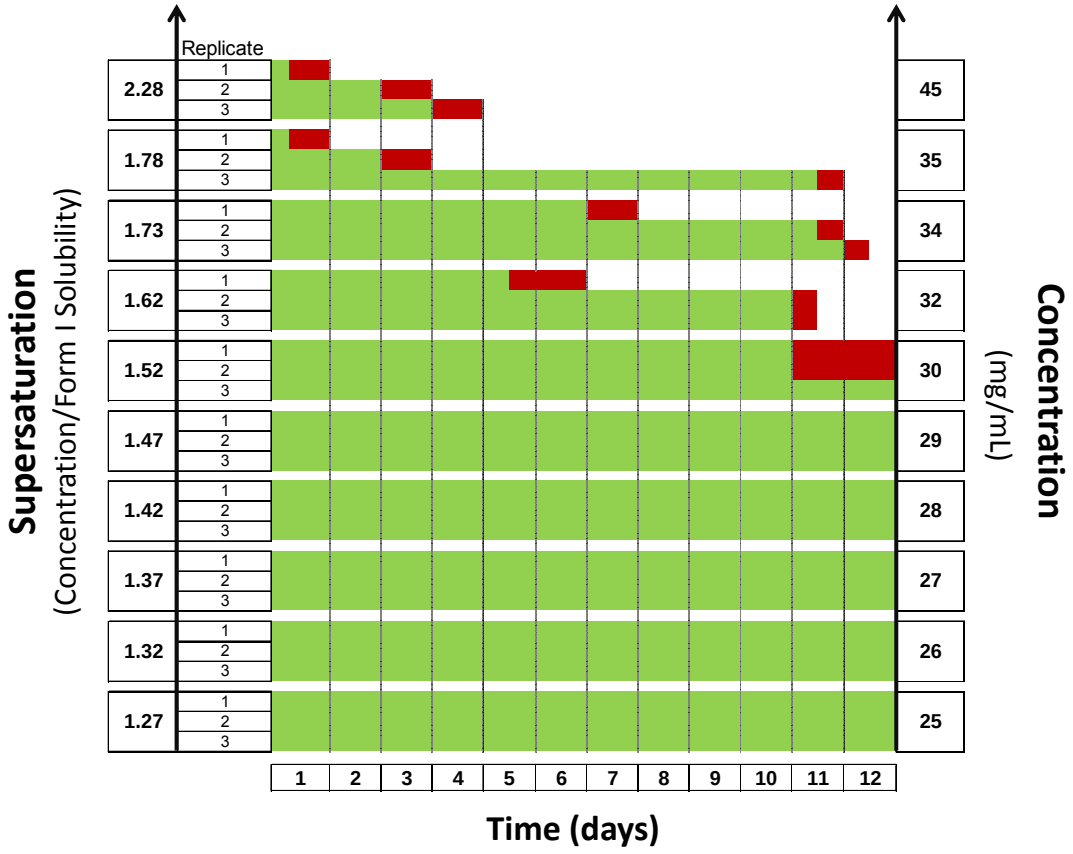

Figure 23. Physical stability of APAP supersaturated solutions in 0.15 M sodium chloride agitated at 50 rpm and 37 °C for 12 days. Supersaturation (S) levels tested were 1.27x – 2.28x of Form I solubility (25 – 45 mg/mL). S of 1.27x (25 mg/mL) is at Form II solubility. Green color indicates clear solutions and red color band represents the time window during which crystallization occurred.

MD Simulation of

APAP Polymorph Dissolution

Molecular dynamics (MD) simulations were conducted to investigate the molecular level dissolution behavior and the solid state differences. The Form I and II virtual crystals for MD simulation were built to match each other as closely as possible in terms of total surface area, the numbers of APAP molecules, as well as the total length of edges (Table 2), all of which are important in dissolution rate comparison.[41] Both crystals were placed in water boxes with additional 40 Å from each side. If the crystals were to dissolve completely, the theoretical molar concentration would be approximately the same (APAP I = 0.282 mM, and APAP II = 0.288 mM) that is about 2-fold of the Form I solubility.[41]

The MD simulation visualized the departure of APAP molecules from the crystal surface into the water phase, which then displayed them by thermal motions (moving around freely in water). Images at 0, 3 and 10 ns are shown in Figure 24 to compare Form I and Form II. As expected, most of the dissolved APAP molecules are initially located on corners and edges for both forms (Figure 25) which has been demonstrated previously.[41] The numbers of molecules leaving the solid surface were plotted as a function of time in Figure 26a. Under this treatment, Form I and II do not exhibit any significant difference in the rate of dissolution. Another comparison between APAP I and APAP II was made for the initial interaction energies for the APAP molecules located on the corners and edges. As we have demonstrated earlier,[41] the interaction energy among the drug molecules would deter dissolution, while the interaction energy between the

drug and water molecules would favor the dissolution. Thus the driving force for dissolution is the difference between these two forces (total interaction energy of APAP with water minus that of APAP with APAP), which is plotted along the *x*-axis in Figure 26*b* indicating that the driving force for dissolution for the molecules on the corner and edge molecules are strikingly similar between Form I and Form II.

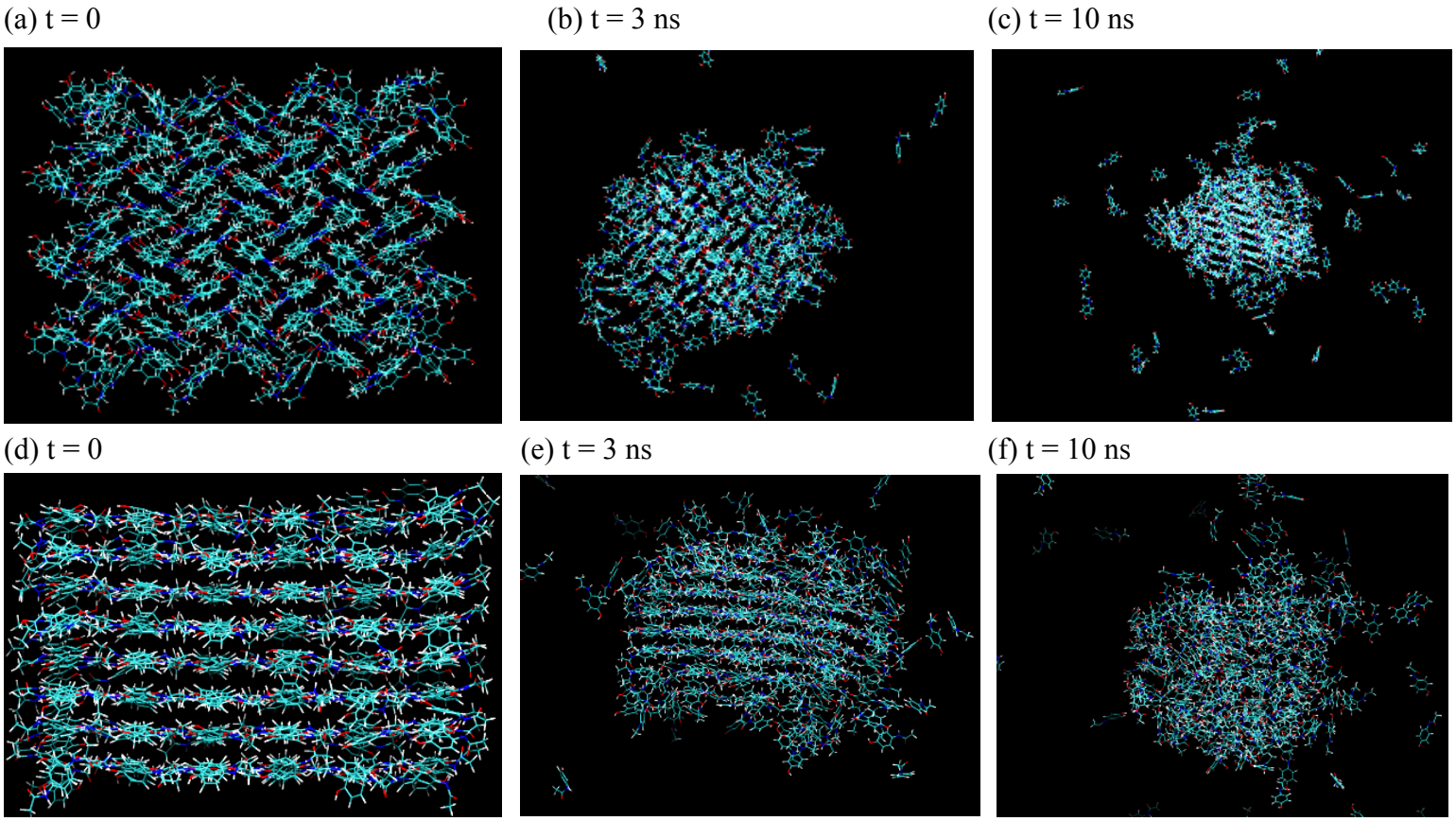

Figure 24. Display of images of two crystals from MD simulations. a to c: APAP I. (a) At 0 ns viewed down crystallographic *c* axis. (b) At 3 ns. (c) At 10 ns. d to f: APAP II. (d) At 0 ns viewed down crystallographic *b* axis. (e) At 3 ns. (f) At 10 ns.

(a)

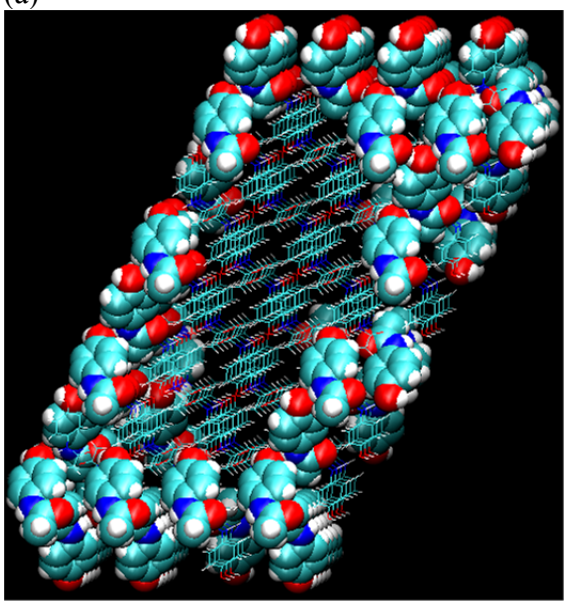

(b)

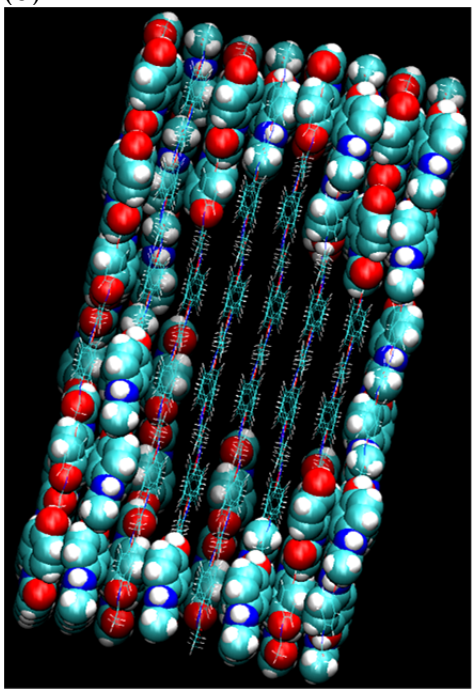

Figure 25. Demonstration of the corner and edge effect in dissolution simulation of a single crystal APAP in 0.15 M NaCl at 37 °C. Undissolved APAPs are shown in line style and dissolved APAPs are in bulky VDW style. (a) APAP I at 10 ns. (b) APAP II at 10 ns.

(a)

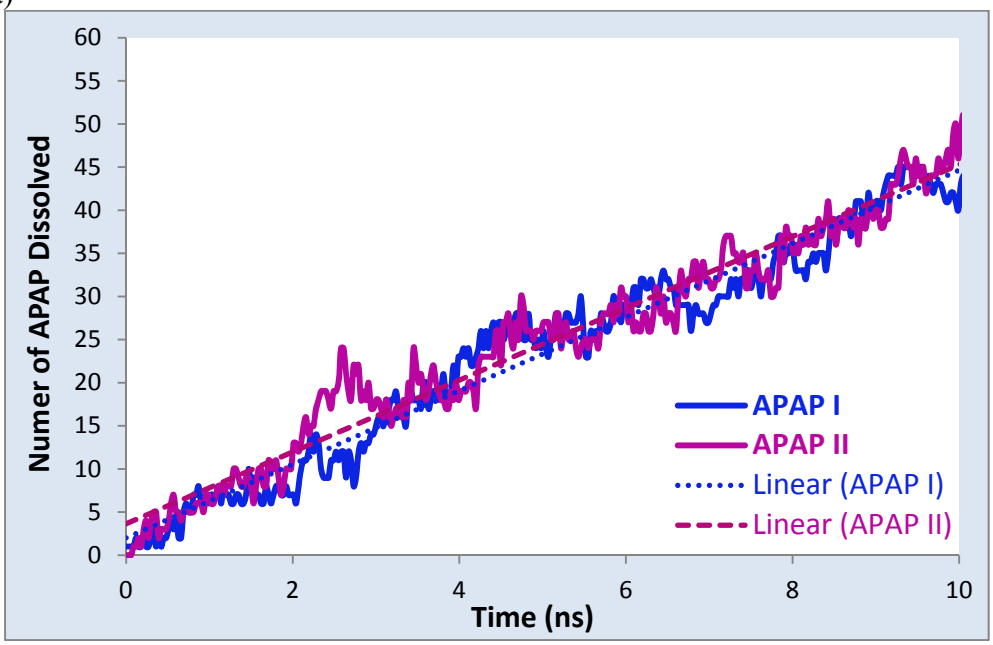

(b)

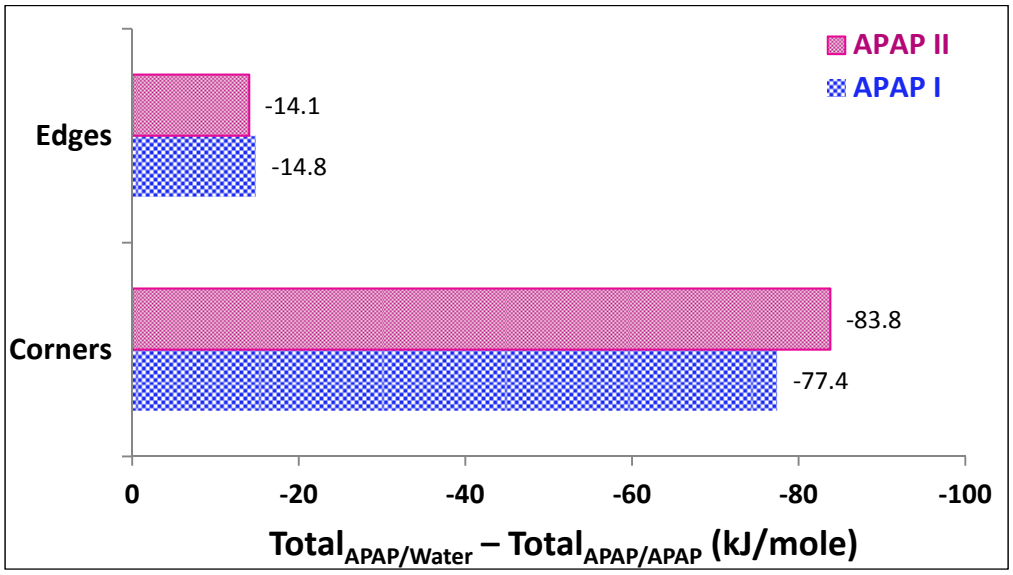

Figure 26. Numbers of molecules leaving the crystal as a function of time and the correlation with the initial total inter- and intra-molecule interaction energies. (a) Numbers of APAP molecules observed outside of the crystal surface from MD simulation of stable polymorph APAP I and metastable polymorph APAP II in 0.15 M sodium chloride at 37 °C. (b) Initial (t = 0 ns) total interaction energy difference between the intra-molecule (APAP/water) and inter-molecule (APAP/APAP) interactions on corners or edges. This difference is the major driving force for initial dissolution.

Differentiation of Form I and II was noticed in the solid state during simulation. As illustrated in Figure 24, the difference between Form I and Form II solid phases is clearly visible. After 10 ns, the undissolved Form I solid retained its long range order shown as well-organized crystal lattice (Figure 24-*c*), while the crystallinity of the remaining Form II solid is limited only to a small area in the center, and the rest of outer layer molecules turned into a thick mass of disordered molecules (Figure 24*f*). This difference was analyzed quantitatively through two methods. Since hydrogen bonding is one of the major forces associating molecules in crystal lattice, the H-bond profile in the solid phase reflects the stability. The percentage of H-bonds broken over time for both crystals were calculated (Figure 27). The stable Form I is shown to be more stable maintaining a higher percentage of intact H-bonds. At 10 ns, 61% of the APAP II H-bonds were broken vs 41% in APAP I. Another analysis of the solid state difference is the radial distribution function of both forms for time 0 and 10 ns (Figure 28). The decrease in the radial distribution function indicates that the molecules have moved from their lattice positions. APAP I retains most of the structural features at the end of 10 ns, with some difference at $\geq$ 17.5 Å away from the center which can be attributed to a loss of molecules in the outer layers due to dissolution. However, APAP II displays a difference at 5 Å and beyond, indicating the loss of crystallinity in regions close to the center of the crystal.

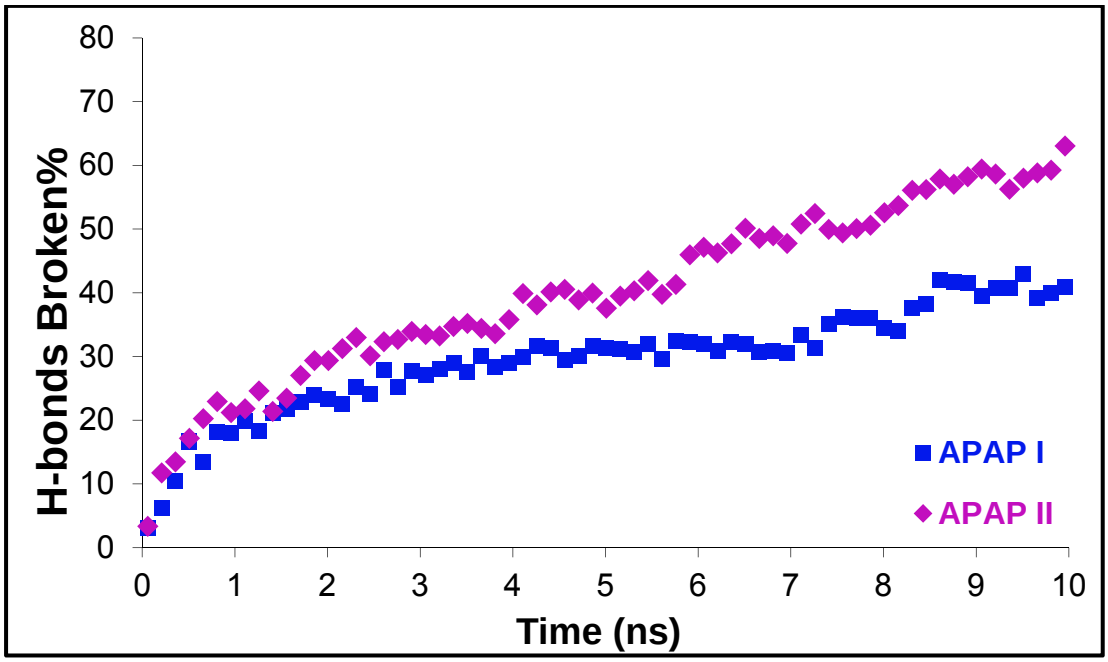

Figure 27. Percentage of H-bonds broken vs time obtained from MD simulation of stable polymorph APAP I and metastable polymorph APAP II in the aqueous solution of sodium chloride at 37 °C.

(a)

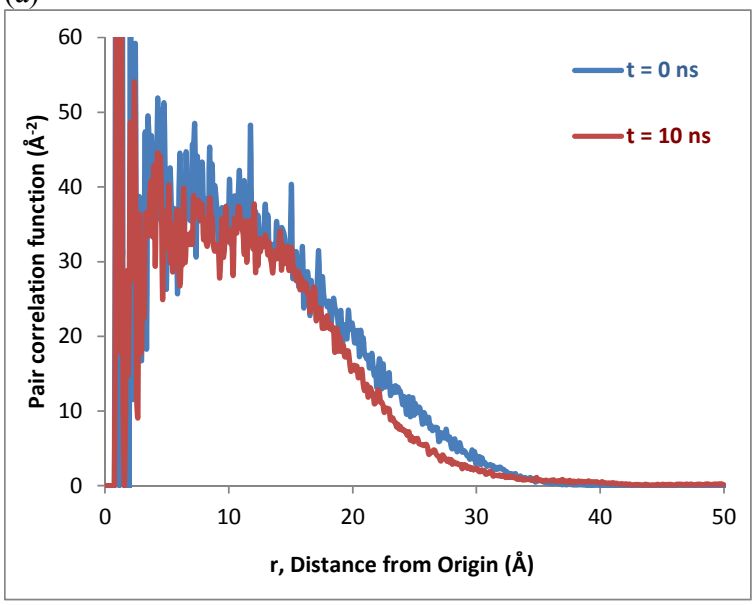

(b)

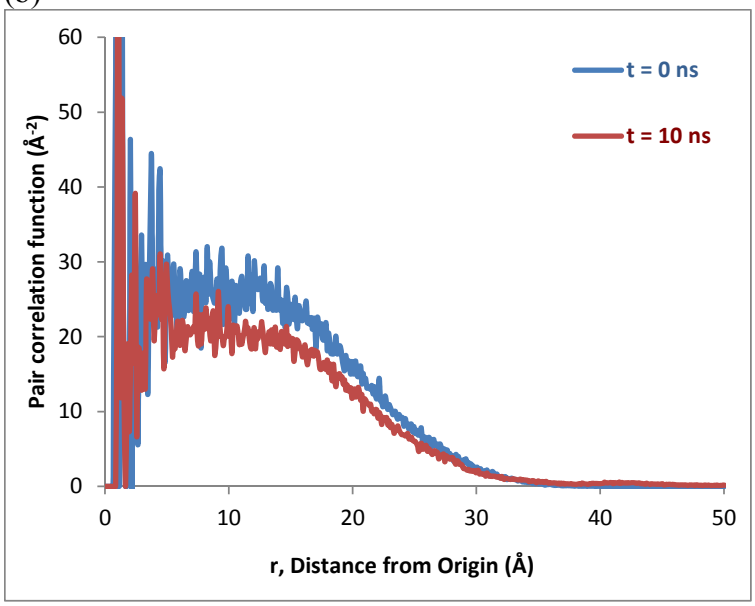

Figure 28. Pair correlation function calculated on the solid phases before and after dissolution simulations in the aqueous solution of sodium chloride at 37 °C. (a) Stable polymorph APAP I crystal. (b) Metastable polymorph APAP II crystal.

Crystallization of APAP Form I on Surfaces of Form II and Amorphous Solids

Surface-driven crystallization was studied by adding the solubility medium to films of Form II or to the amorphous form on a micro cover glass. The changes were viewed under polarized light microscopy (PLM) and further characterized by PXRD. The initial solid was pure Form II by PXRD (Figure 29*f,* bottom pattern). Under PLM, Form II crystal surface layers dissolved gradually as shown as the inward recess (Figure 29*b*,*c,d,e*) compared to time 0 (Figure 29*a*). During the course of dissolution, signs of re-crystallization are visible on the surface starting at 20 min, becoming especially evident at 40 min (Figure 29*e*). The PXRD obtained after 40 min exposure showed the appearance of Form I peaks (Figure 29*f, top pattern*), which demonstrates that the surface re-crystallized solid is the result of Form II to Form I transformation. More importantly, *no new crystals* were observed in the solution phase, and no protruding crystals on the surface, indicating that Form I grew from Form II on surface, a truly surface recrystallization instead of the solution-mediated transformation. In the case of the amorphous form (Figure 30), crystallization was observed instantaneously upon contact with the aqueous solution (Figure 30*b* taken at 25 seconds). The immediate PXRD scan (within 3 min) already showed crystallization to pure Form I (Figure 30*c*). This indicates that when in aqueous solution, the amorphous material crystallizes to the stable Form I rather than to Form II as it does in air.

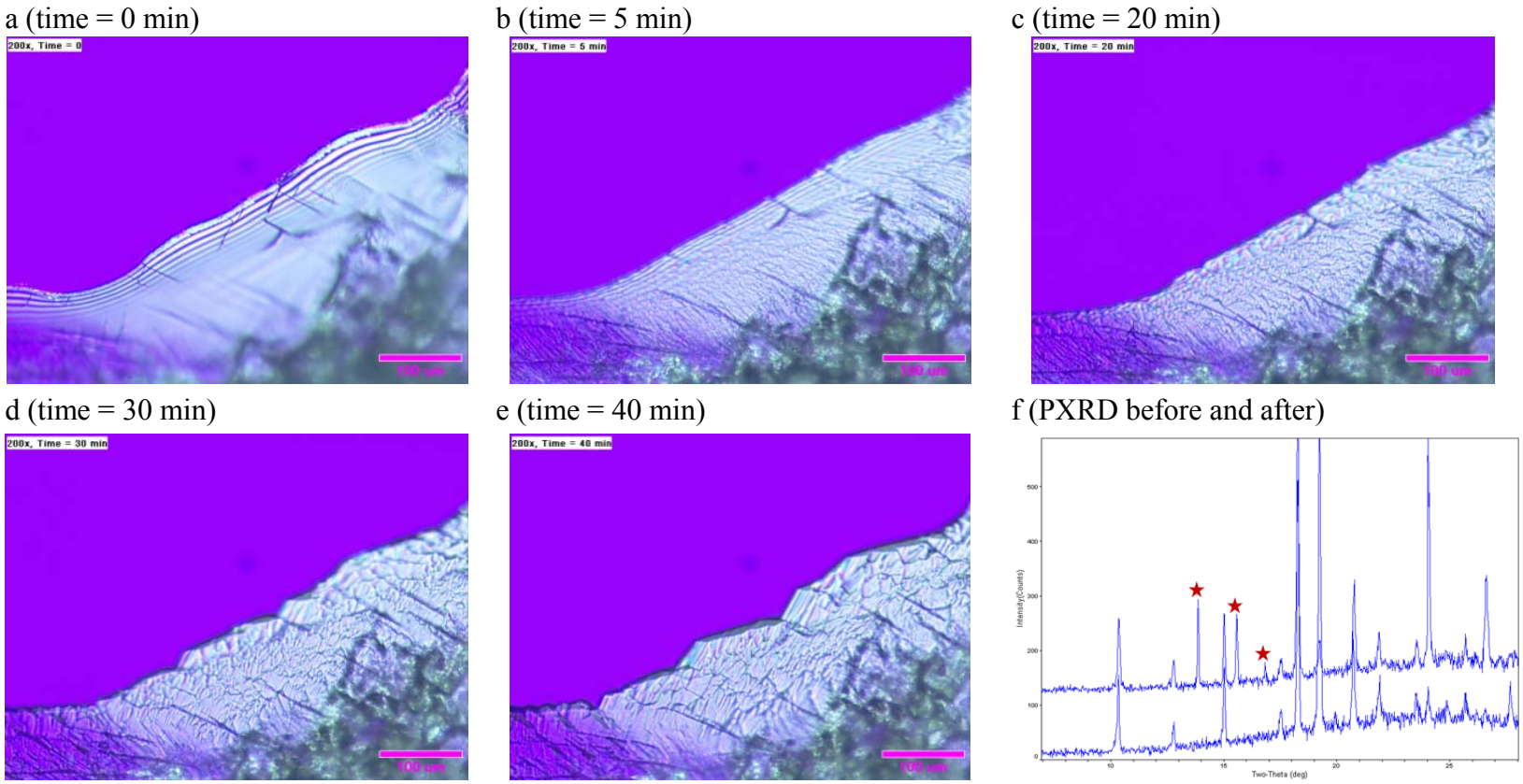

Figure 29. APAP Form II → Form I conversions studied by PLM and PXRD in 0.15 M NaCl at ambient temperature. (a) to (e) PLM images captured at time 0 and at different times after aqueous phase was added. The part of the crystal on lower right corner was at a different height, and therefore was not well focused. (f) PXRD patterns before (bottom) and after (top) aqueous phase was added, with the Form I peaks marked with stars.

a (time = 0)

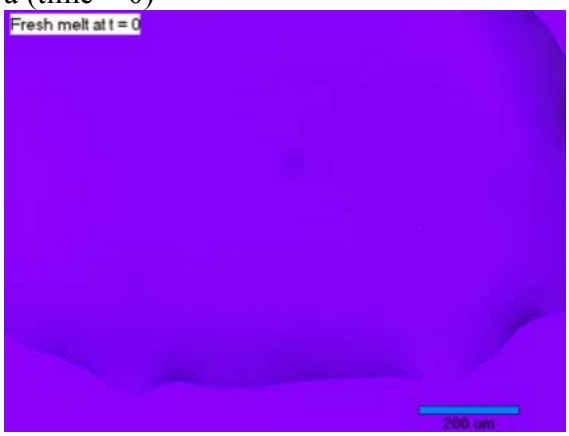

b (time = 25 seconds)

c (PXRD pattern at 3 min)

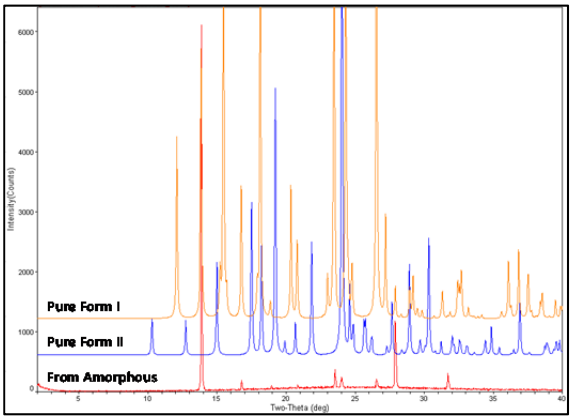

Figure 30. APAP amorphous → Form I conversions studied by PLM and PXRD in 0.15 M NaCl at ambient temperature. (a) PLM image of amorphous form before aqueous phase was added. (b) PLM image at 25 seconds after aqueous phase was added. (c) PXRD pattern of the final solid form shown on the bottom with overlaid pure Form I and Form II patters on the top.

Discussion

Thermodynamic Driving Force for Solution-mediated Polymorphic Transformation

Solution-mediated phase transformation (SMPT) is a process mechanistically defined by three consecutive steps:[17,137,18]

1. Initial dissolution of the metastable phase into the solution to reach and exceed the solubility of the stable phase;
2. Nucleation of the stable phase;
3. Crystal growth of the stable phase coupled with the continuous dissolution of the metastable phase.

Multiple publications report that APAP Form II converts to Form I through (SMPT).[125,121,132] These observations were primarily made in crystallization solvents by cooling a hot organic solvent solution or by adding antisolvent.[121,132,138] Our objective was to understand how crystallization of APAP Form I occurs when Form II is added to a solution with no APAP initially, such as in a dissolution of Form II.

How readily the stable form nucleates in step 3 of SMPT is correlated with the two forms' difference in Gibbs free energy, ΔG. The larger the ΔG is, the higher driving force is for nucleation of the stable form. ΔG is a function of the activity ratio of the two solid forms expressed in the equation of $\Delta G_{II\rightarrow I} = -RTln\frac{a_{Form\ II}}{a_{Form\ I}}$ where R is the ideal gas constant and T is the temperature in Kelvin. If the solubility (which approximates the activity) of the two solid forms could be accurately measured, obtaining the ΔG value would have been straightforward. Unfortunately, measuring APAP Form II solubility is a

two-decade long challenge mainly due to the facile conversion to the stable Form I in solutions.[129,130] The only available and often-cited solubility ratio of 1.3 (APAP Form II over Form I) is from a single, short (60 min) powder dissolution test in water at 37 °C.[139] In the paper, the concentration of APAP measured by UV spectrophotometry plateaued at 10 min with concentrations approaching 17 mg/mL for Form I and 22 mg/mL for Form II (which gives the ratio of 1.3). This Form I solubility of ~17 mg/mL is not consistent with many other publications. For example, at lower temperature of 30 °C the solubility in water is 17.4 mg/mL,[140] at 37 °C the solubility increases to 21.02 ± 0.13 mg/mL in water[141], and to 20.0 ± 0.2 mg/mL in water with 0.15 M NaCl.[41] Therefore, it is probable that saturation had not been reached at 17 mg/mL.

There have also been a number of reported attempts by calorimetry to determine the relative stability of acetaminophen Form I and Form II.[127,104,131,142] The heat capacity (C_p) and fusion data were experimentally determined either by differential scanning calorimetry (DSC) on the *in situ* melt-quenched Form II from,[104] by sublimation and solution calorimetry,[127] or by adiabatic calorimetry on Form II single crystals.[131] Based on the C_p, the thermodynamic functions (enthalpy, H, and entropy, S) were derived, which can then be used to calculate the $\Delta G_{II \rightarrow I}$ using the equation: $\Delta G_{II \rightarrow I} = \Delta H - T\Delta S$. The $\Delta G_{II \rightarrow I}$ from three such reports displayed a large disparity, from approximately –3.0 kJ/mole [104] to –3.9 kJ/mole[127] to –13 kJ/mole[131] at 25 °C, corresponding to Form II/Form I solubility ratios of 3.3, 4.8 and 197.2 respectively. Therefore, a conclusive answer to the energy difference (thus solubility ratio) between APAP polymorphs is still absent.

As discussed above, the free energy difference between the two solid forms is the key to understand the driving force of APAP Form II to I conversion in solution. The solubility measurement is a more straightforward way to determine the free energy difference. The challenge of obtaining accurate solubility measurements for Form II is two-fold. The first is the difficulties in obtaining pure Form II in sufficient quantity. Form II crystallization from ethanol was always contaminated with a small amount of Form I, consistent with the findings from others.[143] Crystallization from the melt[125,143] was found to be reliable, and pure Form II was made reproducibly. Therefore, we have adopted this method in our study. The second challenge is the physical instability of Form II in solution. To counter this, we applied a polymer as crystallization inhibitor to extend the window of physical stability. A very low concentration of PVP (0.02% or 20 ug/mL) was able to inhibit or delay the APAP form conversion without affecting the solubility in our study. Procedurally, changes to the traditional shake flask method are necessary for this difficult measurement. The measurement was directly performed on the micro cover glass which avoided complications such as Form I contamination when grinding and combining different batches. By this new method, minimal sample is required (since pure Form II is difficult to make in large amounts), the solution phase can be collected without filtration, and the residual solid can be easily recovered and analyzed by PXRD.

This new experimental methodology resulted in a successful solubility measurement of APAP Form II in aqueous solution of 0.15 M NaCl at 37 °C. The Form II solubility of 24.7 ± 0.6 mg/mL is reliable supported by the reproducibility among the four Form II replicates (Figure 22), and most convincingly by the PXRD results

confirming the residual solid phase collected at equilibrium being pure or mostly pure Form II (Figure 21). Based on the Form I solubility of 19.7 ± 0.3 mg/mL measured under identical conditions, the solubility ratio of Form II over Form I is calculated to be 1.27 ± 0.04. This ratio is somewhat close to the predicted value using the Hoffman equation[144] (1.2), and is quite far from the predicted value using the ideal solubility equation (1.5).[145] A recent paper[142] reported intrinsic dissolution rates (IDR) of 1.50, 1.33, and 1.31 mg/mL/cm^2, respectively for Form II prepared by melt quenching of three different APAP I materials (coarse, micronized and nano-silica coated), and 1.14 mg/mL/cm^2 for Form I. IDR correlates with solubility, thus an average IDR ratio of Form II over Form I of 1.21 ± 0.09 can be calculated, which is lower but close to our measured solubility ratio although the data are more variable and the remaining tablets were not characterized to identify the final solid form. Our measured solubility ratio of 1.27 ± 0.04 ($\Delta G_{II \rightarrow I}$ = ca. – 0.62 kJ/mole) is significantly below the average solubility ratio (1.7) among the known polymorph systems surveyed by Pudipeddi and Serajuddin.[145] Therefore, the thermodynamic driving force for From II to Form I conversion is quite low.

Since we have determined the solubility ratio of APAP Form II over Form I at 37 °C, we can now address the question: Is the dissolution of Form II able to reach the supersaturation level required for Form I to crystallize? Figure 23 demonstrates that Form I is not able to crystallize from solutions at supersaturations of 1.27x – 1.52x over Form I solubility (1.27x is at Form II solubility) over the course of up to 10 days of agitation at 37 °C. Form II would have had ample time to dissolve and reach saturation before Form I is crystallized from the solution. But the reality is the opposite. This strongly suggests

that primary nucleation through solution-mediated polymorphic transformation is not the mechanism dictating the facile APAP Form II to Form I conversion in solution. The rapid conversion from Form II to Form I in solution must be due to other reasons.

MD Simulation of Differences between APAP Polymorphs during Dissolution

Simulated dissolution profiles of APAP I and APAP II nanocrystals (4.6–4.7 nm as shown in Table 2) were constructed. The numbers of molecules leaving the crystal sphere were found to be almost identical between the two crystals within the 10 ns simulation (Figure 26*a*). This appears to contradict the thermodynamic stability relationship of the stable Form I *vs* the metastable Form II at 37 °C. However, nanoparticles with sizes down to <100 nm can increase saturation solubility,[114] and our calculation indicated a 3.4-fold solubility increase when the particle size is reduced to 4.6 nm.[41] This 3.4 folds higher solubility could attenuate the difference between the two forms if such a difference is small to start with. More importantly, we have demonstrated[41] that the initial dissolution rate is profoundly affected by the corner and edge effect (molecules at corners and edges dissolve first). In nanocrystals of APAP I and II, the molecules that dissolve within 10 ns came mainly from on the corners and edges (Figure 25*a*,*b*). A much higher percentage of molecules become edge or corner bound when the crystal is nanosized rather than macroscopic. Therefore, the corner and edge effect dominates the initial dissolution of a tiny nanocrystal. Further, the driving force for dissolution is the strength of drug molecule interaction with water being greater than drug-drug molecule binding energy.[41] This driving force is favorable since the net interaction energies are negative (Figure

26*b*). A striking closeness between Forms I and II was observed, with comparable net interaction energy values residing in the edges (–14.8 kJ/mole for Form I and –14.1 kJ/mole for Form II), as well as in the corners (–77.4 kJ/mole for Form I and –83.8 kJ/mole for Form II). The similar initial dissolution rate of Form I and II nanocrystals can thus be adequately explained by the similar dissolution driving force inherent in the corner and edges molecules which are the first dissolved molecules. The 3.4x saturation solubility increase over the normal size crystals further masked the real but small difference between the solubility of these two solid forms.

The second analysis of the MD simulation data was to examine the differences in the remaining solid phase between APAP I and II. The results are consistent with the thermodynamic stability relationship. APAP II crystal is less stable than APAP I as shown by higher percentage of H-bond broken (Figure 27) over time. H-bonding is the major force contributing to lattice energy. Fewer H-bonds are associated with a decrease in the heat of fusion of the crystal. The van der Waal forces (the other major force for molecular association) is also expected to be smaller in APAP II based on the visibly more disordered lattice in Figure 24c,*f*. Furthermore, not only the corner and edge molecules but also those on the flat surfaces in APAP II have turned into a disordered state. The visible thick disordered layer surrounding the APAP II crystal was determined by pair correlation function (Figure 28) to be significant. The dense drug layer represents a high concentration of APAP molecules on the crystal surface. This discovery pointed out a link between crystal surface and Form I crystallization rate.

Facile APAP Form II to Form I Transformation through a Surface Facilitated Mechanism

Based on the insight gained from the MD simulations, the Form II surface is poised to offer the supersaturation which the kinetics of Form I crystallization heavily depends on. The visual PLM experiment on Form II dissolving into aqueous solution (Figure 29*a-e*) provides direct evidence of the involvement of the surface layer in the Form II to Form I transition. While the surface of Form II showed evident signs of re-crystallization (which was confirmed by PXRD to be Form II to Form I transformation), the solution phase appears to be completely clear without any nucleation and crystal growth. Furthermore, the conversion on the surface took place relatively quickly; in a matter of ~40 min, Form I peaks were already present in PXRD pattern (Figure 29*f*). This indicates that the surface has cultivated the polymorphic transformation.

Based on the data presented in Figure 29, it can be deduced that the concentration on Form II surface has to be much higher than a supersaturation of 1.52x over Form I solubility, or else the nucleation of Form I could not have taken place rapidly. It is reasonable to believe that such a highly concentrated APAP layer on the Form II surface is created due to the fact that the hydration rate is faster than the molecular diffusion rate from the surface to bulk solution phase. The existence of the high supersaturation sets the stage for potential polymorphic conversion. This phenomenon presumably also exists in other metastable solid systems, but why does it lead to fast solid form conversion in the APAP system? This can be interpreted by the crystallization tendency of APAP. APAP was reported to crystallize from the amorphous state more readily than other studied

compounds due to lower configurational entropy and higher molecular mobility.[146] Lower configurational entropy means higher probability to assume proper orientation and conformation for crystal nucleation, which is intrinsic to the molecular structure of APAP. The molecular mobility, on the other hand, is expected to increase drastically in the dissolution study when compared to the dry amorphous system since water is introduced. Therefore, on the highly supersaturated surface, APAP should have a high tendency to nucleate. This is supported by the data in Figure 30*a,b* where the amorphous phase of APAP crystallizes almost instantaneously once in solution. More specifically, at the hydrated amorphous surface which mimics the highly concentrated APAP molecule layer accumulated on Form II surface observed by MD simulation, it was the stable Form I that has been crystallized. The resultant PXRD pattern represents an unequivocally pure Form I (Figure 30*c*). These data imply that the highly concentrated APAP layer on the Form II surface has facilitated the Form I crystallization.

The evidence presented above leads to the conclusion that the APAP Form II to I conversion in solution is through the surface-facilitated phase transformation (SurFPT), as opposed to the well-known solution-mediated phase transformation (SMPT). We envision the steps of SurFPT (Figure 31) in the following sequence: (a) The Form II surface molecules hydrate immediately once the water is introduced; (b) The hydrated molecules remain on the surface because of the barrier to diffuse into the bulk; (c) The concentration on the surface becomes high enough to crystallize as Form I.

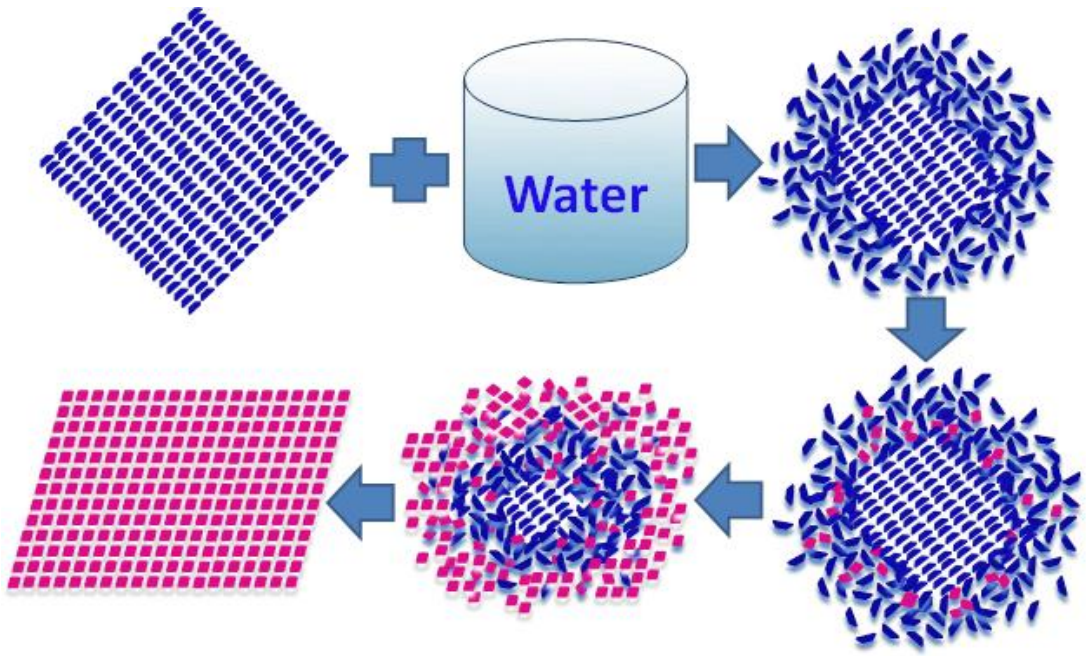

Figure 31. Schematic Illustration of Surface Facilitated Phase Transformation (SurFPT). The metastable form hydrates immediately once the water is introduced. The hydrated molecules quickly accumulate on the surface, approaching a high enough supersaturation level which leads to crystallization into the stable solid form.

As in SMPT, the presence of solvent (water in our study) is a prerequisite for SurFPT. Contrary to SMPT, however, in SurFPT the nucleation takes place on the metastable crystal surface coated with rapidly solvated drug-rich layer rather than in the solution. Sometimes, SMPT could nucleate on foreign particle surfaces (heterogeneous nucleation), however, the crystal growth usually is toward the solution phase creating protruding crystals[147] because the solution phase is supplying the molecules. In the case of SurFPT, the crystal grows beneath the surface (Figure 29) following the seeding by the surface layer crystals. Since accumulation of drug concentration on the surface takes a shorter time, SurFPT mechanism promotes a faster polymorphic conversion for drugs

with higher intrinsic tendency for crystallization, such as APAP. Finally, it can be safely extrapolated that the SurFPT mechanism also should be responsible for the reported APAP Form II to Form I conversion in air under different relative humidity conditions.[143]

Since the SurFPT mechanism could be used in other polymorphic systems, its implication goes beyond the APAP polymorphic pair. Understanding SurFPT benefits formulation and solid state scientists in the research and development of pharmaceutical products. For examples, in the effort to make metastable forms or to measure solubility of metastable forms or to use metastable form to gain solubility advantage, SurFPT is far more detrimental than SMPT. This has caused the failure in measuring the solubility of APAP Form II in the past and in preparing APAP Form II on a large scale which otherwise would provide a lower cost option for processing solid dosage forms. It would also decrease the solubility advantage of a metastable form when the drug is taken *in vivo*, because the solid does not have any chance to dissolve into solution within the absorption window before the stable form crystallizes. The outcome is analogues to the matrix crystallization occurring in amorphous solids which negated the dissolution advantage of the amorphous form.[19]

Conclusions

We presented strong evidence from a series of molecular dynamics simulations and experiments that reveal the root cause for the facile polymorphic conversion of APAP from orthorhombic Form II to monoclinic Form I. APAP Form II undergoes surface-facilitated phase transformation (SurFPT) in contact with the solution. In SurFPT, the nucleation takes place on the metastable crystal surface coated with rapidly solvated

drug-rich layer rather than in the solution where creating sufficient supersaturation takes a longer time. From MD simulations, such a drug-rich layer is evident on the APAP Form II surface but not on the Form I surface. The SurFPT mechanism we have demonstrated with APAP could also exists in other polymorphic systems. This mechanism promotes a faster polymorphic conversion for drugs with higher intrinsic tendency for crystallization, such as APAP. Understanding it helps us select appropriate strategies to circumvent the polymorphic conversion problems during manufacturing of active pharmaceutical ingredients and drug products.

Acknowledgement

The authors acknowledge Dr. Geoff G. Z. Zhang, Dr. Yihong Qiu, and Mr. Rodger Henry at AbbVie, Inc, for insightful discussions, Mr. Jianwei Wu previously at AbbVie for HPLC assistance and AbbVie's Tuition Assistance Program for financial support.

CHAPTER FIVE

DRUG–POLYMER INTERACTIONS AT WATER-CRYSTAL INTERFACES AND IMPLICATIONS FOR CRYSTALLIZATION INHIBITION: MOLECULAR DYNAMICS SIMULATIONS OF AMPHIPHILIC BLOCK COPOLYMER INTERACTIONS WITH TOLAZAMIDE CRYSTALS

Abstract

A diblock copolymer, PEG-*b*-PLA, is effective in modulating the crystal growth of tolazamide, resulting in a crystal morphology change from needles to plates in aqueous media. To understand the molecular mechanism of this crystal surface drug–polymer interaction, we conducted molecular dynamics (MD) simulations on crystal surfaces of tolazamide in water containing PEG-*b*-PLA. To ensure that the polymer structure was fully equilibrated, a 130 ns simulation of the polymer in a large water box was run before initiating 50 ns simulations with each of the crystal surfaces. The simulations successfully demonstrated the differentiated drug–polymer interactions and are consistent with experimental studies. Interaction of PEG-*b*-PLA with the (001) face occurred more rapidly (≤10 ns) and strongly (total interaction energy of –29.1 kJ/mole/monomer) than that with the (010) face (~35 ns, –21.02 kJ/mole/monomer). In addition, there was virtually no interaction with the (100) face. Interestingly, upon dissecting the various contributions to the total interaction energies, van der Waals interactions were identified

as the dominant forces (accounts for 77–93% of total interaction energies) that enabled such strong drug–polymer interactions. It suggests that polymers capable of forming strong hydrophobic interactions are more effective in inhibiting crystallization of poorly water-soluble and hydrophobic drugs in aqueous media (such as gastrointestinal fluid) than those with hydrogen bonding capacities. Such in-depth analysis and understanding facilitate the rational selection of polymers in designing supersaturation-based enabling formulations.

Key words: Tolazamide, poly(ethylene glycol)-block-poly(lactic acid), molecular dynamics simulation, crystallization inhibition by polymers, drug-polymer interaction, crystal surface specific interactions, crystal morphology modification, van der Waals interaction.

Introduction

Synthetic and natural polymers have been widely used in developing and manufacturing pharmaceutical products. The applications include[148,149] (but are not limited to) binding the particles of a solid dosage form, changing the flow properties of active pharmaceutical ingredient (API), masking unpleasant taste of a drug, modifying drug release characteristics, stabilizing suspensions, enabling drug delivery and inhibiting crystallization of APIs. The ability of polymers to inhibit crystallization of drug molecules has promoted intense research in recent years. Polymers are used to stabilize the metastable solid form in formulations, i.e. amorphous solid dispersions (ASD[150-152]), to deliver poorly water-soluble small molecular drugs (Class II and IV in

Biopharmaceutics Classification System[153]) which represent approximately 90% of current pipeline drugs across the pharmaceutical industry.[154] Polymers also are used to maintain supersaturation during dissolution of enabling formulations for maximizing formulation performance.[19,155-157] Finally, polymers can play an important role in modifying the crystal habit during solution crystallization.[158-160]

Crystallization inhibition originates from drug–polymer interactions. Understanding the mechanism of how drug molecules interact with a polymer will help us to select a better polymer for formulating and delivering drug molecules. Molecular dynamics (MD) simulations are well suited for adding insights that would otherwise difficult to gain by experimental methods. The reported use of MD simulation in drug crystallization inhibition by polymers can be divided into two main areas: polymer–drug interactions in amorphous systems which primarily deal with solubility or miscibility[58-63] and crystal systems which address crystal growth inhibition. In the latter, there are only a few published studies in recent years. Zhu *et al.* simulated the interaction of several additives (such as hydroxypropyl methylcellulose, HPMC) in water with crystal surface of fenofibrate[66] and griseofulvin.[65] A short HPMC chain (five repeating units) was constructed and placed into a small water box (1500 water molecules) with the simulation carried over a short duration (600–800 ps). The simulated binding energies between the additives and crystal surface were correlated with the experimental results when these additives were found to reduce the particle size of recrystallized griseofulvin. In 2012, Yani, Chow and Tan reported a 400 ps MD simulation of large polymers (225 monomers for PVP and 62 for HPMC) with different crystal phases of salbutamol sulfate in

vacuum.[64] Hydrogen bonding between PVP and salbutamol sulfate, which was ~40% of the total binding energy, was thought to dominate in prohibiting crystal growth. The water soluble polymers used in drug crystallization inhibition strongly interact with water molecules. As a result, the interaction with drug molecules is expected to change in the presence of water. For examples, Taylor and her group reported that poly(vinylpyrrolidone) (PVP), which is an effective crystallization inhibitor to felodipine in amorphous solid dispersions at low relative humidity (RH) significantly reduced its effectiveness at high RH[161] and even lost its ability in aqueous dissolution medium.[162] The loss of effectiveness was ascribed to the strong interaction of PVP with water molecules. Apparently, more studies are needed to improve upon the MS simulation methodologies (i.e. sufficiently long simulation time under more realistic conditions) in order to demonstrate the validity and utility of MS simulation as an emerging and powerful technique for such applications. More importantly, it is necessary to conduct more careful analysis in interaction energies involved in the drug–polymer interaction for the purpose of understanding the mechanism of crystallization inhibition by polymers in aqueous solutions. The purpose of our present work, therefore, is to develop improved MD simulation methods to study the molecular level mechanism and energetics involved in crystal growth inhibition by polymers in an aqueous solution.

The model system chosen for this study is comprised of tolazamide (TLZ), an oral hypoglycemic agent, and poly(ethylene glycol)-block-poly(lactic acid) (PEG-b-PLA), an amphiphilic block copolymer. Based on the interesting work published by Kuldipkumar et al,[158,163,164] PEG-b-PLA selectively interacted with the (001) phase of the TLZ crystal,

changing the crystal habit from needle to plate shape[158] (shown in Figure 32). PEG-b-PLA exerts this strong habit modification at very low concentration (3–10 ppm) regardless of PEG to PLA monomer ratios in the polymer.[164] Atomic force microscopy with the tip tethered with the polymer or parts of the polymer (PEG or PLA) determined the adhesion forces to individual faces of the single crystals. The adhesion forces were the strongest (264 nN) with (001), the weakest (~5 nN) with (100) and intermediate (170 nN) with (010).[164]

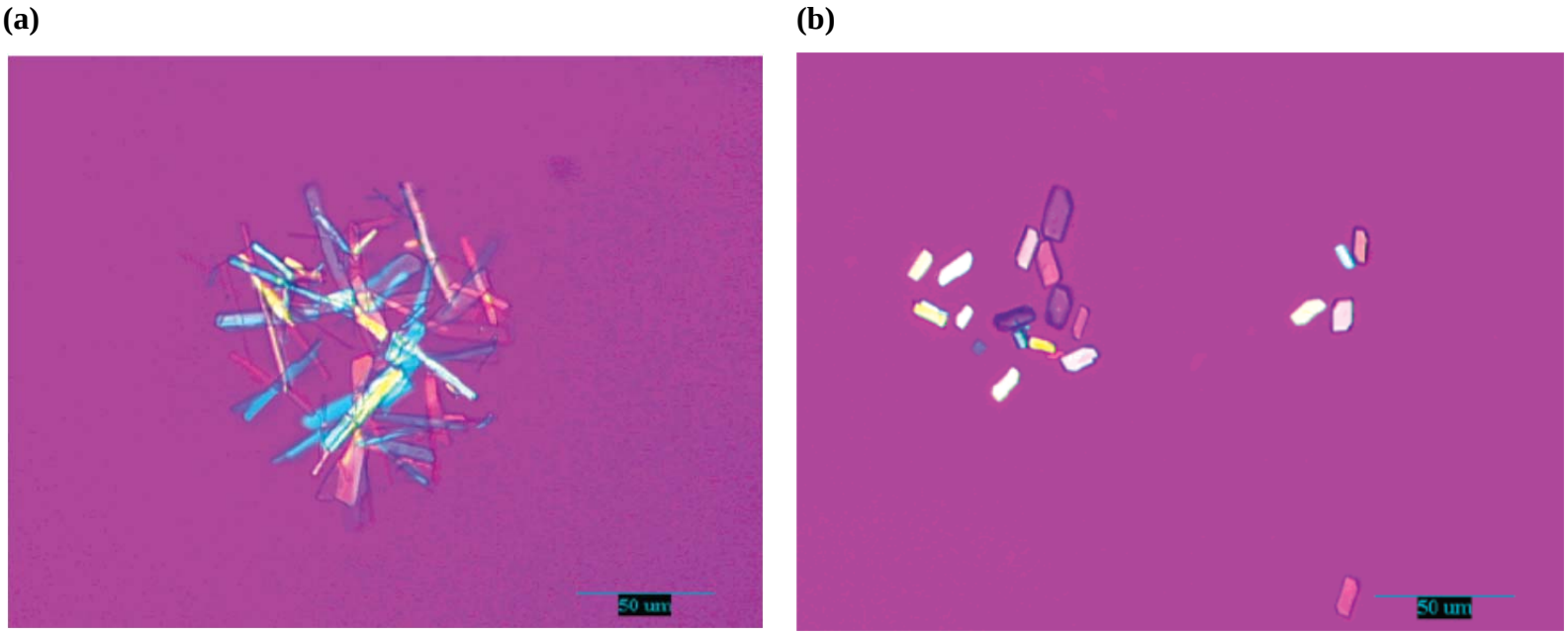

Figure 32. Tolazamide crystals obtained (a) in the absence of PEG-b-PLA and (b) in the presence of 50 μg/mL of PEG-b-PLA.[158] (Photomicrographs used with the permission of *Crystal Growth and Design*).

Our MD simulation was designed to investigate the interactions between TLZ crystals and PEG-b-PLA in water. Large crystal surfaces of (001), (010) and (100) were built respectively into a sizable water box. A representative PEG-*b*-PLA was constructed, first equilibrated with a 130 ns MS simulation in water and then added to another water box containing the crystals. The assembly was simulated for 50 ns to determine how the polymer molecule interacts with each crystal surface. The nature of the polymer interaction with TLZ molecules was quantitatively determined through van der Waals and electrostatic interaction energies. The results from the study strongly correlated with the reported experimental data, allowing an in-depth view of how the molecular interactions responsible for the crystallization inhibition take place at the crystal-water interface. This correlation with experimental results established our MD simulation method, which will allow future applications of this method in studying other drug crystal–polymer interactions.

Experimental

Building the Crystals

The single crystal structure of tolazamide (TLZ, molecular structure in Figure 33*a*) was taken from CABCUD01[165] in the Cambridge Structural Database (Cambridge, UK). The crystal system is triclinic with space group *P*1, Z = 2 and *a* = 6.355 Å, *b* = 9.223 Å, *c* = 13.510 Å, α =101.104°, β = 92.80 ° and γ = 85.72° (Figure 33*b*). The molecules are dimerized by NH-O hydrogen bonds and dimers are packed together through van der Waals interactions only.[165] TLZ is poorly water-soluble (intrinsic solubility of ~70 μg/mL), hydrophobic (CLogP of 2.69) and weakly acidic (pK_a of 5.9 assigned to the

sulfonamide hydrogen).[158,166] Three virtual crystals were constructed from the unit cell using Mercury software (Mercury 2.3, CCDC 2001-2009) following our previous method[41] with some modifications. The (001) surface crystal was built by extending the unit cell at *a*, *b*, and *c* directions for 17, 2 and 8 times, producing the 17 x 12 x 2 crystal lattice. Similarly, the (010) and (100) surfaces were made at 17 x 2 x 8 and 2 x 12 x 8 unit cell repetitions (detailed in Table 3 and Figure 34).

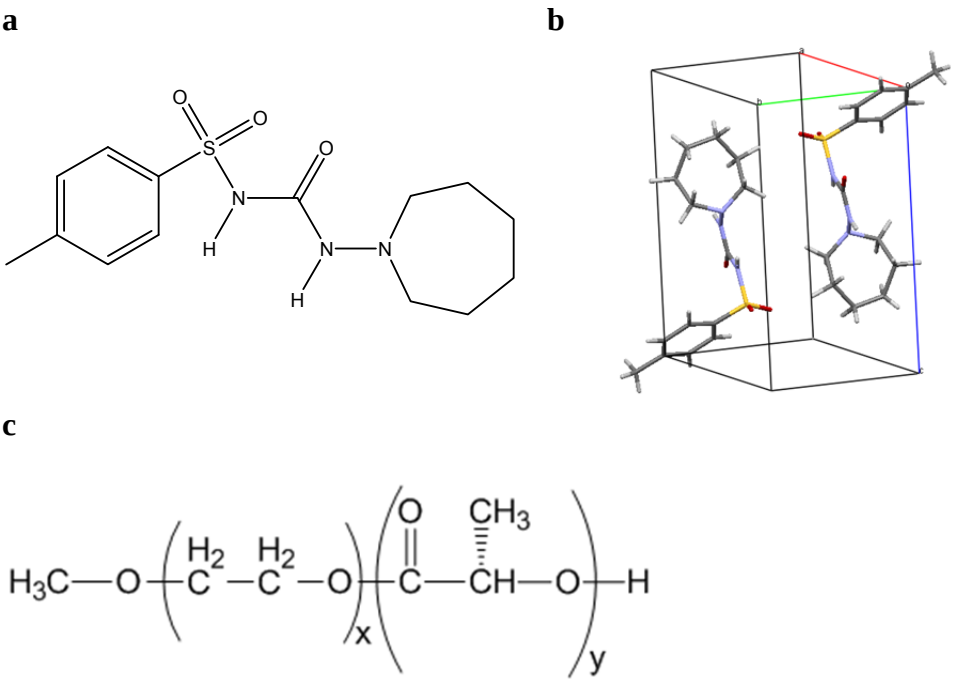

Figure 33. (*a*) Molecular structure of tolazamide. (*b*) Unit cell of tolazamide. (*c*) Molecular formula of PEG-*b*-PLA.

Table 3. Three Crystal Lattices of Tolazamide Built with large (001), (010) and (100) Surfaces.

Surface	Lattice with unit cells	Crystal Dimension (Å)			no. of molecules	Surface Size $\times 10^4$ (Å^2)
		a	b	c		
(001)	17×12×2	108.04	110.68	27.02	816	1.19
(010)	17×2×8	108.04	18.45	108.08	544	1.17
(100)	2×12×8	12.71	110.68	108.08	384	1.17

(a) (001) surface

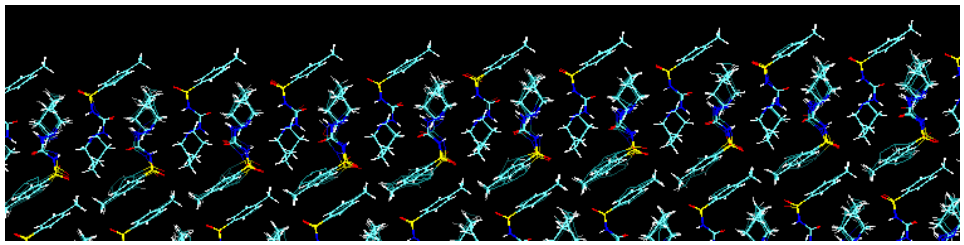

(b) (010) surface

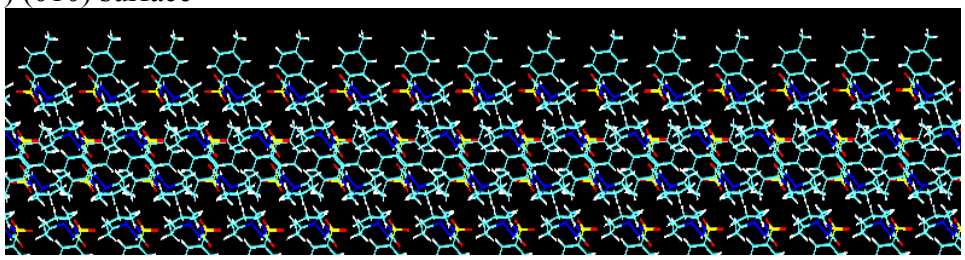

(c) (100) surface

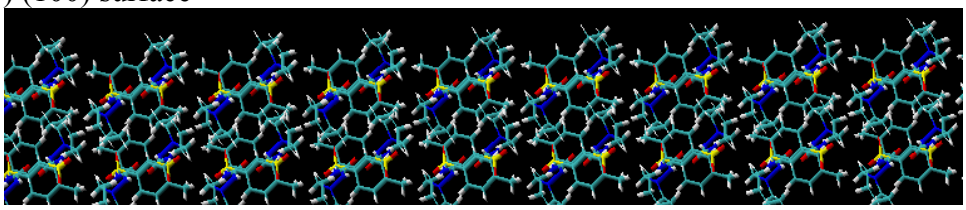

Figure 34. Illustration of the tolazamide molecular packing on three surfaces of crystals used in simulation. (a) (001) surface with the flat face of the methyl benzene ring toward water. (b) (010) surface with the methyl benzene ring oriented toward water perpendicularly. (a) (100) surface with the azepane ring toward water perpendicularly.

The crystals constructed above were prepared using Visual Molecular Dynamics software (VMD, version 1.9, March 2011).[99] The topology and parameters of TLZ for the CHARMM27[39] force field were obtained from the Swiss Institute of Bioinformatics (http://swissparam.ch/). The structure file of the crystals was built using the Automatic PSF Builder function in VMD from the input of the Mercury coordinate file and the TLZ topology file.

Building the Polymer and Obtaining the Hydrated Polymer Structure

The polymer used was a poly(ethylene glycol)-block-poly(lactic acid) (PEG-*b*-PLA) (general formula shown in Figure 33*c*), within the class of amphiphilic diblock copolymers. The PEG-*b*-PLA polymer built for this study contains 22 and 8 repeating units of PEG and PLA, respectively, mimicking a PEG: PLA ratio of 110: 40 in a commercially available PEG-*b*-PLA polymer which was used in the reported TLZ habit modification study.[164] The molecular weight of PEG22-*b*-PLA8 is 1600 g/mol, or 20% of the real polymer. The chemical structure was drawn using ChemDraw (ver 9.0.7, Cambridge, Massachusetts) which was then input into Spartan O2 (Wavefunction, Inc., Irvine, California) to calculate the three-dimensional molecular structure in mol2 format. This was submitted to Swiss Institute of Bioinformatics (http://swissparam.ch/) to obtain the topology and parameters for the CHARMM27[39] force field.

Prior to simulating the polymer-crystal surface interaction in water, the polymer must be equilibrated with water. This was accomplished through a 130 ns MD simulation in water. The steps of energy minimization and production run followed the conditions described in the following section. The polymer was first simulated in a 64×62×53 Å water box for 100 ns, and then in a larger size water box (106×118×114 Å) for another 30 ns. The polymer structure from the end of 130 ns was combined with that of the crystals to simulate the polymer crystal interactions in a water box.

Building the Polymer and Crystals together in Water

Water rather than buffer was selected as the aqueous medium in this simulation since neither the rate of crystallization nor the morphology of TLZ in the presence of PEG-*b*-PLA was affected by changing buffer pH values.[164] The hydrated PEG-*b*-PLA polymer structure and TLZ crystals were built together using VMD software (version 1.9, March 2011).[99] The center of the polymer was positioned at 20 Å away from the center of each crystal surface, and about 4.9×10^4 water molecules (~100 Å distance from the crystal surface) were added to cover the crystal surface and the polymer. The combined structural files were created using the Automatic PSF Builder function in VMD.[99]

MD Simulation

The computer code used for the MD simulations was the parallel, scalable MD program NAMD version 2.9b1.[100] Periodic boundary conditions were used. The cutoffs for nonbonding (van der Waals and electrostatic) interactions were 12 Å. The switch distance was 10 Å, and a 1.0 1–4 scaling factor was used. The polymer and crystal in the water box were first subjected to energy minimization (6000 steps) followed by slow heating from 10 to 298 K over 30000 steps. The temperature and pressure of the system were equilibrated for 10000 steps using a Langevin piston. The system was then allowed to equilibrate for 30000 steps at constant temperature (298 K) and pressure (1 atm). After equilibration, the crystal was fixed so that it does not dissolve into water in the following production run so that the polymer's interaction with the intact crystal surface can be

simulated. Production simulation of the polymer interaction with the intact crystal surface was performed at constant volume and temperature (298 K) for 50 ns.

Analysis of MD Simulation Data

Simulated results were viewed using VMD (version 1.9, March 2011).[99] Interaction energies were calculated using algorithms for the van der Waals (VDW) and electrostatic energies in the NAMD program.[100] These calculations were performed for the whole polymer (PEG22-*b*-PLA8) and the PEG22 and the PLA8 portions of the polymer within 4 Å of the TLZ molecules. Because partial charges exist in an atom due to the different electronegativities of the atoms, the potential function used in the molecular dynamics simulation considers the partial charge in every atom even when the molecules are neutral. The electrostatic interactions, including ion–dipole interactions and H-bonding, and van der Waals interactions, including London dispersion forces and electronic repulsions, were calculated using the partial atomic charges and van der Waals parameters in the CHARMM potential function.[39] Since the block polymer contains more PEG repeating units than PLA, the interaction energy was reported as energy value per monomer. This allows comparison in interaction strength among polymers with different chain lengths.

Results

Visual Analysis

Surface (001)

Initially the polymer moved freely in water but quickly (at 0.5 ns) it approached the surface (Figure 35*a*). At 2 ns the PLA tail made a contact with the surface (Figure 35*b*).

The polymer bent toward the surface (Figure 35c). At 4.5 ns, the PEG tail also touched down (Figure 35*d*). Both PLA and PEG ends gradually pulled the whole polymer down to the surface (Figure 35*e,f*). At 10 ns the polymer flattened itself on the surface (Figure 35*g*), after which there were no further position changes through the end of the 50 ns simulation (Figure 35*h*), although the polymer kept making small movement (vibrating) from 10 to 50 ns. A view from the top of the crystal surface at 50 ns (Figure 35*i*) shows the polymer lays curled and flat on the surface. It appears that the tails of the polymer play a bigger role in initiating the interaction than the other parts of the polymer.

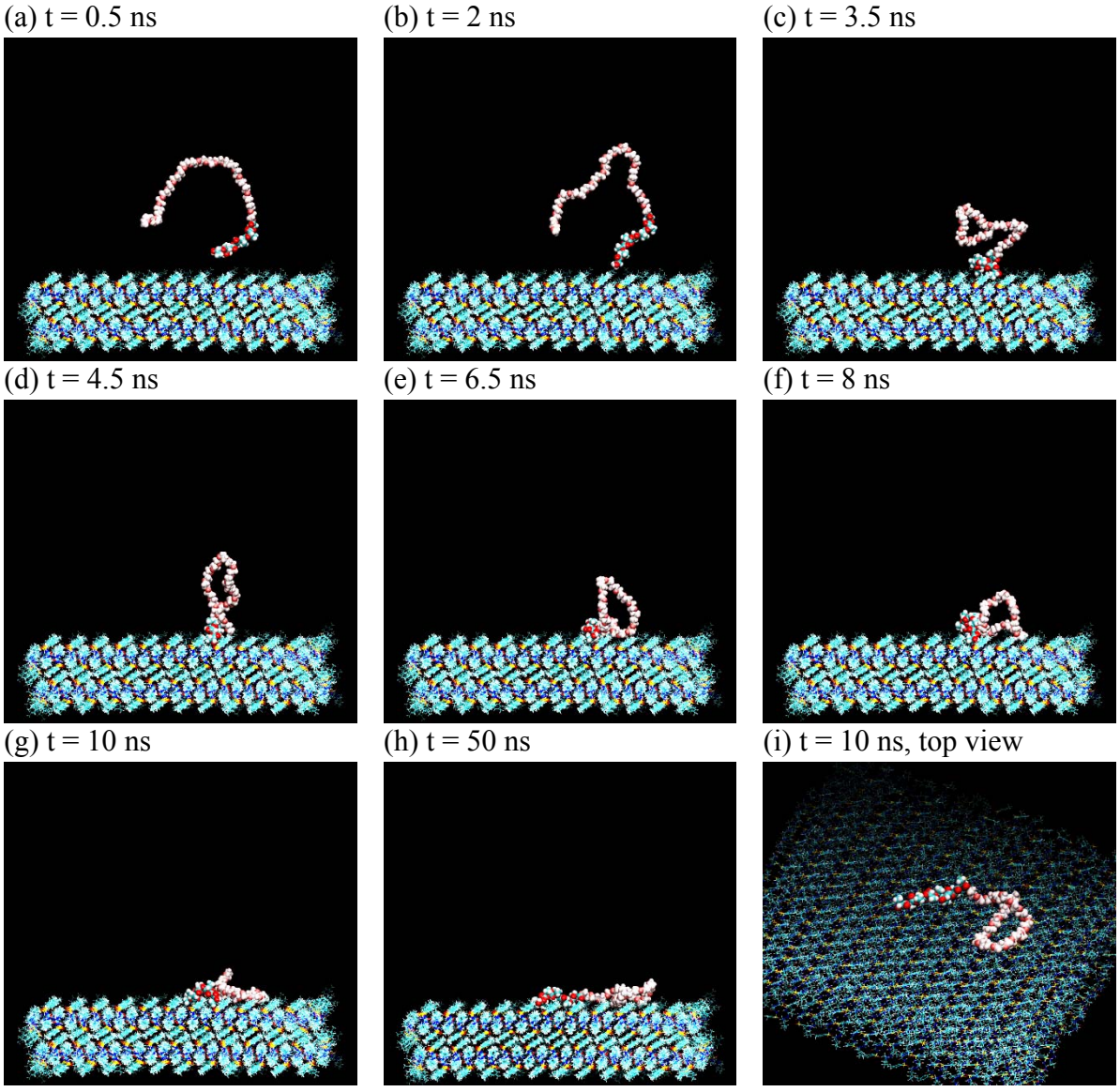

Figure 35**.** Display of images of MD simulation of PEG-b-PLA polymer with TLZ crystal surface (001) at different times. PLA portion is shown as red/blue/white (oxygen is red, carbon is blue and hydrogen is white). PEG as red/beige/pink (oxygen is red, carbon is beige and hydrogen is light pink). For clearer views, water molecules are not shown.

Surface (010)

The polymer behaved differently with the (010) face. The PEG tail was already at the surface at time 0 (Figure 36*a*) indicating this has occurred earlier during the equilibration. However, the faster interaction with the PEG tail did not bring about any faster interaction with the whole polymer. During the period of 0 to 20 ns, there has been simply a single contact between the PEG end and the surface (Figure 36*b,c*), while the PLA part moved around in the water phase. Changes finally took place at 23 ns when the PEG chain gradually lowered to the surface (Figure 35*d,e*). At 50 ns (Figure 35*f*), most of the PEG lied down as a linear chain, but is not coiled as on the (001) surface. As seen with the (001) surface, the initial contact with the crystal surface was made through the tail of the polymer. Interestingly, only a small part of PLA made contact with the (010) surface.

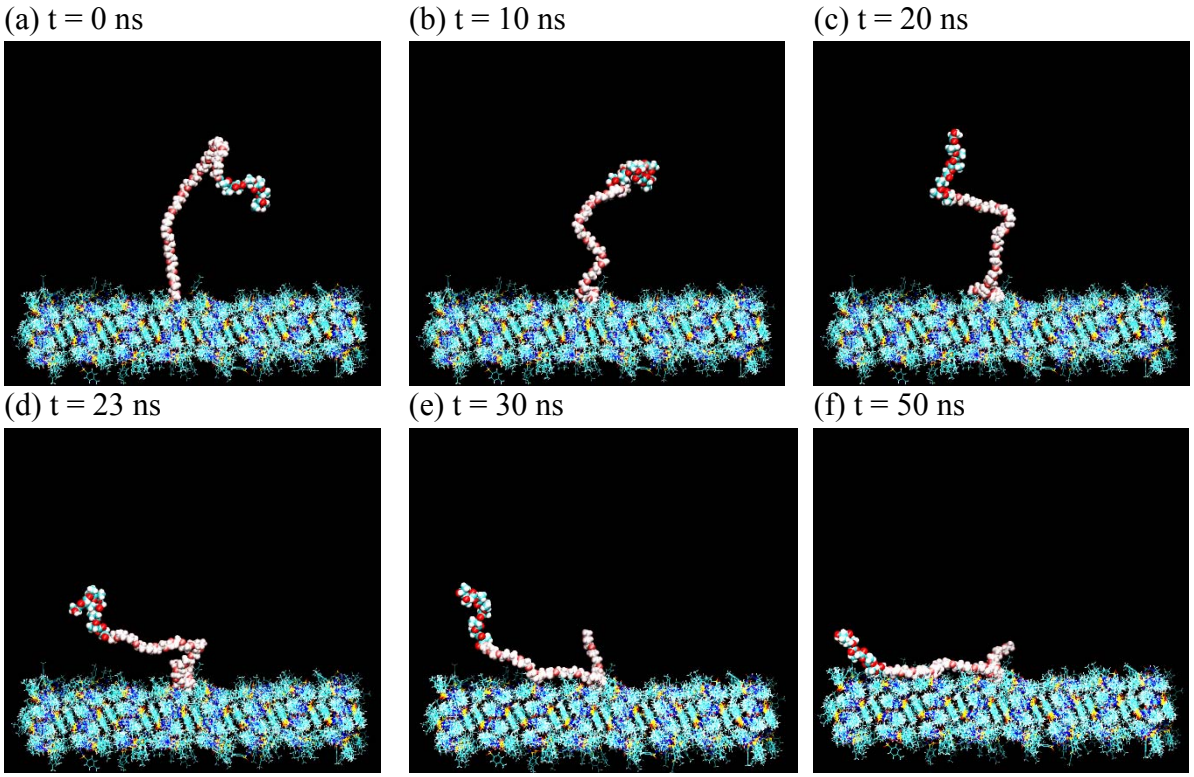

Figure 36. Display of images of MD simulation of PEG-b-PLA polymer with TLZ crystal surface (010) at different times. PLA portion is shown as red/blue/white (oxygen is red, carbon is blue and hydrogen is white). PEG is shown as red/beige/pink (oxygen is red, carbon is beige and hydrogen is light pink). For clearer views, water molecules are not shown.

Surface (100)

The polymer did not interact with the (100) face. From 0 to 10 ns, the polymer sometimes moved closer to the surface (Figure 37*a*), and sometimes moved further away (Figure 37*b*). Starting from 12 ns it gradually diffused from the center toward the edge of the water box (Figure 37*c*). The polymer moved across the (100) surface until it found the (001) face at ~17 ns (Figure 37*d*). Evidently the polymer has little affinity to (100) but its binding to (001) is favored. The polymer settled on the edge of (001) and (100) at 35 ns

(Figure 37*e*) with no changes afterwards. The PEG part interacted with (001) phase, while the PLA part found a space on the edge between (001) and (100) (Figure 37*f*).

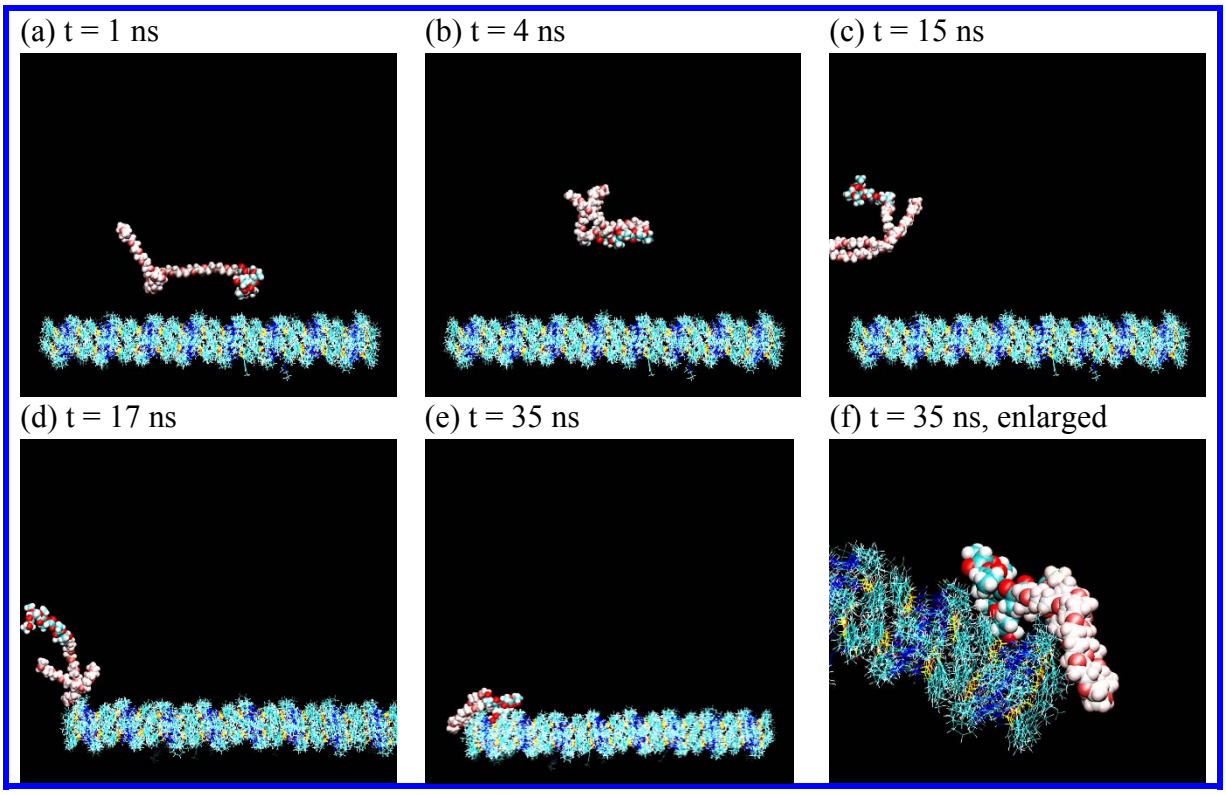

Figure 37. Display of images of MD simulation of PEG-b-PLA polymer with TLZ crystal surface (100) at different times. PLA portion is shown as red/blue/white (oxygen is red, carbon is blue and hydrogen is white). PEG as red/beige/pink (oxygen is red, carbon is beige and hydrogen is light pink). For clearer views, water molecules are not shown.

Interaction Energy Analysis

Interaction energies between each block of the polymer (PLA or PEG) and the three crystal surfaces were calculated to characterize how the crystal surface differentiated interactions with the polymer. The energy level was normalized by the number of monomers in each block in order to compare PLA with PEG. Six plots demonstrating the dynamic changes in VDW and electrostatic energies as a function of simulation time are shown in Figure 38.

(a) (001) face

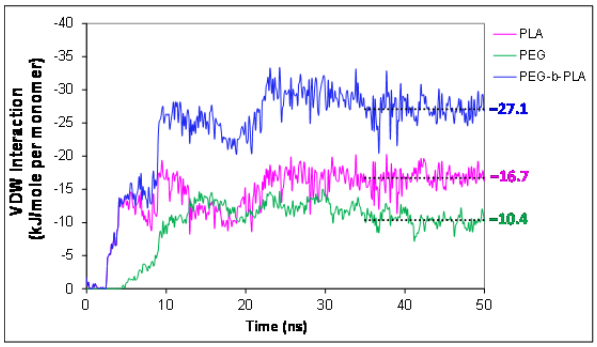

(b) (001) face

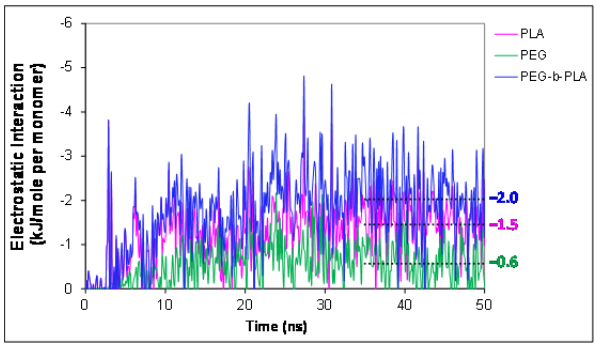

(c) (010) face

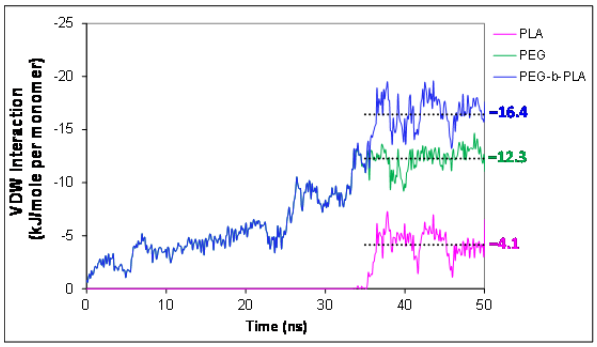

(d) (010) face

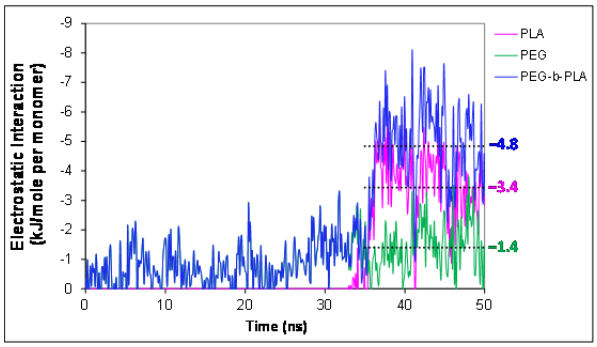

(e) (100) face: 0–17 ns

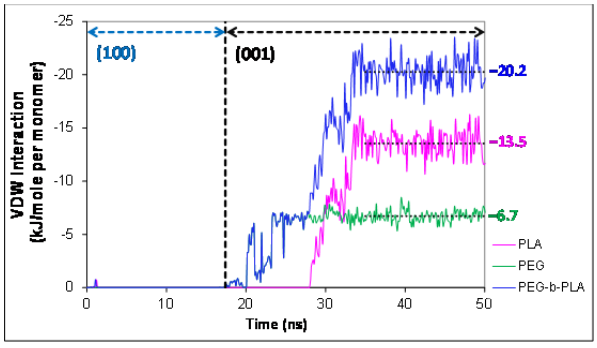

(f) (100) face: 0–17 ns

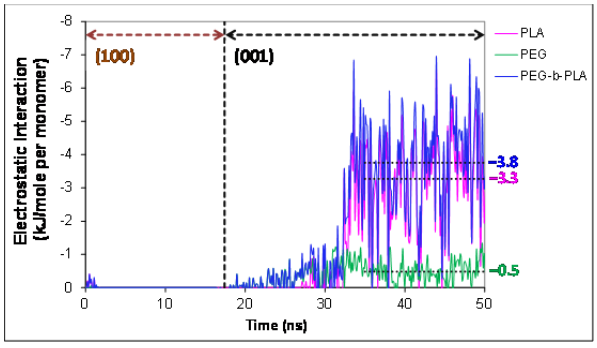

Figure 38. The interaction energies vs time between the polymer (including PEG portion, PLA portion and the whole polymer PEG-*b*-PLA) and the three TLZ crystal surfaces calculated as VDW and electrostatic energy per monomer in both blocks of the polymer.

The onset of increase in interaction energy in Figure 38 exactly coincided with the visually observed polymer-crystal interactions (Figure 35, Figure 36 and Figure 37). Since interaction energy levels plateau after 35 ns, it can be assumed that the interaction between the polymer and the surfaces had approximately reached equilibrium, and the degree of interaction could be estimated by the averaged energy values from 35 to 50 ns for both VDW and electrostatic forces. When the VDW of the whole PEG-*b*-PLA is compared at equilibrium, (001) phase shows significantly stronger interaction (–27.1 ± 1.8 kJ/mole of monomer) than that of the (010) surface (–16.4 ± 1.7 kJ/mole of monomer). When PEG and PLA are compared separately, at the (001) face both PLA and PEG portions contributed to the VDW energy (Figure 38*a*), while at the (010) surface the PEG portion provides the major contribution since the PLA hardly interacted with (010) (Figure 36). There is no interaction with the (100) face for either portion of the block polymer (Figure 38*e,f*).

The van der Waals interaction energy obtained is much larger than the electrostatic interaction energy. This is true regardless of crystal faces and different parts of the polymer. In addition, the electrostatic interaction is mostly contributed by the PLA part.

Discussion

Dependence of Drug Molecular Packing on Drug–Polymer Interactions

The MD simulation indicates that PEG-*b*-PLA in water interacts most strongly with the TLZ (001) phase (Figure 35 and Figure 38*a,b*), less strongly with the (010) face (Figure 36 and Figure 38*c,d*) and almost not all with the (100) face (Figure 37 and Figure

38*e,f*). This is consistent with reported experimental results that the adhesion forces between the polymer and TLZ crystal faces followed the rank ordering of (001) > (010) > (100) with very low measurable forces toward (100).[164]

Intuitively the surface differentiated interaction is due to different TLZ molecular packing on the crystal surface since it is the only variable in the simulation experiment. On the (001) face, the methyl phenyl ring lays almost flat on the surface (Figure 34*a*), providing larger effective surface area to interact with the polymer. When the polymer molecular comes in contact with the (001) face, the sheet of benzene rings offer strong interactions (i.e. van der Waals and hydrophobic interactions). The total van der Waals interaction energy with (001) per monomer exceeded –27 kJ/mole (Figure 38*a*) which leads to stable interactions once contact is made between the polymer and the surface. Within 10 ns, the polymer has already fully coiled on the (001) surface.

The (101) surface also consists of the methyl phenyl ring; however, the ring "stands up" with the methyl group pointing outward (Figure 34*b*). When the polymer comes to this surface, it first encounters the methyl group that is expected to provide fewer VDW and hydrophobic interactions with the polymer. The polymer has to penetrate deeper in order to interact with the benzene ring which takes longer time. The total van der Waals interaction energy per monomer decreased to –16.4 kJ/mole on (010) (Figure 38*c*), a 40% reduction compared to that on (001). This may have contributed to the much slower interaction. Since the weaker interaction compared to the (001) face allows for more movement after contact is made, it took 35 ns for the PEG chain to bind to the (010) surface. Interestingly, the PLA part could not find a place to "lay down" on (010) after

"searching" for 50 ns. This is quite different than the fast and tight binding between PLA and (001). The details of the interface of water–polymer–(001) surface at 50 ns is shown in Figure 39. Parts of the PLA chain snuggly fit into the gaps formed between two layers of the methyl phenyl ring. On (010), the surface molecules appeared to be more mobile and did not form a groove to accommodate the PLA chain (Figure 36*f*). Thus, there is less interaction of the PLA with the (010) surface.

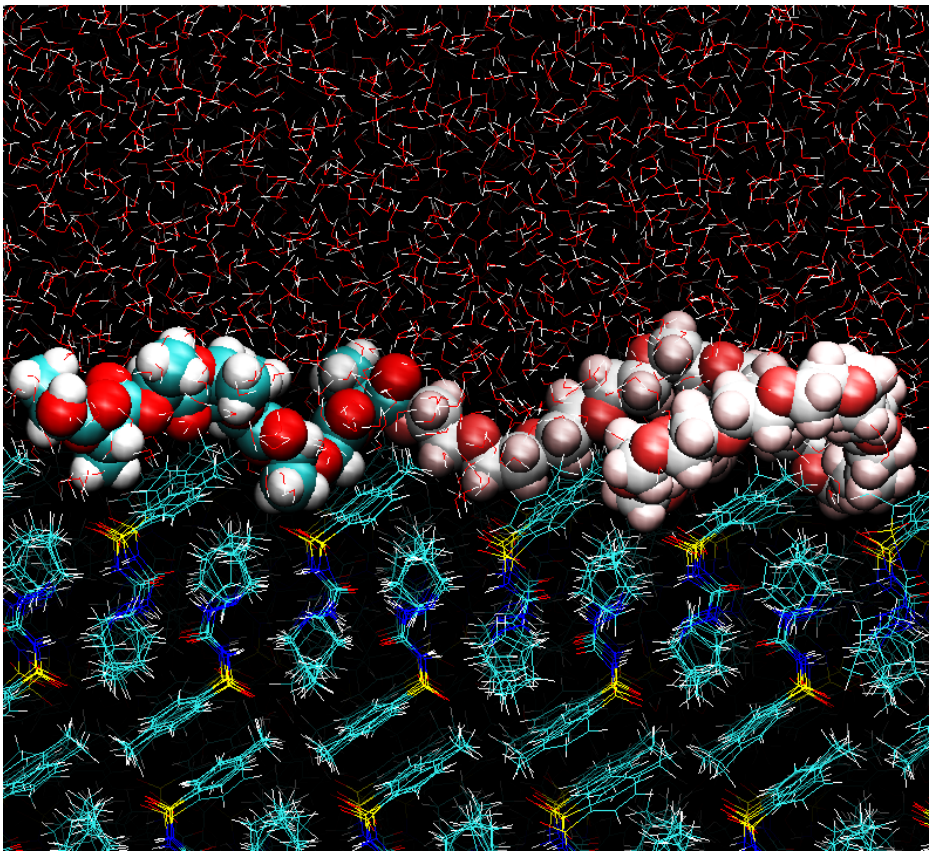

Figure 39. Enlarged image at (001) crystal–water interface to demonstrate the PEG-*b*-PLA polymer–TLZ interaction at 50 ns. The PLA part is located at the left side (color code of the atoms: oxygen is red, carbon is blue and hydrogen is white). The PEG part is at the right side (color code of the atoms: oxygen is red, carbon is beige and hydrogen is light pink).

Lastly, on the (100) surface, the dominant molecular moiety is the azepane perpendicularly facing the water phase (Figure 34c). The van der Waals interactions to hydrocarbons on the azepane are expected to be weaker compared to the phenyl rings. This perhaps explains the lack of the polymer interaction with the (100), and why the polymer prefers to move toward (001) which is adjacent to (100) and interacted with the (001) face instead.

The simulations were able to visualize the crystal surface specific interactions, thus providing direct evidence for understanding the crystal growth inhibition by polymers. As described in the diffusion theory for crystal growth,[25] the overall crystal growth rate in a first order process is controlled by the rate of molecular diffusion from the bulk solution to the crystal surface and the rate of molecule integration into the crystal surface. Alonzo *et al.*[32] have found that in the presence of HPMC, felodipine crystal growth shifted toward an integration-controlled mechanism from the diffusion-controlled mechanism. The visual findings from the simulations support the role of polymers in reducing surface integration rate. The observed rapid and strong adsorption of the PEG-*b*-PLA selectively to (001) provides physical blockage for other TLZ molecules to integrate into the (001) surface for extending the crystals in the (001) direction. This resulted in the TLZ morphology change (Figure 32). However, the polymer–crystal surface specific interaction does not inhibit crystallization because some surfaces are not inhibited and are still free to grow. The MD simulation is potentially a method to screen polymers for intended purposes. For example, if crystal habit modification is needed, the screening will look for specific crystal surface interaction with different polymers. If the objective

is to inhibit crystal growth at all or to obtain significantly reduced particle size, the screening can target the polymers with a universal inhibition across different crystal surfaces. Applying MD simulation for such an application may become a reality relatively sooner due to advances in MD simulation methodology and rapid increases in computational speed.

Importance of VDW Forces in Polymer–Crystal Surface Interaction

The MD simulations demonstrate the important role of VDW forces in TLZ–PEG-b-PLA interactions. Most oxygen atoms (shown as red in Figure 39) in the polymer are oriented toward water, while the atoms on the hydrocarbon chain which are hydrophobic are tightly inserted into the layers of phenyl rings on the (001) face. Thus, the polymer forms hydrophilic and H-bond interactions with water molecules but hydrophobic and van der Waals interactions with the TLZ surface molecules.

The visual observation in Figure 39 is quantitatively captured in Figure 38 where the interaction energy landscape between the polymer and TLZ molecules is presented. The electrostatic interaction energy (Figure 38*b,d,f*) is small compared to VDW interaction energy (Figure 38*a,c,e*). The electrostatic energy, including hydrogen bonding, only accounts for 7.0% of total interaction energies between PEG-*b*-PLA and (001) (2 out of 29 kJ/mole), 23% of that on (010) (4.8 out of 21.3 kJ/mole), and 15.6% of that on (001) at the (001/(100) edge (3.8 out of 24.0 kJ/mole). The small electrostatic interaction is mainly contributed by the PLA block and minimally by the PEG block. This conforms to the chemical structures of the PEG-b-PLA and TLZ. Only one

hydrogen atom at the PLA tail can be donated to form a hydrogen bond (Figure 33*c*). The rest of polymer has multiple hydrogen bond acceptors. The carbonyl oxygen in PLA is a stronger hydrogen acceptor than the ether oxygen in PEG because it is more electronegative. In the TLZ crystal, the methyl phenyl ring on (001) and (010) faces or the azepane on (100) face do not possess strong H-bond donors or acceptors. TLZ molecules in the crystal are dimerized by intermolecular NH–O hydrogen bonds[165] which are not accessible from the surfaces. These data indicate that hydrophobic interactions rather than hydrophilic interactions are responsible for most polymer–TLZ intermolecular interactions.

The above conclusion for TLZ can be applied to many other poorly water-soluble compounds for several reasons. Firstly, more than two third of the marketed poorly soluble drugs (219 out of 318 BCS Class II and IV compounds) surveyed in 2011 are highly hydrophobic (CLogP > 2.50), similar to or more hydrophobic than TLZ (LogP = 2.69).[166] When placed in a polar environment (i.e. water), these non-polar molecules will have a tendency to group together with the non-polar motif of the polymer to minimize the surface area in contact with water. This is the nature of hydrophobic interactions. Therefore, for these crystal surfaces, formation of hydrophobic interaction with polymers would be much more energetically favorable.

Another important factor to consider is the role of water. The interaction of a polymer with a drug in dry state (i.e. in amorphous solid dispersion where H-bonding with polymers is important for physical stability) changes when water is introduced. Formation of drug–polymer H-bonds in aqueous solutions should be less favorable due to

the strong competition from water. Since water is 55 M and an excellent H-bond donor and acceptor, it would dominate the H-bond sites on the crystal surface as well as on the polymers. An MD simulation study on adsorption of polyethylene glycol (PEG) on the surface of dicalcium silicate showed that the absorption energy decreased more than 10-fold in the presence of water compared to under vacuum due to the added interaction of water with the PEG and dicalcium silicate.[167]

Thirdly, the VDW interactions are not as weak as often perceived. Although hydrogen bonding (bond energy of 8–30 kJ/mole)[168] is in general stronger than VDW forces (bond energy of 4–41 kJ/mole)[168] on a per interaction basis, the total interaction energy from the VDW forces could overwhelm the contribution from hydrogen bonding due to the larger numbers of VDW interactions. The sum of many VDW interactions can be very strong as exemplified in the TLZ and PEG-*b*-PLA system where the VDW interaction energy with the (001) face is 27.1 kJ/mol/monomer (Figure 38a), reaching the level of a strong H-bond (O–H→O bonding energy is 25 kJ/mol).[168] This explains how a ppm level of PEG-*b*-PLA was able to block the (001) surface growth.[158]

The lack of experimental techniques to accurately measure the level of hydrophobic interactions between the polymer and the drug may have been why the hydrophobic interactions have not been emphasized in the past. Recently more work has recognized the role of hydrophobic interactions in crystallization inhibition. In 2013, IIevbare *et al.*[169] reported a comprehensive study on the crystal growth rate of three structurally diverse hydrophobic drugs (celecoxib, efavirenz, and ritonavir) in the presence of 22 different polymers in aqueous solution. Despite the different chemical properties and

structures of the model compounds, nonspecific hydrophobic drug−polymer interactions appeared to be important in determining the impact of a given polymer on crystal growth for of all three drugs. Among the 22 polymers, specific intermolecular interactions were only found between PVPVA [(poly(vinylpyrrolidone vinyl acetate)] and celecoxib and efavirenz. The same group reported again in 2013[157] that the effectiveness of these 22 polymers in inhibiting nucleation from aqueous solutions appeared to depend on the hydrophobicity of the polymer relative to that of the drugs (celecoxib, efavirenz and ritonavir). Powell *et al.*[170] studied crystal growth in organic glasses (amorphous form) of three poorly soluble hydrophobic drugs (nifedipine, felodipine and indomethacin) in the presence of 1% polymers. Interestingly, among the seven polymers tested, the ability to inhibit crystal growth is not well ordered by the strength of host−polymer hydrogen bonds, but correlates extremely well with the neat polymer's glass transition temperature (T_g), suggesting that the mobility of polymer chains is an important factor in inhibiting crystal growth in organic glasses. This study was focused on amorphous solids rather than crystal growth in aqueous solution. However, the outcome of the study indicated that H-bonds are not dominating stabilization factors and there may be other reasons why these polymers are so effective at merely 1%.

Therefore, for poorly water-soluble and highly hydrophobic compounds, polymers capable of forming a hydrophobic interaction would be more important than those with hydrogen bonding capacities. The MD simulation is capable of providing both VDW and electrostatic interaction energies to clearly delineate this insight. With the positive results from this study, it is encouraging to conduct more MD simulation studies in the future

using different drug–polymer systems in order to assess the broad impact of VDW interactions in drug crystallization inhibitions.

Conclusions

We employed MD simulations to study the interaction of an amphiphilic diblock copolymer (PEG-*b*-PLA) with tolazamide (001), (010) and (100) crystal surfaces in water. The very different behaviors of the polymer on each surface can be explained by different TLZ molecular packing on the surface layer and the differences in polymer–TLZ interaction energies. The results from the simulations demonstrated the polymer's strong interaction with (001), weaker interaction with (010) and minimal to no interaction with (100), which matched remarkably well with the reported crystal habit alteration by the preferential interaction of PEG-*b*-PLA primarily with the (001) and partially with (010).[158,164] The MD simulations suggest that for poorly water-soluble and hydrophobic drugs, such as tolazamide, the hydrophobic interaction is perhaps more important in establishing polymer-drug interaction in aqueous solutions. The implication of this conclusion is that during selection of polymers to inhibit crystallization and to maintain supersaturation during dissolution of enabling formulations, it is more important to look for polymers that can engage strong hydrophobic interactions rather than focusing solely on hydrogen binding capabilities. The consistency between the simulation and experimental results increased the confidence in further developing MD simulations as a tool to investigate polymer–drug interactions.

Acknowledgement

The authors acknowledge Dr. Geoff G. Z. Zhang, and Dr. Yihong Qiu, at AbbVie, Inc for scientific discussions, Mr. Rodger Henry, at AbbVie, Inc. for providing the TLZ single crystal structure file and AbbVie's Tuition Assistance Program for financial support.

CHAPTER SIX

GENERAL CONCLUSIONS

This dissertation applied primarily molecular dynamics simulations to investigate fundamental processes involved in the pharmaceutical aqueous mass transfer phenomena which are important in drug product research and development. The three separate but cohesive studies addressed the following questions. First, how does a drug crystal dissolve into aqueous medium at the molecular level? Secondly, by what mechanism can one polymorph rapidly convert to another in some cases? Thirdly, how do polymers interact with a crystal surface to slow down the crystallization or polymorphic conversion? Interesting results were obtained in each of the three investigations.

In the simulations of acetaminophen crystal Forms I and II dissolving into aqueous medium, we found that dissolution of the molecules from a crystal surface is not a random process. The order of the molecules entering the solution is strongly correlated with the drug–drug and drug–water interaction energies. The molecules at corners and edges quickly dissolved (corner and edge effect, shown in Figure 40) and those on different crystal faces dissolved at different rates (crystal face differentiated dissolution or morphology affected dissolution). Because of the corner and edge effect, there was no difference in the dissolution rate between the two acetaminophen polymorphs. In addition, these two nano-sized crystals exhibited much higher dissolution rate than regular size crystals which could not be accounted for by solubility and surface area

differences. The significance of these findings is two-fold; (1) the crystal morphology is expected to play a role in the initial dissolution rate, and (2) the existing dissolution equations based on surface area may not be able to estimate the dissolution rate of nanocrystals which have greater proportion of their molecules in corners and edges and countless defects created during milling.

(a) (b)

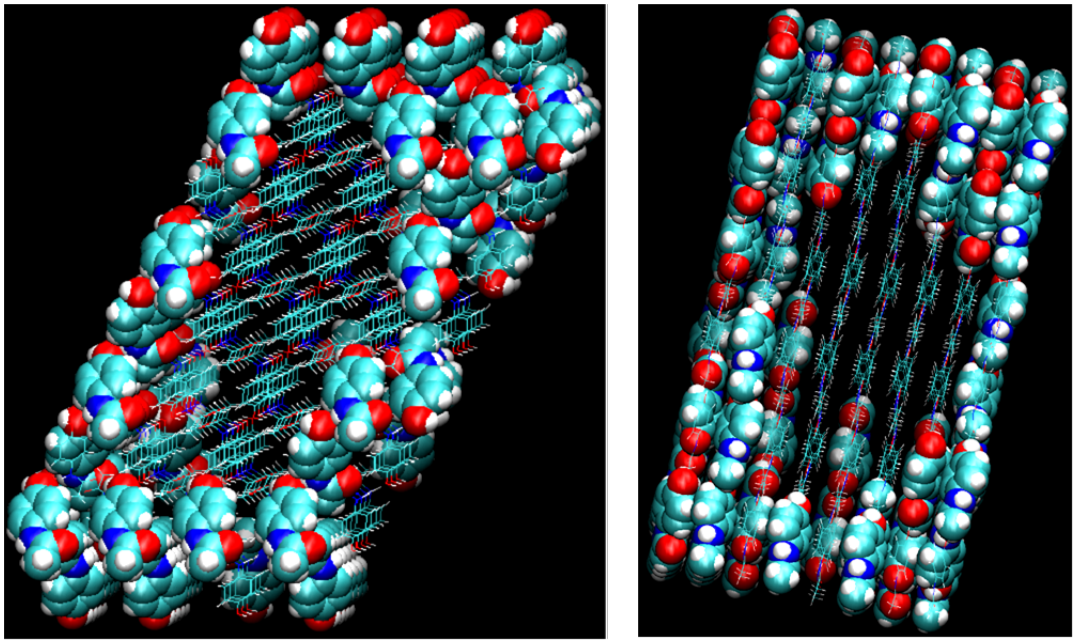

Figure 40. Corner and edge effect in drug crystal dissolution. Simulated from dissolution of ~4.5 nm acetaminophen single crystal in 0.15 M NaCl at 37 °C. Undissolved drug molecules are shown in line style and dissolved ones are in bulky VDW style. (a) Form I at 10 ns. (b) Form II at 10 ns.

In the second study, a series of MD simulations and experimental methods were utilized to identify which force (thermodynamic or kinetic) is responsible for the rapid polymorphic transformation of acetaminophen Form II to Form I in solutions. Using a new solubility method, we reported the first time an accurate measured thermodynamic solubility of Form II at 37°C. This allowed us to calculate the solubility ratio of Form II to Form I, which represents the thermodynamic driving force for the conversion. This value is only 1.27 ± 0.04 and was not high enough to create the supersaturation level to nucleate Form I. Finally, the molecular dynamics (MD) simulation suggested that large numbers of acetaminophen molecules were accumulating on the surface of Form II once in contact with water. This thick disordered molecular layer on Form II surface provides high local acetaminophen concentration for fast Form I crystallization. This was further supported by the rapid surface recrystallization of Form I from a Form II crystal in solution observed by polarized light microscopy and powder X-ray diffraction. The images from polarized light microscopy (Figure 29) showed no new crystals growing toward the solution phase, which is a truly surface crystallization phenomenon. Therefore, we identified a unique polymorphic transition mechanism, termed as SurFPT (surface facilitated phase transformation), as illustrated shown in Figure 41. This new mechanism promotes faster polymorphic transformation than the well-known mechanism of solution-mediated phase transformation (SMPT).

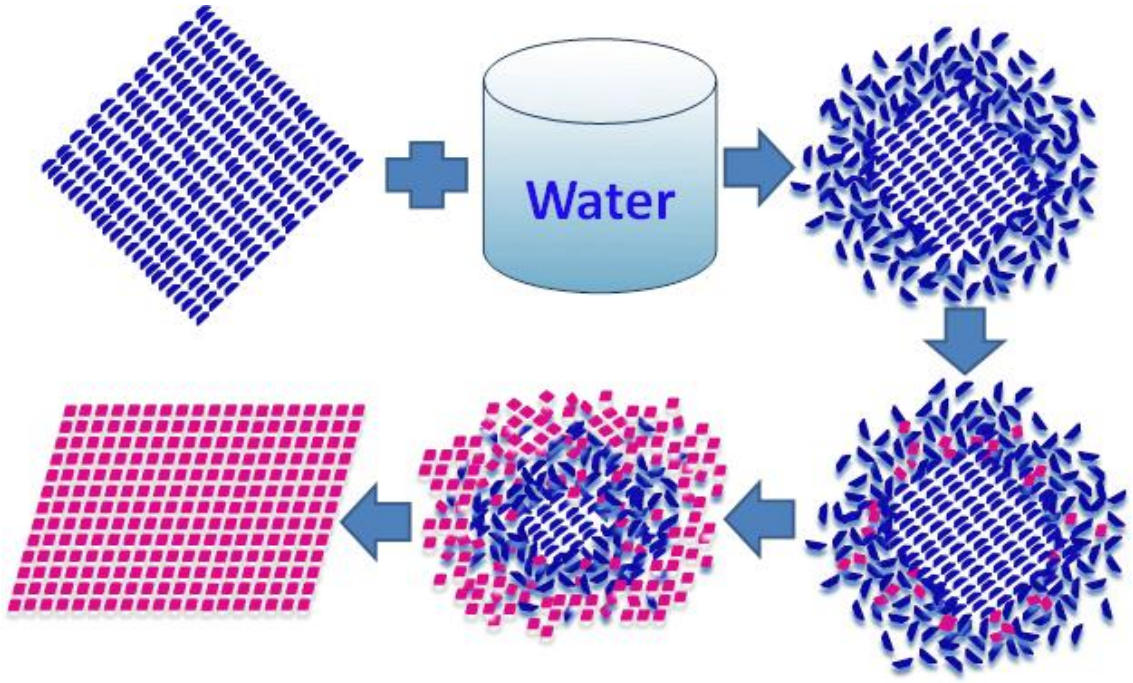

Figure 41. Schematic illustration of surface facilitated phase transformation (SurFPT). The metastable form hydrates at once when the water is introduced. The hydrated molecules quickly accumulate on the surface, approaching a high enough supersaturation level which leads to crystallization into the more stable solid form.

The third study simulated tolazamide crystal surfaces in the presence of hydrated PEG-*b*-PLA, a diblock copolymer for 50 ns in a large water box. In this simulation the crystals were not allowed to dissolve so that the molecular interaction of the crystal surface with the polymer was visualized and the interaction energies were calculated. The results from the simulations demonstrated the polymer's strong interaction with the (001) face, weaker interaction with the (010) face and minimal to no interaction with the (100) face, which matched remarkably well with the reported crystal habit alteration by the preferential interaction of PEG-*b*-PLA primarily with the (001) face and partially with the (010) face. Interestingly, van der Waals interactions were identified as the dominant

forces, accounting for 77–93% of total interaction energy and enabling strong drug–polymer interactions on the (001) and (010) faces. These strong van der Waals interactions require a tight fit between the polymer and the crystal surface, as seen in Figure 42. These findings suggest that polymers capable of forming strong hydrophobic interactions are more effective in inhibiting crystallization of poorly water-soluble and hydrophobic drugs in aqueous media than those with hydrogen bonding capacities. Such in-depth analysis and understanding facilitate the rational selection of polymers in designing supersaturation-based enabling formulations.

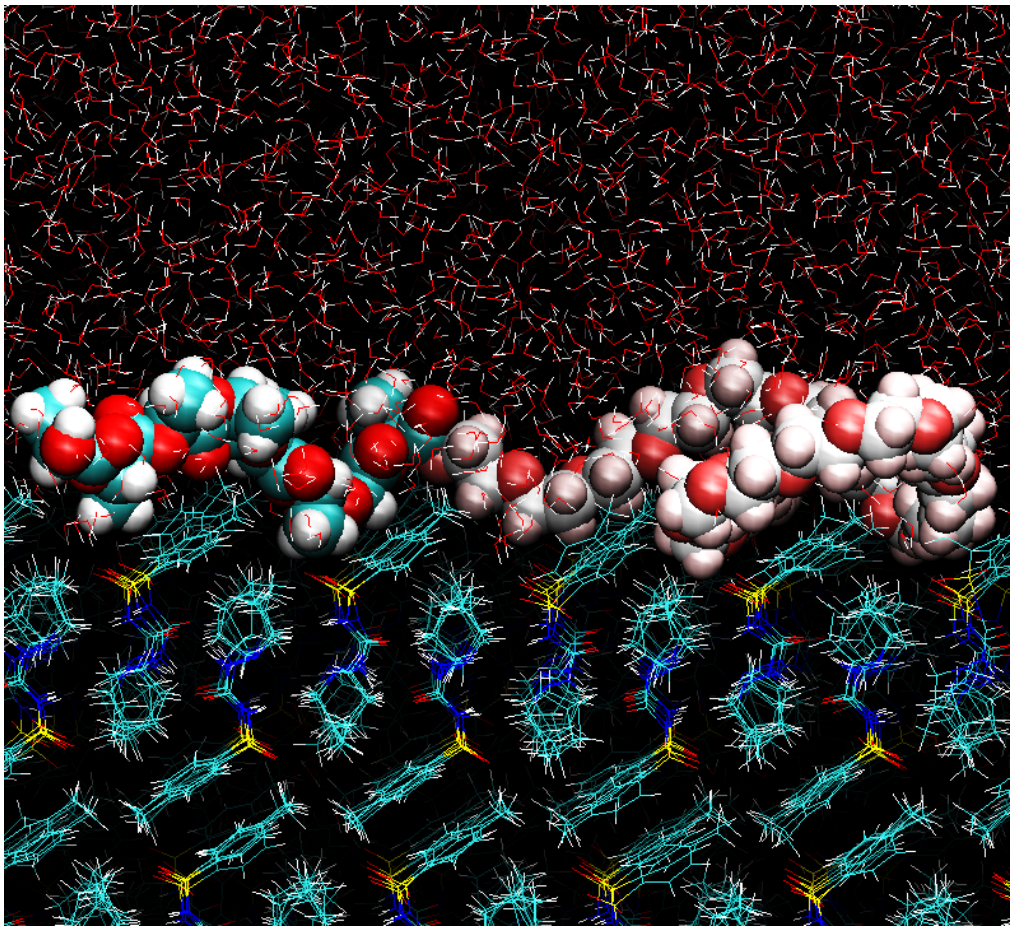

Figure 42. PEG-b-PLA polymer–TLZ interaction at the (001) crystal –water interface at 50 ns. The PLA part is located at the left side (color code of the atoms: oxygen is red, carbon is blue and hydrogen is white). The PEG part is at the right side (color code of the atoms: oxygen is red, carbon is beige and hydrogen is light pink).

CHAPTER SEVEN

FUTURE RESEARCH

Based on the recently available literature, we believe that the application of MD simulation in pharmaceutical research and development is still at an early phase. The results from this dissertation demonstrated that this new technique can significantly elevate our understanding in drug dissolution, polymorphic transformation and drug–polymer interactions. Future studies should not only continue in these topics, but also expand into other topics. Several ideas for future studies are outlined below.

Formulation Excipient Interaction with Drug Molecules

Drug–Polymer Interaction at the Crystal Surface

It is proposed to evaluate more polymer and drug systems. Structures and parameters for polymers frequently used in pharmaceutical formulations such as PVP, PVPVA, HPMC, HPMC-AS, HPC, etc. with or without H-bond capabilities can be populated as a database. Their interaction with various drug crystals with varied hydrophobicity can then be studied using our established MD simulation methodology. The purposes are (1) to evaluate the interaction forces (van der Waals or H-bonding or ionic) that are important (i.e. the broad impact of van der Waals interaction), and (2) to determine if the method is viable as a screening tool for rational selection of polymers.

Drug–Polymer–Surfactant Interaction and Its Impact on Crystallization

Surfactants are also frequently used in pharmaceutical formulation. Their role in crystallization of drug molecules in solution will be also very interesting. They can be studied using the same methodology in the presence or absence of polymers.

Pharmaceutical Nanoparticle Systems

Dissolution of Drug Nanoparticles

We have found that the APAP nanocrystals dissolved very quickly. The fast rate of dissolution could not be explained by existing knowledge based on the surface area or solubility. Larger crystals in sizes more close to real nanoparticles (such as 50–100 nm) can be studied in water when computationally possible. This will help (1) to understand the dissolution rate with respect to different nano sizes (i.e. at what sizes the dissolution rate can be described by the equations established for macrosize crystals) and (2) whether or not the diffusion layer exists. Another interesting study will be to compare the dissolution behavior of nanocrystals that are water soluble and poorly water-soluble.

The work presented in this dissertation demonstrates that all of these future studies are, or soon will be, possible.

CHAPTER EIGHT

DISCLOSURE

AbbVie and Loyola University Chicago jointly participated in the study design, research, data collection, analysis and interpretation of data, writing, reviewing, and approving the publication. Kenneth W. Olsen is a professor at Loyola University Chicago, and has no additional conflicts of interest to report. Yi Gao is an employee of AbbVie and may own AbbVie stock.

APPENDIX A

BUILDING CRYSTAL STRUCTURES

The following is a set of instructions on how to build a crystal surface using Mercury and VMD.

Open Mercury software and load the drug single crystal structure file. Click "Packing" to show the unit cell. On the main menu, select Calculate - Packing/Slicing. Type in the numbers of unit cells to build to the right side of the column under "Pack". Maximum of 10 unit cell can be entered. To build more than 10 unit cells, enter 10 on the right column, then enter minus number (i.e. -7) to the left side column. 17 unit cells will be built.

Using the building of tolazamide (TLZ) 17x2x8 lattice (010) face as an example, in "a" direction, enter 10 on the right column, then enter a minus number (i.e. -7) to the left side column. In "b" direction, enter 2 on the right column. Finally, in the "c" direction, enter 8 on the right column. It will take a long time for Mercury to build this large lattice. To check if a correct crystal face is made, under Calculate\Planes\New Plane, type h=0, k=1 and l=0 (010 phase). It showed (010) is the large surface in 17x2x8 lattice which is correct. Save it as a pdb file.

The lattice file (.pdb) will be viewed as a single chain by VMD rather than as multiple TLZ molecules. Therefore the following procedure needs to be done to convert the original pdb to a useful pdb file.

- Open the file via Word. Edit/Replace. Replace "UNK" with "TLZ" (the number spaces between UNK and next column, 1, should remain the same). Save it again using the original file name of "010_17x2x8.pdb". Hit OK.

- Delete the rows that do not need to be changed (first few rows until HETATM, and rows after HETATM). There are hundreds of pages to delete after HETATM. To speed up, select the starting point to delete, hold down shif/ctrl and hit “End”. This will select all from the selected rows. Hit “delete”. Save the file as “010_17x2x8_deleted un-needed rows.pdb”. Hit OK.
- Launch Excel program, File/Open “010_17x2x8_deleted un-needed rows.pdb”/Fixed Width. Click “Next”. Using the mouse to move the arrows that divide each columns to collapse the vertical lines before and after the column, 1, and leave only one line right before 1 (not 1.00). Be sure to collapse all vertical lines.
- Click next to open in Excel and save it as “010_17x2x8_deleted un-needed rows _clapsed.xls”.
- Insert 3 columns before the divided line (right before the number 1)
- In the 1st new column, type in Space. Copy/paste to the rest of rows.
- In the 3rd new column, type %. Copy/paste to the rest of rows.
- In the 2nd column, type 1 to the first 42 row (because 42 atoms form one molecule of TLZ). In the 43st row type in 1+row1, then copy all the way down (Shift/Page down to move faster). There will be 408 molecules in total. Copy down together with the 1st and 3rd columns can save time.
- Select the 2nd new column, go to Format Cell/Number/Custom, type in 00#, than hit OK. Now all of the numbers are in the format of 001, 002…., 099…, 408.

- Save it again as “010_17x2x8_deleted un-needed rows_clapsed.xls”. The next step is to Save it as file type CSV (select comma delimited, *.csv). 010_17x2x8_deleted un-needed rows_clapsed.csv. Hit YES when the next dialogue shows up.
- Open 010_17x2x8_deleted un-needed rows_clapsed.csv in Wordpad.
- Replace “,Space,” with two spaces
- Replace “,%,1” with no space
- After done, there should be 2 spaces before the molecule number, and 6 spaces after the molecule number.
- Save it as .txt file “010_17x2x8_ deleted un-needed rows.txt”. Close the file and open in Wordpad again.
- Open the original pdb file, “010_17x2x8.pdb” also in Wordpad. Select the first a few rows before HETATM, copy and paste to the beginning of 010_17x2x8_ deleted un-needed rows.txt file. Then select all rows after HETATM (shift/ctrl/END), copy and paste to the end of above txt file.
- Save the final text file as 010_17x2x8.pdb_finalized.pdb. This file can be opened from VMD shown as single chain for each TLZ molecule.

APPENDIX B

CALCULATION OF INTERACTION ENERGIES

The following is a set of VMD instructions for making the PDB files needed to measure the interaction energies, and scripts to calculate interaction energies in the NAMD program.

Interaction Energy between APAP and Surrounding APAPs

Using APAP# 241 as an example, the first thing to do is to identify the APAP# surrounding the APAP#241.

1. In VMP, load the psf and pdb files.
2. Run the following in tk console.

```
set sel [atomselect top "resname APAP and same resid as (resname APAP and within 4 of resid 241)"]
$sel writepdb 241.pdb
```

Open the 241.pdb file and 7 APAP# were shown: 242 50 49 33 177 114 178. The 2nd step is to create the following.

```
set basename apap1_40A
[atomselect top all] set beta 0
 [atomselect top "resname APAP and resid 242 50 49 33 177 114 178"] set beta 1
 [atomselect top "resid 241"] set beta 2
 [atomselect top all] writepdb $basename-interact_241.pdb
```

The above interact_241.pdb file is used to calculate the interaction of APAP#241 with surrounding APAPs within 4 A.

Interaction Energy between APAP and Surrounding Water

Similarly, use the following to create files for calculation.

```
set basename apap1_40A_APAPwater
[atomselect top all] set beta 0
 [atomselect top "resname TIP3"] set beta 1
```

[atomselect top "resname APAP and resname APAP and resid 4"] set beta 2
[atomselect top all] writepdb $basename-interact_4.pdb

Interaction Energy between APAP and NaCl

With Na+:

set basename apap1_40A_APAP_Na
[atomselect top all] set beta 0
[atomselect top "resname SOD"] set beta 1
[atomselect top "resname APAP and resid 61"] set beta 2
[atomselect top all] writepdb $basename-interact_61.pdb

With Cl-:

set basename apap1_40A_APAP_Cl
[atomselect top all] set beta 0
[atomselect top "resname CLA"] set beta 1
[atomselect top "resname APAP and resid 61"] set beta 2
[atomselect top all] writepdb $basename-interact_61.pdb

Interaction Energy between TLZ Crystal Surface

and PEG-*b*-PLA Diblock Copolymer in Water

The whole polymer was defined as segname O3. For (001) face, the selection of the PLA

and PEG was defined by the following.

PLA part: index 34290 to 34307 or index 34456 to 34510

PEG part: index 34272 to 34289 or index 34308 to 34455

set basename tlz_peg_interact_z
[atomselect top all] set beta 0
[atomselect top "resname TLZ"] set beta 1
[atomselect top "segname O3"] set beta 2
[atomselect top all] writepdb $basename-all.pdb

set basename tlz_peg_interact_z
[atomselect top all] set beta 0
[atomselect top "resname TLZ"] set beta 1
[atomselect top "index 34290 to 34307 or index 34456 to 34510"] set beta 2

[atomselect top all] writepdb $basename-pla.pdb

The index numbers for (100) face are: PLA part index 16312 to 16366 or index 16146 to 16163. PEG part index 16164 to 16311 or index 16128 to 16145.

The index numbers for (001) face are: PLA part index 23032 to 23086 or index 22866 to 22883. PEG part index 22884 to 23031 or index 22848 to 22865.

MAMD Script to Calculate Interaction Energies

An example script is shown below for the calculation of the PEG chain with the TLZ crystal (001) face.

```
# initial config
coordinates     tlz_peg_all_z_wb_autopsf.pdb
temperature     0

# output params
outputname      tlz_peg-interact_z_peg
binaryoutput    no

# integrator params
timestep        2.0

# force field params
structure       tlz_peg_all_z_wb_autopsf.psf
paraTypeCharmm      on
parameters      par_all27_prot_lipid_apap.inp
parameters      Tolazamide.par
parameters      Spartan_min1_pdb.par
exclude         scaled1-4
1-4scaling      1.0
switching       on
switchdist      10.0
cutoff          12.0
pairlistdist    13.5
stepspercycle   40

# Atoms in group 1 have a 1 in the B column; group 2 has a 2.
```

```
pairInteraction          on
pairInteractionFile      tlz_peg_interact_z-peg.pdb
pairInteractionCol       B
pairInteractionGroup1 1
pairInteractionGroup2 2

# First frame saved was frame 1000.
set ts 150

coorfile open dcd tlz_peg_all_z_wb_prod_1-50_stride400.dcd

# Read all frames until nonzero is returned.
while { ![coorfile read] } {
  # Set firstTimestep so our energy output has the correct TS.
  firstTimestep $ts
  # Compute energies and forces, but don't try to move the atoms.
  run 0
  incr ts 150
}
coorfile close
```

APPENDIX C

CALCULATIION OF NUMERS OF MOLECULES DISSOLVED WITH TIME

The following are steps to calculate the numbers of molecules dissolved from the crystals into water.

Claculation of APAP Form I Dissolved with Time

The first step is to identify the 4 APAP resid numbers (167, 218, 234 and 26) located in the center of the crysal. Then use the VMD to calculate the numbers of molecules dissolving by the following steps.

- Load dcd file of APAP1_4x4x4_40A water (1-10 stride 100) and the PSF file.
- Under Extension/Analysis/RMSD Trajectory tool, enter “resname APAP and resid 167 218 234 26”. Click “Align” to fix the molecule so that they do not move during calculation.
- In Representation, create one with “resname APAP and not within X of (resname APAP and resid 167 218 234 26)”. X is the radius of the crystal and was found to be 29 for APAP1 in oder to inclue all of the molecules in the crystal at time 0.
- Run the following sripit.

```
#get the number of frames
set mol top
set num_steps [molinfo $mol get numframes]
#open file for writing
set fil [open number_apap_disolved.dat w]
#loop over all frames in the trajectory
for {set i 0} {$i < $num_steps} {incr i} {
#select apaps and count

set sel [atomselect top "type OH1 and resname APAP and not within 29 of (resname
APAP and resid 167 218 234 26)"]
$sel frame $i
$sel update
set num_apap [$sel num]
```

```
puts $fil "$i $num_apap"
}
close $fil
```

Calculation of APAP Form II Dissolved with Time

Similarly, the first step is to identify the 4 molecules located in the center of the Form II crystal. The script is listed in the following.

```
#get the number of frames
set mol top
set num_steps [molinfo $mol get numframes]
#open file for writing
set fil [open number_apap_disolved.dat w]
#loop over all frames in the trajectory
for {set i 0} {$i < $num_steps} {incr i} {
#select apaps and count
set sel [atomselect top "type OH1 and resname APAP and not within 27 of (resname
APAP and resid 19 126 162 271)"]
$sel frame $i
$sel update
set num_apap [$sel num]
puts $fil "$i $num_apap"
}
close $fil
```

APPENDIX D

ANALYSIS OF THE LOG FILE FOR INTERACTION ENERGIES

Steps to plot the log file for interaction energy profile is described below using simulation file of APAP1_4x4x4_40 A water box as an exmple.

- launch VMD.
- Extensions/Analysis/NAMD plot.
- Under File, select the log file for plot (e.g corner1.log, a txt file).
- Click the energy to plot (Electric, VWD and total).
- Go back to File/Plot selected data.
- A plot will show up. In the plot, go to File/Export Xmgrace, then save it as corner1.arg file (click No and ignore the subsequent error message). Each log file will generate 3 arg files (elect, VDW and total).
- The saved file can be opened in Excel. From Excel, File/Open .arg file, select delimited/next/Space/next until finish.
- Plot elect, VDW and total as 3 groups.

APPENDIX E

CALCULATION OF PAIR CORRELATION FUNCTION G(R)

Below are the steps to calculate g(r), pair correlation function as a function of frame number by the VMD program, using APAP1 as an example.

1. VMD/Load the dcd file of APAP1 at stride 100 and the PSF file.
2. Locate the center molecule (resid 167).
3. Under Extention/Analysis/Trajectory tool, delete “protein”. Enter “resname APAP and resid 167”. Click “Align” to fix the structure.
4. Under Extention/Analysis/Radial Pair Distribution Function g(r), set up the following: Selection 1 = resname APAP and resid 167. Selection 2 = resname APAP. Frame number: from 0 to 0. Step = 1. Delta r = 0.1. Max = 50 (cover the diameter of the crystal). Click “use PBC”. Click “display g(r)”. Click “Save file” to save it under a designated folder. Finally, click “computer g(r)”.
5. The file generated can be plotted using Excel.

APPENDIX F

CALCULATION OF NUMBERS OF HYDROGEN BONDS

Below are steps to calculate the numbers of hydrogen bonds as a function of frame number by the VMD program, using APAP1 as an example.

1. In VMD main menu, File/New molecule/Browse/Load the following files.

   APAP1_40A_autopsf_ion.psf

   APAP1_40A_autopsf_ion_prod_1to10_stride100.dcd

2. Go to Main menu/Extensions/Analysis/Hbond

   a. Selection: resname APAP

   b. Frames: all

   c. Click to select "Update selection every frame?"

   d. Selection 1 is: both

   e. Donor/acceptor distance: 3.0

   f. Angle cut-off: 20

   g. Calculation detailed information for: unique hbond

   h. Output options

      i. Select "Plot the data to multiplot"

      ii. Directory is automatically selected

      iii. Frame/bond data: hbond.dat

      iv. Details output file: hbond_details.dat

      i. Click "Find hydrogen bonds"

Note that it will take a long time (~15 min) to finish the calculation. Three files will be saved: gr0.dat, hbonds.dat and hbonds-details.dat. The hbond.dat file can be opened from the Excel and plotted.

REFERENCES

(1) Dokoumetzidis, A.; Macheras, P.: A century of dissolution research: From Noyes and Whitney to the Biopharmaceutics Classification System. *Int. J. Pharm.* **2006**, *321*, 1-11.

(2) Xu, C.; Zou, M.; Liu, Y.; Ren, J.; Tian, Y.; Yan, J.; Wang, Y.; Cheng, G.: Pharmacokinetics of carbamazepine polymorphs and dihydrate in rats, related to dogs and humans. *Arch. Pharmacal Res.* **2011**, *34*, 1973-1982.

(3) Kobayashi, Y.; Ito, S.; Itai, S.; Yamamoto, K.: Physicochemical properties and bioavailability of carbamazepine polymorphs and dihydrate. *Int. J. Pharm.* **2000**, *193*, 137-146.

(4) Noyes, A. A.; Whitney, W. R.: The rate of solution of solid substances in their own solutions. *J. Am. Chem. Soc.* **1897**, *19*, 930-4.

(5) Nernst, W.: Theory of reaction velocity in heterogenous systems. *Z. Phys. Chem., Stoechiom. Verwandtschaftsl.* **1904**, *47*, 52-55.

(6) Wang, J.; Douglas, R. F.: Fundamentals of Dissolution. In *Developing Solid Oral Dosage Forms Pharmaceutical Theory and Practice*; 1st ed.; Qiu, Y., Chen, Y., Zhang, G. G. Z., Eds.; Academic Press: New York, USA, 2009; pp 309-318.

(7) Uddin, R.; Nadia Saffoon, K. B. S.: Dissolution and Dissolution Apparatus: A Review. *International Journal of Current Biomedical and Pharmaceutical Research* **2011**, *1*, 201-207.

(8) Wang, J.; Flanagan, D. R.: General Solution for Diffusion-Controlled Dissolution of Spherical Particles. 1. Theory. *J. Pharm. Sci.* **1999**, *88*, 731-738.

(9) Wang, J.; Flanagan, D. R.: General solution for diffusion-controlled dissolution of spherical particles. 2. Evaluation of experimental data. *J. Pharm. Sci.* **2002**, *91*, 534-542.

(10) Grant, D. J. W.: Theory and origin of polymorphism. *Drugs Pharm. Sci.* **1999**, *95*, 1-33.

(11) Brittain, H. G.; Grant, D. J. W.: Effects of polymorphism and solid-state solvation on solubility and dissolution rate. *Drugs Pharm. Sci.* **1999**, *95*, 279-330.

(12) Zhang, G. G. Z.; Zhou, D.: *Chapter 2 Crystalline and Amorphous Solids*; 1st ed.; Academic Press: New York, 2009.

(13) Burger, A.; Ramberger, R.: On the polymorphism of pharmaceuticals and other molecular crystals. I. Theory of thermodynamic rules. *Mikrochim. Acta* **1979**, *2*, 259-71.

(14) Dudognon, E.; Correia, N. T.; Danede, F.; Descamps, M.: Solid-Solid Transformation in Racemic Ibuprofen. *Pharm. Res.* **2013**, *30*, 81-89.

(15) Higuchi, T.; Shefter, E.: The influence of hydrate and solvate formation on rates of solution and solubility of crystalline drugs. *Sci. Sect. Am. Pharm. Assoc., Preprint Papers, Las Vegas, Nevada* **1962**, 9 pp.

(16) Chen, D.; Haugstad, G.; Li, Z. J.; Suryanarayanan, R.: Water sorption induced transformations in crystalline solid surfaces: characterization by atomic force microscopy. *J. Pharm. Sci.* **2010**, *99*, 4032-4041.

(17) Zhang, G. G. Z.; Law, D.; Schmitt, E. A.; Qiu, Y.: Phase transformation considerations during process development and manufacture of solid oral dosage forms. *Adv. Drug Delivery Rev.* **2004**, *56*, 371-390.

(18) Greco, K.; Bogner, R.: Solution-mediated phase transformation: Significance during dissolution and implications for bioavailability. *J. Pharm. Sci.* **2012**, *101*, 2996-3018.

(19) Alonzo, D. E.; Zhang, G. G. Z.; Zhou, D.; Gao, Y.; Taylor, L. S.: Understanding the Behavior of Amorphous Pharmaceutical Systems during Dissolution. *Pharm. Res.* **2010**, *27*, 608-618.

(20) Greco, K.; McNamara, D. P.; Bogner, R.: Solution-mediated phase transformation of salts during dissolution: Investigation using haloperidol as a model drug. *J. Pharm. Sci.* **2011**, *100*, 2755-2768.

(21) Croker, D. M.; Davey, R. J.; Rasmuson, A. C.; Seaton, C. C.: Solution-mediated phase transformations between co-crystals. *CrystEngComm* **2013**, *15*, 2044-2047.

(22) Mullin, J. W.: Nucleation. *Cryatallization* **2001**, 181–215.

(23) Higuchi, T.: Some physical chemical aspects of suspension formulation. *J. Am. Pharm. Assoc. (1912-1977)* **1958**, *47*, 657-60.

(24) Graham, D.: Physical Chemistry Course 435 at Loyola University Department of Chemistry. **2007**, Chapter 18.

(25) Mullin, J. W.: Crystal Growth. In *Crystallization*; 4th ed.; Mullin, J. W., Ed.; Elsevier, 2004; pp 216-284.

(26) Simonelli, A. P.; Mehta, S. C.; Higuchi, W. I.: Inhibition of sulfathiazole crystal growth by polyvinylpyrrolidone. *J. Pharm. Sci.* **1970**, *59*, 633-8.

(27) Char, K.; Frank, C. W.; Gast, A. P.: Fluorescence studies of polymer adsorption. 2. A simple model describing adsorbed polymer rearrangement. *Langmuir* **1989**, *5*, 1096-105.

(28) Duro, R.; Souto, C.; Gomez-Amoza, J. L.; Martinez-Pacheco, R.; Concheiro, A.: Interfacial adsorption of polymers and surfactants: implications for the properties of disperse systems of pharmaceutical interest. *Drug Dev. Ind. Pharm.* **1999**, *25*, 817-829.

(29) Eskilsson, K.; Tiberg, F.: Equilibrium and kinetic properties of triblock copolymers at hydrophobic surfaces. *Macromolecules* **1997**, *30*, 6323-6332.

(30) Furusawa, K.; Tagawa, T.: Adsorption behavior of water soluble polymers with lower critical solution temperature. *Colloid Polym. Sci.* **1985**, *263*, 353-60.

(31) Kislenko, V. N.; Berlin, A. A.; Kawaguchi, M.; Kato, T.: Mathematical Models of Polymer Adsorption at a Porous Adsorbent Surface. *Langmuir* **1996**, *12*, 768-73.

(32) Alonzo, D. E.; Raina, S.; Zhou, D.; Gao, Y.; Zhang, G. G. Z.; Taylor, L. S.: Characterizing the Impact of Hydroxypropylmethyl Cellulose on the Growth and Nucleation Kinetics of Felodipine from Supersaturated Solutions. *Cryst. Growth Des.* **2012**, *12*, 1538-1547.

(33) McCammon, J. A.; Gelin, B. R.; Karplus, M.: Dynamics of folded proteins. *Nature (London)* **1977**, *267*, 585-90.

(34) Brooks, B. R.; Brooks, C. L., III; Mackerell, A. D., Jr.; Nilsson, L.; Petrella, R. J.; Roux, B.; Won, Y.; Archontis, G.; Bartels, C.; Boresch, S.; Caflisch, A.; Caves, L.; Cui, Q.; Dinner, A. R.; Feig, M.; Fischer, S.; Gao, J.; Hodoscek, M.; Im, W.; Kuczera, K.; Lazaridis, T.; Ma, J.; Ovchinnikov, V.; Paci, E.; Pastor, R. W.; Post, C. B.; Pu, J. Z.; Schaefer, M.; Tidor, B.; Venable, R. M.; Woodcock, H. L.; Wu, X.; Yang, W.; York, D. M.; Karplus, M.: CHARMM: The biomolecular simulation program. *J. Comput. Chem.* **2009**, *30*, 1545-1614.

(35) Karplus, M.; Kuriyan, J.: Molecular dynamics and protein function. *Proc. Natl. Acad. Sci. U. S. A.* **2005**, *102*, 6679-6685.

(36) Markwick, P. R. L.; McCammon, J. A.: Studying functional dynamics in bio-molecules using accelerated molecular dynamics. *Phys. Chem. Chem. Phys.* **2011**, *13*, 20053-20065.

(37) Schlick, T.: Theoretical and Computational Approaches to Biomolecular Structure. In *Molecular Modeling and Simulation: An Interdisciplinary Guide*; 1st ed.; Marsden, J. E., Sirovich, L., Wiggins, S., Antman, S. S., Eds.; Springer: New York, 2006; pp 199-224.

(38) Adcock, S. A.; McCammon, J. A.: Molecular dynamics: Survey of methods for simulating the activity of proteins. *Chem. Rev. (Washington, DC, U. S.)* **2006**, *106*, 1589-1615.

(39) MacKerell, A. D., Jr.; Bashford, D.; Bellott, M.; Dunbrack, R. L.; Evanseck, J. D.; Field, M. J.; Fischer, S.; Gao, J.; Guo, H.; Ha, S.; Joseph-McCarthy, D.; Kuchnir, L.; Kuczera, K.; Lau, F. T. K.; Mattos, C.; Michnick, S.; Ngo, T.; Nguyen, D. T.; Prodhom, B.; Reiher, W. E., III; Roux, B.; Schlenkrich, M.; Smith, J. C.; Stote, R.; Straub, J.; Watanabe, M.; Wiorkiewicz-Kuczera, J.; Yin, D.; Karplus, M.: All-Atom Empirical Potential for Molecular Modeling and Dynamics Studies of Proteins. *J. Phys. Chem. B* **1998**, *102*, 3586-3616.

(40) Schlick, T.: Molecular Dynamics: Basics. In *Molecular Modeling and Simulation: An Interdisciplinary Guide*; 1st ed.; Marsden, J. E., Sirovich, L., Wiggins, S., Antman, S. S., Eds.; Springer: New York, 2006; pp 383-416.

(41) Gao, Y.; Olsen, K. W.: Molecular dynamics of drug crystal dissolution: simulation of acetaminophen form I in water. *Mol Pharm* **2013**, *10*, 905-17.

(42) Ohtaki, H.; Fukushima, N.: Dissolution of an sodium chloride crystal with the (1 1 1) and (-1-1-1) faces. *Pure Appl. Chem.* **1989**, *61*, 179-85.

(43) Ohtaki, H.; Fukushima, N.; Hayakawa, E.; Okada, I.: Dissolution process of sodium chloride crystal in water. *Pure Appl. Chem.* **1988**, *60*, 1321-4.

(44) Ohtaki, H.; Mikami, M.; Tago, Y.: Molecular dynamics simulations for dissolution and nucleation processes of alkali halide crystals in water. Pt. 1 ed.; North-Holland, 1993; pp 265-8.

(45) Liu, L.-M.; Laio, A.; Michaelides, A.: Initial stages of salt crystal dissolution determined with ab initio molecular dynamics. *Phys. Chem. Chem. Phys.* **2011**, *13*, 13162-13166.

(46) Karplus, M.: Molecular dynamics of biological macromolecules: A brief history and perspective. *Biopolymers* **2003**, *68*, 350-358.

(47) Sen, A.; Ganguly, B.: A computational study toward understanding the separation of ions of potassium chloride microcrystal in water. *Theor. Chem. Acc.* **2012**, *131*, 1-13.

(48) de Leeuw, N. H.; Parker, S. C.; Harding, J. H.: Molecular dynamics simulation of crystal dissolution from calcite steps. *Phys. Rev. B: Condens. Matter Mater. Phys.* **1999**, *60*, 13792-13799.

(49) Spagnoli, D.; Cooke, D. J.; Kerisit, S.; Parker, S. C.: Molecular dynamics simulations of the interaction between the surfaces of polar solids and aqueous solutions. *J. Mater. Chem.* **2006**, *16*, 1997-2006.

(50) Piana, S.; Gale, J. D.: Understanding the Barriers to Crystal Growth: Dynamical Simulation of the Dissolution and Growth of Urea from Aqueous Solution. *J. Am. Chem. Soc.* **2005**, *127*, 1975-1982.

(51) Hayakawa, D.; Ueda, K.; Yamane, C.; Miyamoto, H.; Horii, F.: Molecular dynamics simulation of the dissolution process of a cellulose triacetate-II nano-sized crystal in DMSO. *Carbohydr. Res.* **2011**, *346*, 2940-2947.

(52) Toroz, D.; Hammond, R. B.; Roberts, K. J.; Harris, S.; Ridley, T.: Molecular dynamics simulations of organic crystal dissolution: The lifetime and stability of the polymorphic forms of para-amino benzoic acid in aqueous environment. *J. Cryst. Growth* **2014**, Ahead of Print.

(53) Li, Y.-C.; Rissanen, S.; Stepniewski, M.; Cramariuc, O.; Rog, T.; Mirza, S.; Xhaard, H.; Wytrwal, M.; Kepczynski, M.; Bunker, A.: Study of Interaction Between PEG Carrier and Three Relevant Drug Molecules: Piroxicam, Paclitaxel, and Hematoporphyrin. *J. Phys. Chem. B* **2012**, *116*, 7334-7341.

(54) Costache, A. D.; Sheihet, L.; Zaveri, K.; Knight, D. D.; Kohn, J.: Polymer-Drug Interactions in Tyrosine-Derived Triblock Copolymer Nanospheres: A Computational Modeling Approach. *Mol. Pharmaceutics* **2009**, *6*, 1620-1627.

(55) Kasimova, A. O.; Pavan, G. M.; Danani, A.; Mondon, K.; Cristiani, A.; Scapozza, L.; Gurny, R.; Moller, M.: Validation of a Novel Molecular Dynamics Simulation Approach for Lipophilic Drug Incorporation into Polymer Micelles. *J. Phys. Chem. B* **2012**, *116*, 4338-4345.

(56) Samanta, S.; Roccatano, D.: Interaction of Curcumin with PEO-PPO-PEO Block Copolymers: A Molecular Dynamics Study. *J. Phys. Chem. B* **2013**, *117*, 3250-3257.

(57) Subashini, M.; Devarajan, P. V.; Sonavane, G. S.; Doble, M.: Molecular dynamics simulation of drug uptake by polymer. *J. Mol. Model.* **2011**, *17*, 1141-1147.

(58) Shahzad, Y.; Sohail, S.; Arshad, M. S.; Hussain, T.; Shah, S. N. H.: Development of solid dispersions of artemisinin for transdermal delivery. *Int. J. Pharm. (Amsterdam, Neth.)* **2013**, *457*, 197-205.

(59) Fule, R.; Meer, T.; Sav, A.; Amin, P.: Solubility and dissolution rate enhancement of lumefantrine using hot melt extrusion technology with physicochemical characterisation. *J. Pharm. Invest.* **2013**, *43*, 305-321.

(60) Gupta, J.; Nunes, C.; Vyas, S.; Jonnalagadda, S.: Prediction of Solubility Parameters and Miscibility of Pharmaceutical Compounds by Molecular Dynamics Simulations. *J. Phys. Chem. B* **2011**, *115*, 2014-2023.

(61) Maus, M.; Wagner, K. G.; Kornherr, A.; Zifferer, G.: Molecular dynamics simulations for drug dosage form development: thermal and solubility characteristics for hot-melt extrusion. *Mol. Simul.* **2008**, *34*, 1197-1207.

(62) Patel, S. K.; Lavasanifar, A.; Choi, P.: Roles of Nonpolar and Polar Intermolecular Interactions in the Improvement of the Drug Loading Capacity of PEO-b-PCL with Increasing PCL Content for two Hydrophobic Cucurbitacin Drugs. *Biomacromolecules* **2009**, *10*, 2584-2591.

(63) Xiang, T.-X.; Anderson, B. D.: Molecular dynamics simulation of amorphous indomethacin-poly(vinylpyrrolidone) glasses: Solubility and hydrogen bonding interactions. *J. Pharm. Sci.* **2013**, *102*, 876-891.

(64) Yani, Y.; Chow, P. S.; Tan, R. B. H.: Molecular Simulation Study of the Effect of Various Additives on Salbutamol Sulfate Crystal Habit. *Mol. Pharmaceutics* **2011**, *8*, 1910-1918.

(65) Zhu, W.; Romanski, F. S.; Dalvi, S. V.; Dave, R. N.; Silvina Tomassone, M.: Atomistic simulations of aqueous griseofulvin crystals in the presence of individual and multiple additives. *Chem. Eng. Sci.* **2012**, *73*, 218-230.

(66) Zhu, W.; Romanski, F. S.; Meng, X.; Mitra, S.; Tomassone, M. S.: Atomistic simulation study of surfactant and polymer interactions on the surface of a fenofibrate crystal. *Eur. J. Pharm. Sci.* **2011**, *42*, 452-461.

(67) Duffy, D. M.; Rodger, P. M.: Modeling the interaction between the poly(octadecyl acrylate) inhibitor and an n-octacosane crystal. *Phys. Chem. Chem. Phys.* **2000**, *2*, 4804-4811.

(68) Zhang, S.-G.; Wang, F.-Y.; Tan, X.-Y.: MOLECULAR DYNAMICS SIMULATION THE HYDROXYAPATITE SCALE INHIBITION MECHANISM OF WATER-SOLUBLE POLYMERS. *J. Theor. Comput. Chem.* **2010**, *9*, 889-902.

(69) Zeng, J.-P.; Qian, X.-R.; Wang, F.-H.; Shao, J.-L.; Bai, Y.-S.: Molecular dynamics simulation on the interaction mechanism between polymer inhibitors and calcium phosphate. *J. Chem. Sci. (Bangalore, India)* **2014**, Ahead of Print.

(70) Wang, S.; Zhang, J.; Lu, G.: Molecular dynamics simulation on mechanism of scale inhibition of polymer. *Zhongguo Shiyou Daxue Xuebao, Ziran Kexueban* **2007**, *31*, 144-147.

(71) Dali, M. V.; Carstensen, J. T.: Effect of change in shape factor of a single crystal on its dissolution behavior. *Pharm. Res.* **1996**, *13*, 155-62.

(72) Gao, Y.; Carr, R. A.; Spence, J. K.; Wang, W. W.; Turner, T. M.; Lipari, J. M.; Miller, J. M.: A pH-Dilution Method for Estimation of Biorelevant Drug Solubility along the Gastrointestinal Tract: Application to Physiologically Based Pharmacokinetic Modeling. *Mol. Pharmaceutics* **2010**, *7*, 1516-1526.

(73) Grant, D. J. W.; Higuchi, T.: Dissolution Rates of Solids. In *Solubility Behavior of Organic Compounds*; Saunders, W. H. J., Ed.; John Wiley & Sons: New York, 1990; pp 474-538.

(74) Pedersen, P. V.; Brown, K. F.: Theoretical isotropic dissolution of nonspherical particles. *J. Pharm. Sci.* **1976**, *65*, 1437-42.

(75) Sperry, D. C.; Thomas, S. J.; Lobo, E.: Dissolution Modeling of Bead Formulations and Predictions of Bioequivalence for a Highly Soluble, Highly Permeable Drug. *Mol. Pharmaceutics* **2010**, *7*, 1450-1457.

(76) Schlick, T.: Biomolecular Structure and Modeling: Historical Perspective. In *Molecular Modeling and Simulation: An Interdisciplinary Guide*; 1st ed.; Marsden, J. E., Sirovich, L., Wiggins, S., Antman, S. S., Eds.; Springer: New York, 2006; pp 1-27.

(77) Fischer, S.; Olsen, K. W.; Nam, K.; Karplus, M.: Unsuspected pathway of the allosteric transition in hemoglobin. *Proc. Natl. Acad. Sci. U. S. A.* **2011**, *108*, 5608-5613, S5608/1-S5608/6.

(78) Golden, S. D.; Olsen, K. W.: Identification of ligand-binding pathways in truncated hemoglobins using locally enhanced sampling molecular dynamics. *Methods Enzymol.* **2008**, *437*, 459-475, color pl. 18, 19.

(79) Lindorff-Larsen, K.; Piana, S.; Dror, R. O.; Shaw, D. E.: How fast-folding proteins fold. *Science (Washington, DC, U. S.)* **2011**, *334*, 517-520.

(80) Klein, M. L.; Shinoda, W.: Large-Scale Molecular Dynamics Simulations of Self-Assembling Systems. *Science (Washington, DC, U. S.)* **2008**, *321*, 798-800.

(81) Mathe, J.; Aksimentiev, A.; Nelson, D. R.; Schulten, K.; Meller, A.: Orientation discrimination of single-stranded DNA inside the α-hemolysin membrane channel. *Proc. Natl. Acad. Sci. U. S. A.* **2005**, *102*, 12377-12382.

(82) Zou, X.; Ma, W.; Solov'yov, I. A.; Chipot, C.; Schulten, K.: Recognition of methylated DNA through methyl-CpG binding domain proteins. *Nucleic Acids Res.* **2012**, *40*, 2747-2758.

(83) Gullingsrud, J.; Schulten, K.: Lipid bilayer pressure profiles and mechanosensitive channel gating. *Biophys. J.* **2004**, *86*, 3496-3509.

(84) Heller, H.; Schaefer, M.; Schulten, K.: Molecular dynamics simulation of a bilayer of 200 lipids in the gel and in the liquid crystal phase. *J. Phys. Chem.* **1993**, *97*, 8343-60.

(85) Karplus, M.; McCammon, J. A.: Molecular dynamics simulations of biomolecules. *Nat. Struct. Biol.* **2002**, *9*, 646-652.

(86) Nicholson, J.; Hupp, T. R.: The molecular dynamics of MDM2. *Cell Cycle* **2010**, *9*, 1878-1881.

(87) Salsbury, F. R., Jr.: Molecular dynamics simulations of protein dynamics and their relevance to drug discovery. *Curr. Opin. Pharmacol.* **2010**, *10*, 738-744.

(88) Wang, H.; Laughton, C. A.: Molecular modelling methods to quantitate drug-DNA interactions. *Methods Mol. Biol. (Totowa, NJ, U. S.)* **2010**, *613*, 119-131.

(89) Yarnitzky, T.; Levit, A.; Niv, M. Y.: Homology modeling of G-protein-coupled receptors with X-ray structures on the rise. *Curr. Opin. Drug Discovery Dev.* **2010**, *13*, 317-325.

(90) Xiang, T. X.; Anderson, B. D.: Molecular distributions in interphases: statistical mechanical theory combined with molecular dynamics simulation of a model lipid bilayer. *Biophys. J.* **1994**, *66*, 561-72.

(91) Xiang, T.-x.; Anderson, B. D.: Mean molecular potentials in a model lipid bilayer: a molecular dynamics simulation. *J. Chem. Phys.* **1995**, *103*, 8666-78.

(92) Xiang, T.-x.; Anderson, B. D.: Molecular dissolution processes in lipid bilayers: A molecular dynamics simulation. *J. Chem. Phys.* **1999**, *110*, 1807-1818.

(93) Xiang, T.-X.; Anderson, B. D.: A molecular dynamics simulation of reactant mobility in an amorphous formulation of a peptide in poly(vinylpyrrolidone). *J. Pharm. Sci.* **2004**, *93*, 855-876.

(94) Li, T.; Morris, K. R.; Park, K.: Influence of Solvent and Crystalline Supramolecular Structure on the Formation of Etching Patterns on Acetaminophen Single Crystals: A Study with Atomic Force Microscopy and Computer Simulation. *J. Phys. Chem. B* **2000**, *104*, 2019-2032.

(95) Li, T.; Park, K.; Morris, K. R.: Understanding the Formation of Etching Patterns Using a Refined Monte Carlo Simulation Model. *Cryst. Growth Des.* **2002**, *2*, 177-184.

(96) Costache, A. D.; Sheihet, L.; Zaveri, K.; Knight, D. D.; Kohn, J.: Polymer-Drug Interactions in Tyrosine-Derived Triblock Copolymer Nanospheres: A Computational Modeling Approach. *Mol. Pharmaceutics* **2009**, *6*, 1620-1627.

(97) Sun, T.; Shao, X.; Cai, W.: Self-assembly behavior of β-cyclodextrin and imipramine. A Free energy perturbation study. *Chem. Phys.* **2010**, *371*, 84-90.

(98) Haisa, M.; Kashino, S.; Kawai, R.; Maeda, H.: The monoclinic form of p-hydroxyacetanilide. *Acta Crystallogr., Sect. B* **1976**, *B32*, 1283-5.

(99) Humphrey, W.; Dalke, A.; Schulten, K.: VMD: visual molecular dynamics. *J Mol Graph* **1996**, *14*, 33-8, 27-8.

(100) Phillips, J. C.; Braun, R.; Wang, W.; Gumbart, J.; Tajkhorshid, E.; Villa, E.; Chipot, C.; Skeel, R. D.; Kale, L.; Schulten, K.: Scalable molecular dynamics with NAMD. *J Comput Chem* **2005**, *26*, 1781-802.

(101) Garekani, H. A.; Ford, J. L.; Rubinstein, M. H.; Rajabi-Siahboomi, A. R.: Formation and compression characteristics of prismatic polyhedral and thin plate-like crystals of paracetamol. *Int. J. Pharm.* **1999**, *187*, 77-89.

(102) Kalantzi, L.; Reppas, C.; Dressman, J. B.; Amidon, G. L.; Junginger, H. E.; Midha, K. K.; Shah, V. P.; Stavchansky, S. A.; Barends, D. M.: Biowaiver monographs for immediate release solid oral dosage forms: acetaminophen (paracetamol). *J Pharm Sci* **2006**, *95*, 4-14.

(103) Lee, H. G.; Zhang, G. G. Z.; Flanagan, D. R.: Cocrystal intrinsic dissolution behavior using a rotating disk. *J. Pharm. Sci.* **2011**, *100*, 1736-1744.

(104) Sacchetti, M.: Thermodynamic analysis of DSC data for acetaminophen polymorphs. *J. Therm. Anal. Calorim.* **2001**, *63*, 345-350.

(105) Byrn, S. R.; Pfeiffer, R. R.; Stowell, J. G.: Drugs as Molecular Solids. In *Solid-State Chemistry of Drugs*; 2nd ed.; SSCI, Inc.: West Lafayette, Indiana, 1999; pp 3-40.

(106) Grant, D. J. W.; Higuchi, T.: Specific Interactions in Solubility Phenomena. In *Solubility Behavior of Organic Compounds*; Saunders, W. H. J., Ed.; John Wiley & Sons: New York, 1990; pp 143-163.

(107) Grant, D. J. W.; Higuchi, T.: Intermolecular Interactions and Their Influence on Solubility. In *Solubility Behavior of Organic Compounds*; Saunders, W. H. J., Ed.; John Wiley & Sons: New York, 1990; pp 62-82.

(108) Danesh, A.; Connell, S. D.; Davies, M. C.; Roberts, C. J.; Tendler, S. J. B.; Williams, P. M.; Wilkins, M. J.: An in situ dissolution study of aspirin crystal planes (100) and (001) by atomic force microscopy. *Pharm. Res.* **2001**, *18*, 299-303.

(109) Prasad, K. V. R.; Ristic, R. I.; Sheen, D. B.; Sherwood, J. N.: Dissolution kinetics of paracetamol single crystals. *Int. J. Pharm.* **2002**, *238*, 29-41.

(110) Chow, A. H. L.; Grant, D. J. W.: Physical factors influencing the aqueous dissolution rate of acetaminophen crystals doped with p-acetoxyacetanilide: evaluation by multiple linear regression. *Int. J. Pharm.* **1989**, *51*, 129-35.

(111) Chan, H. K.; Grant, D. J. W.: Influence of compaction on the intrinsic dissolution rate of modified acetaminophen and adipic acid crystals. *Int. J. Pharm.* **1989**, *57*, 117-24.

(112) Mullin, J. W.: Nucleation. *Cryatallization* **2004**, 181–215.

(113) Erdemir, D.; Lee, A. Y.; Myerson, A. S.: Nucleation of Crystals from Solution: Classical and Two-Step Models. *Acc. Chem. Res.* **2009**, *42*, 621-629.

(114) Grant, D. J. W.; Brittain, H. G.: Solubility of pharmaceutical solids. *Drugs Pharm. Sci.* **1995**, *70*, 321-86.

(115) Bhargava, B. L.; Klein, M. L.: Initial Stages of Aggregation in Aqueous Solutions of Ionic Liquids: Molecular Dynamics Studies. *J. Phys. Chem. B* **2009**, *113*, 9499-9505.

(116) Schindler, M.; Mutter, A.; Hawthorne, F. C.; Putnis, A.: Prediction of crystal morphology of complex uranyl-sheet minerals. II. Observations. *Can. Mineral.* **2004**, *42*, 1651-1666.

(117) Chan, H. K.; Doelker, E.: Polymorphic transformation of some drugs under compression. *Drug Dev. Ind. Pharm.* **1985**, *11*, 315-32.

(118) Jacob, S.; Nair, A. B.; Patil, P. N.; Panda, B. P.: Solid state crystallinity, amorphous state, and its implications in the pharmaceutical process. *Int. J. Pharm. Sci. Res.* **2011**, *2*, 472-482.

(119) Yu, L.: Polymorphism in Molecular Solids: An Extraordinary System of Red, Orange, and Yellow Crystals. *Acc. Chem. Res.* **2010**, *43*, 1257-1266.

(120) Vippagunta, S. R.; Brittain, H. G.; Grant, D. J. W.: Crystalline solids. *Adv. Drug Delivery Rev.* **2001**, *48*, 3-26.

(121) Al-Zoubi, N.; Kachrimanis, K.; Malamataris, S.: Effects of harvesting and cooling on crystallization and transformation of orthorhombic paracetamol in ethanolic solution. *Eur. J. Pharm. Sci.* **2002**, *17*, 13-21.

(122) Heng, J. Y. Y.; Williams, D. R.: Wettability of Paracetamol Polymorphic Forms I and II. *Langmuir* **2006**, *22*, 6905-6909.

(123) Lopez-Mejias, V.; Knight, J. L.; Brooks, C. L., III; Matzger, A. J.: On the Mechanism of Crystalline Polymorph Selection by Polymer Heteronuclei. *Langmuir* **2011**, *27*, 7575-7579.

(124) Martino, P. D.; Guyot-Hermann, A. M.; Conflant, P.; Drache, M.; Guyot, J. C.: A new pure paracetamol for direct compression: the orthorhombic form. *Int. J. Pharm.* **1996**, *128*, 1-8.

(125) Nichols, G.; Frampton, C. S.: Physicochemical Characterization of the Orthorhombic Polymorph of Paracetamol Crystallized from Solution. *J. Pharm. Sci.* **1998**, *87*, 684-693.

(126) Rossmann, M.; Braeuer, A.; Leipertz, A.; Schluecker, E.: Manipulating the size, the morphology and the polymorphism of acetaminophen using supercritical antisolvent (SAS) precipitation. *J. Supercrit. Fluids* **2013**, *82*, 230-237.

(127) Perlovich, G. L.; Volkova, T. V.; Bauer-Brandl, A.: Polymorphism of paracetamol. Relative stability of the monoclinic and orthorhombic phase revisited by sublimation and solution calorimetry. *J. Therm. Anal. Calorim.* **2007**, *89*, 767-774.

(128) Fachaux, J. M.; Hermann, A. M. G.; Guyot, J. C.; Conflant, P.; Drache, M.; Huvenne, J. P.; Bouche, R.: Compression ability improvement by solvation/desolvation process: Application to paracetamol for direct compression. *Int. J. Pharm.* **1993**, *99*, 99-107.

(129) Espeau, P.; Ceolin, R.; Tamarit, J.-L.; Perrin, M.-A.; Gauchi, J.-P.; Leveiller, F.: Polymorphism of paracetamol: relative stabilities of the monoclinic and orthorhombic phases inferred from topological pressure-temperature and temperature-volume phase diagrams. *J. Pharm. Sci.* **2005**, *94*, 524-539.

(130) Fioritto, A. F.; Bhattachar, S. N.; Wesley, J. A.: Solubility measurement of polymorphic compounds via the pH-metric titration technique. *Int. J. Pharm.* **2007**, *330*, 105-113.

(131) Boldyreva, E. V.; Drebushchak, V. A.; Paukov, I. E.; Kovalevskaya, Y. A.; Drebushchak, T. N.: DSC and adiabatic calorimetry study of the polymorphs of paracetamol. *J. Therm. Anal. Calorim.* **2004**, *77*, 607-623.

(132) Sudha, C.; Srinivasan, K.: Supersaturation dependent nucleation control and separation of mono, ortho and unstable polymorphs of paracetamol by swift cooling crystallization technique. *CrystEngComm* **2013**, *15*, 1914-1921.

(133) Garekani, H. A.; Ford, J. L.; Rubinstein, M. H.; Rajabi-Siahboomi, A. R.: Formation and compression characteristics of prismatic polyhedral and thin plate-like crystals of paracetamol. *Int. J. Pharm.* **1999**, *187*, 77-89.

(134) Lang, M.; Grzesiak, A. L.; Matzger, A. J.: The Use of Polymer Heteronuclei for Crystalline Polymorph Selection. *J. Am. Chem. Soc.* **2002**, *124*, 14834-14835.

(135) Wen, H.; Morris, K. R.; Park, K.: Synergic Effects of Polymeric Additives on Dissolution and Crystallization of Acetaminophen. *Pharm. Res.* **2008**, *25*, 349-358.

(136) Haisa, M.; Kashino, S.; Maeda, H.: Orthorhombic form of p-hydroxyacetanilide. *Acta Crystallogr., Sect. B* **1974**, *30B*, 2510-12.

(137) Zhang, G. G. Z.; Zhou, D.: *Amorphous and Crystalline Solids*; 1st ed.; Academic Press: New York, 2009.

(138) Barthe, S. C.; Grover, M. A.; Rousseau, R. W.: Observation of Polymorphic Change through Analysis of Focused Beam Reflectance Measurement Data: Transformation of Paracetamol from Form II to Form I. *Cryst. Growth Des.* **2008**, *8*, 3316-3322.

(139) Sohn, Y. T.: Study on the polymorphism of acetaminophen. *Yakche Hakhoechi* **1990**, *20*, 97-104.

(140) Granberg, R. A.; Rasmuson, A. C.: Solubility of Paracetamol in Pure Solvents. *J. Chem. Eng. Data* **1999**, *44*, 1391-1395.

(141) Lee, H. G.; Zhang, G. G. Z.; Flanagan, D. R.: Cocrystal intrinsic dissolution behavior using a rotating disk. *J. Pharm. Sci.* **2011**, *100*, 1736-1744.

(142) Boldyreva, E. V.; Shakhtshneider, T. P.; Ahsbahs, H.; Sowa, H.; Uchtmann, H.: Effect of High Pressure on the Polymorphs of Paracetamol. *J. Therm. Anal. Calorim.* **2002**, *68*, 437-452.

(143) Kachrimanis, K.; Fucke, K.; Noisternig, M.; Siebenhaar, B.; Griesser, U. J.: Effects of Moisture and Residual Solvent on the Phase Stability of Orthorhombic Paracetamol. *Pharm. Res.* **2008**, *25*, 1440-1449.

(144) Hoffman, J. D.: Thermodynamic driving force in nucleation and growth processes. *J. Chem. Phys.* **1958**, *29*, 1192-3.

(145) Pudipeddi, M.; Serajuddin, A. T. M.: Trends in solubility of polymorphs. *J. Pharm. Sci.* **2005**, *94*, 929-939.

(146) Zhou, D.; Zhang, G. G. Z.; Law, D.; Grant, D. J. W.; Schmitt, E. A.: Physical stability of amorphous pharmaceuticals: importance of configurational thermodynamic quantities and molecular mobility. *J. Pharm. Sci.* **2002**, *91*, 1863-1872.

(147) Murphy, D.; Rodriguez-Cintron, F.; Langevin, B.; Kelly, R. C.; Rodriguez-Hornedo, N.: Solution-mediated phase transformation of anhydrous to dihydrate carbamazepine and the effect of lattice disorder. *Int. J. Pharm.* **2002**, *246*, 121-134.

(148) Qiu, L. Y.; Bae, Y. H.: Polymer Architecture and Drug Delivery. *Pharm. Res.* **2006**, *23*, 1-30.

(149) Omidian, H.; Kinam Park, P. S.: Chapter 20: Pharmaceutical Polymers. In *Martin's Physical Pharmacy and Pharmaceutical Sciences*; 6th ed.; Sinko, P., Singh, Y., Eds.; Wolter Kluwer Health/Lippincott Williams & Wilkins.: New York, 2010; pp 492.

(150) Pina, M. F.; Zhao, M.; Pinto, J. F.; Sousa, J. J.; Craig, D. Q. M.: The Influence of Drug Physical State on the Dissolution Enhancement of Solid Dispersions Prepared Via Hot-Melt Extrusion: A Case Study Using Olanzapine. *J. Pharm. Sci.* **2014**, *103*, 1214-1223.

(151) Priemel, P. A.; Laitinen, R.; Barthold, S.; Grohganz, H.; Lehto, V.-P.; Rades, T.; Strachan, C. J.: Inhibition of surface crystallization of amorphous indomethacin particles in physical drug-polymer mixtures. *Int. J. Pharm. (Amsterdam, Neth.)* **2013**, *456*, 301-306.

(152) Sun, Y.; Zhu, L.; Wu, T.; Cai, T.; Gunn, E. M.; Yu, L.: Stability of Amorphous Pharmaceutical Solids: Crystal Growth Mechanisms and Effect of Polymer Additives. *AAPS J.* **2012**, *14*, 380-388.

(153) Amidon, G. L.; Lennernaes, H.; Shah, V. P.; Crison, J. R.: A theoretical basis for a biopharmaceutic drug classification: the correlation of in vitro drug product dissolution and in vivo bioavailability. *Pharm. Res.* **1995**, *12*, 413-20.

(154) Lipp, R.: The innovator pipeline: bioavailability challenges and advanced oral drug delivery opportunities. *Am. Pharm. Rev.* **2013**, *16*, 10, 12, 14-16.

(155) Alonzo, D. E.; Gao, Y.; Zhou, D.; Mo, H.; Zhang, G. G. Z.; Taylor, L. S.: Dissolution and precipitation behavior of amorphous solid dispersions. *J. Pharm. Sci.* **2011**, *100*, 3316-3331.

(156) Gao, P.; Guyton, M. E.; Huang, T.; Bauer, J. M.; Stefanski, K. J.; Lu, Q.: Enhanced Oral Bioavailability of a Poorly water-soluble Drug PNU-91325 by Supersaturatable Formulations. *Drug Dev. Ind. Pharm.* **2004**, *30*, 221-229.

(157) Ilevbare, G. A.; Liu, H.; Edgar, K. J.; Taylor, L. S.: Maintaining Supersaturation in Aqueous Drug Solutions: Impact of Different Polymers on Induction Times. *Cryst. Growth Des.* **2013**, *13*, 740-751.

(158) Kuldipkumar, A.; Tan, Y. T. F.; Goldstein, M.; Nagasaki, Y.; Zhang, G. G. Z.; Kwon, G. S.: Amphiphilic Block Copolymer as a Crystal Habit Modifier. *Cryst. Growth Des.* **2005**, *5*, 1781-1785.

(159) Munk, T.; Baldursdottir, S.; Hietala, S.; Rades, T.; Kapp, S.; Nuopponen, M.; Kalliomaki, K.; Tenhu, H.; Rantanen, J.: Crystal Morphology Modification by the Addition of Tailor-Made Stereocontrolled Poly(N-isopropyl acrylamide). *Molecular Pharmaceutics* **2012**, *9*, 1932-1941.

(160) Oaki, Y.; Imai, H.: Morphological Evolution of Inorganic Crystal into Zigzag and Helical Architectures with an Exquisite Association of Polymer: A Novel Approach for Morphological Complexity. *Langmuir* **2005**, *21*, 863-869.

(161) Rumondor, A. C. F.; Jackson, M. J.; Taylor, L. S.: Effects of Moisture on the Growth Rate of Felodipine Crystals in the Presence and Absence of Polymers. *Cryst. Growth Des.* **2010**, *10*, 747-753.

(162) Konno, H.; Handa, T.; Alonzo, D. E.; Taylor, L. S.: Effect of polymer type on the dissolution profile of amorphous solid dispersions containing felodipine. *Eur. J. Pharm. Biopharm.* **2008**, *70*, 493-499.

(163) Kuldipkumar, A.; Kwon, G. S.; Zhang, G. G. Z.: Determining the Growth Mechanism of Tolazamide by Induction Time Measurement. *Cryst. Growth Des.* **2007**, *7*, 234-242.

(164) Kuldipkumar, A. K., G. S.; Zhang, G. G. Z.: Modulating Crystal Morphology Using Amphiphilic Block Copolymers: Crystallization of Tolazamide and Elucidating the Mechanism. *Journal of Pharmaceutical Sciences* **2014**, *TDB*, TDB.

(165) Koo, C. H.; Suh, J. S.; Yeon, Y. H.; Watanabe, T.: The crystal and molecular structure of 1-(hexahydro-1H-azepin-1-yl)-3-(p-tolylsulfonyl)urea: tolazamide (C14H21N3O3S). *Arch. Pharmacal Res.* **1988**, *11*, 74-9.

(166) Benet, L. Z.; Broccatelli, F.; Oprea, T. I.: BDDCS Applied to Over 900 Drugs. *AAPS J.* **2011**, *13*, 519-547.

(167) Yu, H.; Wang, B.; Pan, X.; Liu, H.; Bi, S.: Molecular dynamics simulation of adsorption of polyethylene glycol on surface of dicalcium silicate. *Huagong Xuebao (Chin. Ed.)* **2013**, *64*, 943-948.

(168) Martin, A.: States of Matter. In *Physical Pharmacy*; 4th ed.; Martin, A., Ed.; Lippincott Williams & Wilkins: Baltimore, USA, 1993; pp 22-52.

(169) Ilevbare, G. A.; Liu, H.; Edgar, K. J.; Taylor, L. S.: Impact of Polymers on Crystal Growth Rate of Structurally Diverse Compounds from Aqueous Solution. *Mol. Pharmaceutics* **2013**, *10*, 2381-2393.

(170) Powell, C. T.; Cai, T.; Hasebe, M.; Gunn, E. M.; Gao, P.; Zhang, G.; Gong, Y.; Yu, L.: Low-Concentration Polymers Inhibit and Accelerate Crystal Growth in Organic Glasses in Correlation with Segmental Mobility. *J. Phys. Chem. B* **2013**, *117*, 10334-10341.

VITA

The author, Yi Gao was born and raised in Tonglu, Zhejiang Province, China. She attended China Pharmaceutical University, in Nanjing, China where she earned a Bachelor of Science in Pharmacy in 1982 and a Master of Science in Pharmaceutical Microbiology in 1986.

Currently, she is a Principal Research Scientist and Group Leader with Pharmaceutical Sciences, AbbVie Inc. (formerly Abbott Laboratories), North Chicago. Prior to joining AbbVie in 1992, she was a research assistant at The University of Iowa and assistant lecturer at China Pharmaceutical University. She started pursuing her doctoral degree in Chemistry at Loyola University in 2005 on a part-time basis. She resides in Vernon Hills, Illinois.